UCRL 10107
c.2

University of California

Ernest O. Lawrence Radiation Laboratory

MEASUREMENT OF $\frac{G}{M}$ FOR MUONS

Berkeley, California

DISCLAIMER

UCRL-10107

UNIVERSITY OF CALIFORNIA

Lawrence Radiation Laboratory
Berkeley, California

Contract No. W-7405-eng-48

MEASUREMENT OF $\frac{G}{M}$ FOR MUONS

Gordon McDonald Bingham

(Ph. D. Thesis)

May 1962

MEASUREMENT OF $\frac{G}{M}$ FOR MUONS

Contents

MEASUREMENT OF $\frac{Q}{M}$ FOR MUONS

Gordon McDonald Bingham
(Thesis)

ABSTRACT

A free running "muon stroboscope" was used to measure the ratio of the precession frequencies of muons (f) and protons in water (f_p) for the same magnetic field. The stroboscope frequency was 200 Mc/sec. The results obtained were:

Positive muons stopping in bromoform $(\frac{f}{f_p})^+ = 3.18336 \pm 0.00007$

Negative muons stopping in water $(\frac{f}{f_p})^-_{H_2O} = 3.1808 \pm 0.0004.$

The first ratio is assumed to be also that of the free particles and leads to the following values for $(g/m)^+$ and m^+:

$$(g/m)^+ = (9.6840 \pm 0.0002) \times 10^{-3}\ m_e^{-1}$$

$$m^+ = (206.766 \pm 0.005)\ m_e$$

where m_e is the electron mass. A diamagnetic correction is applied to the second ratio and an equivalent value $(g/m)^-_{H_2O}$ is obtained for negative muons stopping in water:

$$(g/m)^-_{H_2O} = (9.6760 \pm 0.0013) \times 10^{-3}\ m_e^{-1}\ .$$

Assuming equal masses for positive and negative muons we obtain:

$$\frac{g^-(H_2O) - g^+}{g^+} = -(8.3 \pm 1.4) \times 10^{-4}\ .$$

The present experiment is in quite reasonable agreement with the recent Columbia experiment of Hutchinson et al. From the combined results of

both experiments we have

$$m^+ = (206.765 \pm 0.002)\, m_e \quad (12 \text{ p.p.m.})$$

and

$$\frac{g^-(H_2O) - g^+}{g^+} = -(8.9 \pm 0.8) \times 10^{-4} \quad .$$

I. INTRODUCTION

The muon and the electron pose one of the most interesting questions in particle physics.[1] They have widely different masses, yet they are very similar in all other respects. In the hope of obtaining a clue to the answer of this question, it is of interest to measure accurately the magnetic moment of the muon and to compare this experimental result with that predicted by quantum electrodynamics. The muon g value is given by quantum electrodynamics (Q.E.D.) as[2,3,4,5]

$$g = 2\left(1 + \frac{\alpha}{2\pi} + 0.75\ \frac{\alpha^2}{\pi^2} + \ldots\ \right)$$
$$= 2(1.001165) \qquad (1)$$

where α is the fine structure constant. The behaviour of Q.E.D. at small distances is not well understood and it has been suggested that the theory may not be valid for distances $\frac{h}{\lambda_o c} \sim 10^{-13} - 10^{-14}$ cm. In this case it is necessary to introduce a momentum cutoff $\lambda_o c$ into the integrals involved in Eq. (1) . This results in a muon g value as follows[6]

$$g = 2\left(1 + \frac{\alpha}{2\pi}\left[1 - \frac{2}{3}\left(\frac{m}{\lambda_o}\right)^2\right] + \ldots\ \right) \qquad (2)$$

where m is the muon mass. Electron proton scattering results indicate[7] that the correction term in Eq. (2) is less than $0.02\ \frac{\alpha}{2\pi}$. Thus an experimental determination of g to an accuracy of 1 in 10^5 or better could yield information on quantum electrodynamics at small distances, in addition to information on differences between electrons and muons. It will develop later that the present experiment is, strictly speaking, a determination of the ratio $\frac{g}{m}$ because m is not known to the accuracy that is achieved here.

Lee and Yang pointed out[8] the possibility of experimentally determining the muon g value. It is based on parity nonconservation in the pion-muon-electron decay chain, which results in polarization of the muon spin along the muon direction of motion and then the asymmetric decay of the muon with respect to its spin direction. The angular distribution of electrons, $\frac{df(\theta'')}{d\Omega}$, from the decay of polarized muons at rest is given by[9]

$$\frac{df(\theta'')}{d\Omega} = \frac{1}{4\pi}(1 + a' \cos\theta'') \qquad (3)$$

where θ'' is the angle between the muon spin and the direction of electron emission, and Ω is the solid angle. Eq. (3) has been averaged over the electron energy distribution. The V-A theory of muon decay, which appears to be in good agreement with experiment, predicts that $a' = \pm 1/3$ where the positive sign is for positive muons and the negative sign is for negative muons. The electron distribution is peaked backwards relative to the line of flight of the muons, for both positive and negative muons. It is thus inferred by the V-A theory that, in the pion rest frame, positive muons are polarized opposite to their line of flight and negative muons are polarized along their line of flight.

Experimentally, polarized muons are obtained from the decay in flight of pions and the muon beam so obtained may not be completely polarized. Also the muons must be brought to rest in a suitable target material which may result in further depolarization. The experimental distribution corresponding to Eq. (3) is written

$$\frac{df(\theta')}{d\Omega} = \frac{1}{4\pi}(1 + a \cos\theta') \qquad (4)$$

where the asymmetry coefficient $a = R_p a'$ and R_p is the muon polarization

at decay. For the remainder of this report we will assume that muons carry a "polarization vector" which is approximately along the muon beam line, for both positive and negative muons. We refer θ' to this vector and so a will be negative for both positive and negative muons. Experiments[8,10] have shown that positive muon beams from cyclotrons have almost complete polarization and that this polarization may be retained by suitable choice of target material. Work[11] done at the Berkeley 184" synchrocyclotron, with a positive beam arrangement reasonably similar to the one used here, implied an average value $R_p = 0.857 \pm .024$. In the present experiment bromoform was used for the positive muon work because of its high R_p value, its high density, and the small magnetic field shift experienced by the stopped muons. From CP invariance[12] it is expected that the magnitude of the beam polarization is the same for both positive and negative muons if the same beam setup is used. Experiments with negative muons show that they are almost completely depolarized even with the most favorable choice of target material.[13,14] Water was used as the target material in the negative meson work of this experiment mainly for convenience. The asymmetry coefficient (Eq. 4) is expected to have a magnitude ~ 0.04 with a water target. There are no known target materials whose use results in an appreciably higher value for negative muons. Schiff[15] has observed the rate at which negative muons are transferred to impurities (e.g. neon) when stopped in liquid hydrogen. If we assume similar behaviour for oxygen, then the negative muons will be transferred to the oxygen in water in times $\sim 10^{-10}$ sec. Thus the negative muon target of this experiment is really the oxygen in water.

The experiment to be described here is a precession type experiment. Polarized muons are brought to rest in a target (bromoform for

positive muons, water for negative muons) located in a homogeneous magnetic field H. The frequency of precession of the muons about the field direction is given by

$$f = \frac{g\, e\, H}{4\, \pi\, m\, c} \qquad (5)$$

where it has been assumed that the muon and electron have equal charge. The resulting rotation of the muon "polarization vector" is viewed by a system whose behaviour is very similar to that of a stroboscope. The present experiment essentially determines the value of H at which the stroboscope frequency f_o is equal to the muon precession frequency f. This value is called the "resonance" field, H(res). In fact however, the magnetic field is not measured directly. Instead, the corresponding proton resonance frequency f_p is measured for protons in water. Thus at resonance we have

$$\left.\begin{aligned} f_p &= f_p\,(res) \\ f &= f_o \end{aligned}\right\} \qquad (6)$$

In this experiment we determine the values $f_p(res)$ for the cases in which positive muons are stopped in bromoform and negative muons are stopped in water. Then since f_o is accurately known, we have determined the precession frequency ratio $\frac{f}{f_p}$ for muons and protons in the same magnetic field. (In the present discussion we will neglect any corrections due to the fact that the muons and protons are not free.) Now the muon has a finite mean life τ given by $\tau = 2.2\ \mu$ sec. and so the uncertainty principle will impose a lower limit ($\Delta f \sim 1/2\pi\tau$) on the error in f. Thus for an accurate determination of f it is necessary to operate at high precession frequencies and consequently at high magnetic fields. In the present case the value $f_o = 200$ Mc/sec. was chosen with the limitations being the maximum available magnetic field and electronic difficulties. From the

determinations of other workers (see below) the associated magnetic field and proton frequency are respectively 14.7 kilogauss and 62.8 Mc/sec. From Eq. (5) and a similar equation for the proton in the same magnetic field H we obtain

$$\frac{g}{m} = \frac{f}{f_p} \frac{g_p}{m_p} \tag{7}$$

where g_p is the proton g value and m_p is the proton mass. The best values of these constants are[16] $g_p = 2(2.79275 \pm 0.00003)$ and $m_p = (1836.12 \pm 0.02)\, m_e$ where m_e is the electron mass. The best value for the muon mass, obtained from experiments other than the present type, comes from mesic X-ray work and is[17,18,19] $m = (206.76 \pm .02)m_e$. Thus a measurement of the ratio $\frac{f}{f_p}$ correct to 2 parts in 10^5, as in this experiment, is actually a determination of the ratio g/m, as stated earlier. The value of g has been measured[20] by the "(g-2) experiment," the most recent value obtained being $g = 2(1.001162 \pm 0.000005)$. Thus it is possible to obtain an accurate value of m from this experiment.

Measurements of the ratio $\frac{f}{f_p}$ have already been made by a number of workers. The most accurate value obtained is that of Hutchinson et al[21] and was reported immediately prior to the running of this experiment. They obtained the value $\frac{f}{f_p} = 3.18334 \pm 0.00005$ as the average value for positive muons stopping in several different materials. Their report also listed values obtained for negative muons stopping in various materials. They used the relation

$$\frac{g}{m} = \frac{f/f_p}{f_e/f_p} \frac{g_e}{m_e} \tag{8}$$

rather than Eq. (7) in the calculation of g/m. In Eq. (8) $\frac{f_e}{f_p}$ is the ratio of the precession frequency of an electron to that of a proton in

same magnetic field and g_e is the electron g value. In this way it is possible to take advantage of the accurate determinations $g_e = 2(1.0011609 \pm 0.0000024)$ by Schupp et al[22] and $\frac{f_e}{f_p} = 658.22759 \pm .00004$ as discussed by Dumond.[23] It must be noted that the electrons were free and the protons were in water for the latter determination. Thus a diamagnetic correction must be applied before this determination is used in Eq. (8).

In the following section it will develop that the major difference between this experiment and the recent experiments of other workers is that no pulsed oscillators are used here. The timing of the incoming muon and the decay electron is done simply and immediately relative to a crystal controlled free running oscillator, the "200 Mc/sec oscillator." This oscillator generates the muon stroboscope frequency f_o .

II. MUON STROBOSCOPE

A. Principle of Operation

The operation of the apparatus is best understood by first briefly considering the case where polarized muons are stopped in a field free region. It is desired to determine the magnitude of the asymmetry coefficient a, and the polarization direction ϕ with respect to an array of four identical counters spaced 90° apart as shown in Fig. 1. The "polarization vector" has been shown by the arrow at the centre. The counters are denoted F(i.e. forward as seen from the muon in the polarization direction) R, B, L and the same four symbols are also used to denote the corresponding number of electrons detected from a given number of stopped muons. We assume that the counters have small solid angles. Then from Eq. (4) we have

$$\tan \phi = \frac{R - L}{F - B} \tag{9}$$

and

$$|a| = \frac{2\sqrt{(F-B)^2 + (R-L)^2}}{\Sigma} \tag{10}$$

where $\Sigma = F + B + R + L$. The above relations will be used in the stroboscope discussion.

A simplified block diagram of the symmetric muon stroboscope is shown in Fig. 2. Here polarized muons are stopped in a target located in a uniform magnetic field H. It has been assumed that the muon orbit direction makes an angle ϕ with the axis of the β counter at the instant the muon crosses the μ counter. The incoming muon is detected by the "μ counter" and the decay electron is detected by the "β counter." The counter signals are then sent to the corresponding fast mixer units. These units each contain four mixing circuits labelled I, II, III, IV and A, B, C, D as shown. Each mixing circuit has two inputs, one from the 200 Mc/sec oscillator and one from the appropriate counter. The oscillator inputs

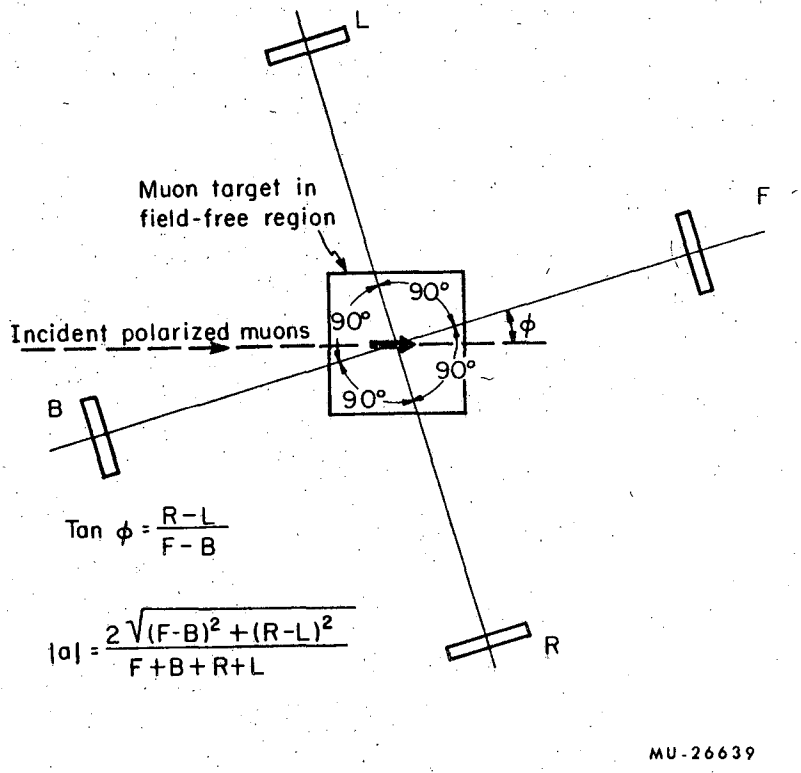

Fig. 1 Determination of muon polarization with respect to counter array consisting of four identical counters F.R.B.L. spaced 90° apart.

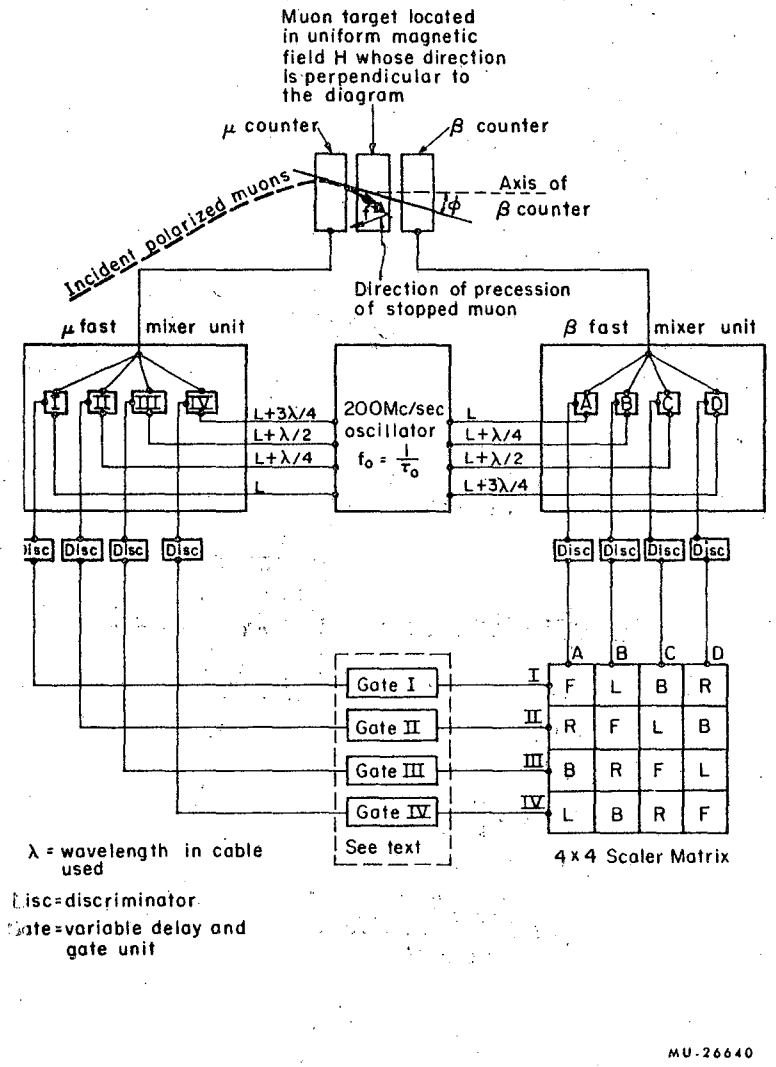

Fig. 2. Simplified block diagram of symmetric muon stroboscope. The Angle between muon orbit and axis of β counter at instant muon crosses μ counter is denoted by ϕ.

are such that I and A, II and B, etc., are in phase but successive quarter wavelength delays are added in going from I to II, II to III, etc. Each mixing circuit is capable of detecting counter signals during an interval of approximately one quarter cycle at the negative peak of the 200 Mc/sec wave, the actual width of this interval being determined by the setting of the discriminator which views the output of the mixing circuit. Thus each fast mixer unit may be thought of as a set of four switches operating at a frequency of 200 Mc/sec, each switch having an on time of approximately 1 nanosec. with successive quarter cycle delays between successive switches. As can be seen from Fig. 2, the four outputs of each fast mixer unit go to a 4 x 4 scaler matrix. Four identical variable delay and gate units, gates I to IV, are included in the μ fast mixer channels to allow variation of the interval, the electron gate, in which decay electrons are accepted. Because of the difficulty of setting gates I - IV so that they are all closely the same, a slightly different arrangement was in fact used and will be described in Section III E. The position of the muon-electron event on the 4 x 4 scaler matrix is a measure of the phase difference (relative to the 200 Mc/sec oscillator) between the muon arrival and the electron emergence. The scalers and their average associated electron-muon phase differences are (referring to Fig. 2)

F scalers — phase difference $0 + 2n\pi$

L scalers — $\frac{\pi}{2} + 2n\pi$

B scalers — $\pi + 2n\pi$

R scalers — $\frac{3\pi}{2} + 2n\pi$

The reason for the designation F, L, B, R will become clear below.

We will now consider the operation of the muon stroboscope at resonance, i.e. the magnetic field H has been adjusted so that the frequency of precession $f = f_0$. Let us suppose that a μ counter signal arrives in the on time of mixing circuit I (hereafter on times will be referred to as

"slots") and triggers gate I. Then any β counter signal which occurs during the gate I and slot A will correspond to a forward count F in the scheme of Figure 1. (We assume equal signal delays between each counter and its fast mixer unit.) Thus the IA element of the 4 x 4 scaler matrix is marked "F". Similarly any β counter signal which occurs in gate I and slot B corresponds to a left count L in the scheme of Fig. 1. The remaining matrix labels may be obtained in this same way. It must be noted that a symmetric muon stroboscope has been assumed, i.e. all slots have equal widths, the pairs I and A, II and B, etc. are exactly in phase with successive phase shifts of exactly $\frac{\pi}{2}$ between successive pairs. In this case it is meaningful to use the same symbol on four scalers as shown, since each member of a particular group of four will show the same average number of counts as both muons and electrons arrive randomly relative to the 200 Mc/sec oscillator. The muon stroboscope essentially sets up a system of counters as in Fig. 1 but in a frame of reference rotating at frequency f_o. The only difference is that, because the "polarization vector" rotates through about 90^o during a slot (assuming slots are about $1/(4 f_o)$ wide), the muon stroboscope will see a slightly lower asymmetry than the asymmetry obtained in Fig. 1. It must be noted that the labels on the 16 matrix elements are strictly true only for $f = f_o$.

Now the operation of the muon stroboscope will be considered for the situation where the magnetic field is not at its resonance value, i.e. $f \neq f_o$. In the spirit of Eq. (9) we will define the phase angle θ of the "polarization vector" relative to the rotating frame as

$$\tan \theta = \frac{R^s - L^s}{F^s - B^s} \qquad (11)$$

where R^s = sum of the four R scalers, etc. Similarly we can define (for

use later) the asymmetry coefficient A as seen by the muon stroboscope.

$$A = \frac{-2\sqrt{(F^S-B^S)^2 + (R^S-L^S)^2}}{\Sigma^S} \qquad (12)$$

When $f \neq f_o$ the polarization vector will rotate (angular velocity $\dot{\theta}$) relative to the rotating frame that has been set up by the muon stroboscope. From analogy with a conventional stroboscope we would expect a relation of the form $\theta = 2\pi(f-f_o)T_{av} + \Phi$ where T_{av} is the average time interval for muon precession and Φ is a constant which we call "the initial phase." Since the muon stroboscope essentially "photographs" the phase angle θ by means of the decay electrons that are emitted, we expect T_{av} to be determined by the particular electron gate that has been set. (In part B, below, the anticipated θ relation is shown to follow as a close approximation to Eq. (11).) So far we have not shown how the resonance field is determined. Because the initial phase is not known to the present experimental accuracy, it is necessary to use a phase difference method[24,21]. At resonance we will have $\theta = \Phi$ regardless of the electron gate in use, since both the "polarization vector" and the rotating frame have the same frequency ($f = f_o$). Thus the phase angle θ was obtained experimentally as a function of f_p (and hence also f) for two different electron gates. The first gate, the early gate, extends from time T_e to $(T_e + G)$ after the muon enters the system and the second gate, the late gate, extends from time T_l to $(T_l + G)$. Then $f_p(res)$ was obtained as the proton frequency at which there was zero phase difference between the early and late results. In the scheme of Fig. 2, T_e and T_l were the delays set on gates I to IV for two separate runs at a given proton frequency f_p. The same gate width G was used for both runs. The procedure was then repeated for a series of values of f_p.

The factors which determine the actual value of initial phase may be set out as follows —

(a) The angle ϕ of Fig. 2.

(b) The precession frequency of the muon between the time it crosses the μ counter and the time it comes to rest. The relation[25] which gives the frequency of precession, $f(\gamma)$, for a muon of total energy $m\gamma c^2$ moving perpendicular to the field lines of a uniform magnetic field H is

$$f(\gamma) = \frac{eH}{2\pi m\gamma c}\left[1 + \left(\frac{g-2}{2}\right)\gamma\right] \qquad (13)$$

For $\gamma = 1$, Eq. (13) reduces to Eq. (5) as expected. Also it is seen that $f(\gamma) < f(1)$. There is an additional lowering of the initial muon precession frequency due to the fact that the initial part of the muon orbit (between the counter and the target) is through a slighly lower magnetic field. However this additional effect is negligible here.

(c) The apparent direction of the axis of the β counter. This is set by the β orbits in the magnetic field. It can also be influenced by the distribution of stopped muons in the target.

(d) The direction of the "polarization vector" for the incident muon beam. It may be orientated at a small angle relative to the beam direction.

(e) The relative signal delay between each counter and its fast mixer unit. This is discussed later.

B. Approximate Theory of Symmetric Muon Stroboscope.

In order to keep the mathematics workable, it is necessary to use simplifying approximations. It is assumed that the finite target size and the finite solid angle of the β counter may both be neglected here. In Appendix 1 the effect of finite solid angle is considered in a simple case and it is shown to be of no importance in this experiment. The

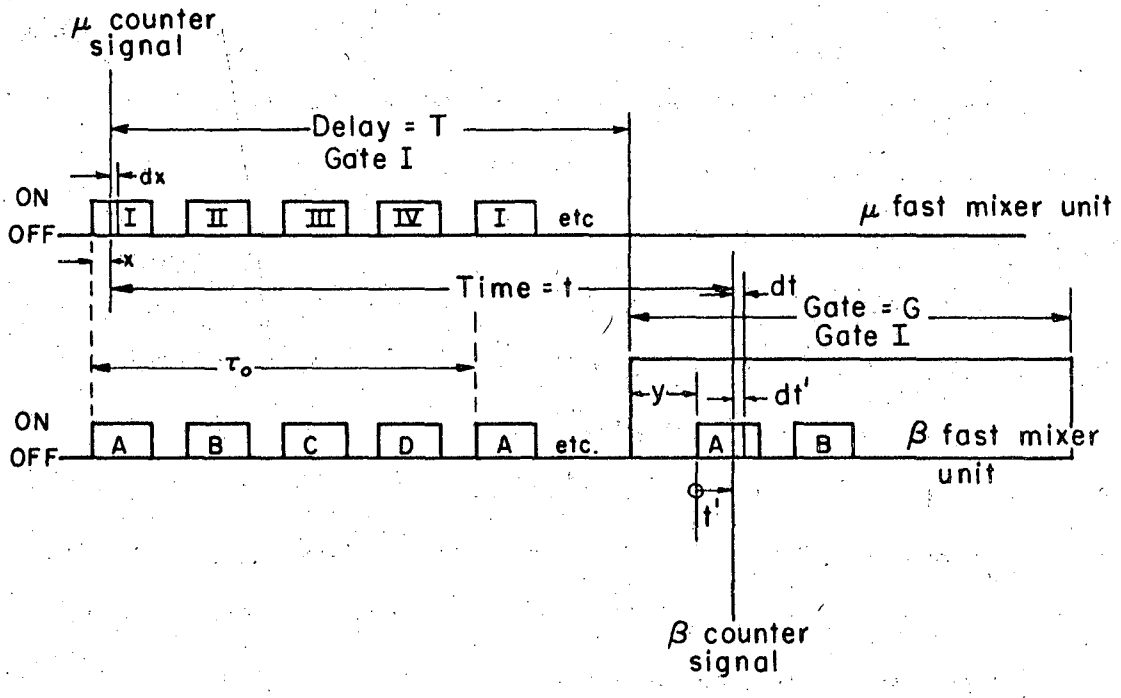

τ_o = stroboscope period (5 nanosec).

All slots I, II, III, IV, A, B, C, D are $\tau_o/6$ wide and spaced $\tau_o/4$.

μ and β fast mixers are exactly in phase and both are free running.

T = Delay, G = Gate, set on the four identical units Gate I-IV of Fig. 2.

Fig. 3. Timing diagram for symmetric muon stroboscope. Notice that T and G are not to scale.

effect of the magnetic field and energy loss on the electron orbits will also be neglected. We will just continue to use the distribution of Eq. (4). Any timing jitter existing in the system will be assumed to be small, i.e. $\ll 1$ nanosec. We will assume a symmetric muon stroboscope with slot widths of $\frac{\tau_o}{6}$. The timing diagram is then as shown in Fig. 3. T and G are the delay and gate settings on the four identical variable delay and gate units. Clearly T and G are not to scale. We consider the case in which a μ counter signal arrived at time x after the start of slot I. Then gate I will be triggered as indicated. It is then assumed that a β counter signal arrives at time t' after the beginning of the first A slot within gate I. This slot begins at time y after start of gate ϕ. We wish to determine the total number F_o of IA events coming from the first A slot within the gate, for a run in which N_μ polarized muons were stopped in the target. We have

$N_\mu f_o dx$ = total number of muons which arrived in interval dx at x for all I slots (since the stroboscope is free running).

$(\Phi + 2\pi ft)$ = total phase angle of "polarization vector" at time t after arrival (relative to axis of β counter).

Thus from Eq. (4) we obtain the number of IA events due to muons in dx at x of all I slots and electrons in dt at t in the first A slot within gate,

$$d^2F_o = (N_\mu f_o\, dx)\left(\frac{\Delta\Omega}{4\pi}\right)\left[1 + a\cos(\Phi + 2\pi ft)\right](e^{-t/\tau}\,\frac{dt}{\tau} \qquad (14)$$

where $\Delta\Omega$ is the β counter solid angle. From Fig. 3 we have $t = T + y + t'$ and $N' = f_o(T + y + x)$ where N' is an integer. Thus we may rewrite Eq. (14) as

$$d^2F_o = N_\mu f_o\, dx\,\frac{\Delta\Omega}{4\pi}\, e^{-T/\tau}\,\frac{dt'}{\tau}\left\{1 + a\cos\left[\Phi + 2\pi(f-f_o)T + 2\pi ft' - 2\pi f_o x\right]\right\} \qquad (15)$$

where $y \ll T$ and $y + t' \ll \tau$ have been used. Integrating on t' and x and using $(f - f_o) \approx 0$ (since for the range used in this experiment

$|f - f_o| \leq 10^{-3} f_o$) we obtain

$$F_o = \frac{N_\mu \Delta\Omega e^{-T/\tau}}{144\,\pi f_o \tau} \left\{ 1 + \frac{2a}{\pi^2} \cos \left[\Phi + 2\pi (f-f_o)\, T \right] . \right\} \quad (16)$$

Similarly by making the substitution $t' \rightarrow t' + n\tau_o$ in Eqs. (15) and (16) the number of IA counts, F_n, due to muons in all I slots and electrons in the $(n+1)^{th}$ slot within gate G, is obtained.

$$F_n = \frac{N_\mu \Delta\Omega e^{-(T+n\tau_o)/\tau}}{144\,\pi f_o \tau} \left\{ 1 + \frac{2a}{\pi^2} \cos \left[\Phi + 2\pi(f-f_o)(T+ n\tau_o) \right] \right\} . \quad (17)$$

Thus the total number of IA counts is given by

$$F = \sum_{n=0}^{N} k\, e^{-(T+n\tau_o)/\tau} \left\{ 1 + \frac{2a}{\pi^2} \cos \left[\Phi + 2\pi(f-f_o)(T+ n\tau_o) \right] \right\} \quad (18)$$

where $k = \frac{N_\mu \Delta\Omega}{144\,\pi f_o \tau}$ and N = number of cycles within the gate G, i.e. $N = \frac{G}{\tau_o}$. With the symmetric stroboscope being considered here, Eq. (18) is also the expression for the II B, III C and IV D counts.

We will consider the I B element of the matrix now. To obtain its counts, L, it is merely necessary to make the substitution $t' \rightarrow t' + \frac{\tau_o}{4}$ in Eq. (15) and proceed exactly as above. In a similar manner the B and R counts may be obtained, the complete final results being summarized in the following equations

$$F = \sum_{n=0}^{N} k\, e^{-(T+n\tau_o)/\tau} \left\{ 1 + \frac{2a}{\pi^2} \cos \left[\Phi + 2\pi(f-f_o)(T+n\tau_o) \right] \right\}$$

$$L = \sum_{n=0}^{N} k\, e^{-(T+n\tau_o)/\tau} \left\{ 1 - \frac{2a}{\pi^2} \sin \left[\Phi + 2\pi\, (f-f_o)(T + n\tau_o) \right] \right\} \quad (19)$$

$$B = \sum_{n=0}^{N} k\, e^{-(T+n\tau_o)/\tau} \left\{ 1 - \frac{2a}{\pi^2} \cos \left[\Phi + 2\pi(f-f_o)(T+n\tau_o) \right] \right\}$$

$$R = \sum_{n=0}^{N} k\, e^{-(T+n\tau_o)/\tau} \left\{ 1 + \frac{2a}{\pi^2} \sin \left[\Phi + 2\pi(f-f_o)(T+n\tau_o) \right] \right\}$$

From Eq. (11) we have

$$\tan\theta = \frac{\sum_{n=0}^{N} e^{-n\tau_o/\tau} \sin\left[\Phi + 2\pi(f-f_o)(T+n\tau_o)\right]}{\sum_{n=0}^{N} e^{-n\tau_o/\tau} \cos\left[\Phi + 2\pi(f-f_o)(T+n\tau_o)\right]} \qquad (20)$$

From Eq. (20) the expression for θ is obtained,

$$\theta = \Phi + 2\pi(f-f_o)\,T + \beta \qquad (21)$$

with

$$\beta = \text{Arg.}\left\{\sum_{n=0}^{N} e^{n\tau_o\left[2\pi(f-f_o)i-1/\tau\right]}\right\}.$$

A more explicit expression, giving $\tan\beta$, may be obtained by performing the summation of the geometric series above and using $\frac{\tau_o}{\tau} \approx 2 \times 10^{-3} \ll 1$.

$$\tan\beta = \frac{\sin 2\pi(f-f_o)G - 2\pi(f-f_o)\tau\left[e^{G/\tau}\cos 2\pi(f-f_o)G\right]}{\cos 2\pi(f-f_o)G - e^{G/\tau} - 2\pi(f-f_o)\tau \sin 2\pi(f-f_o)G} \qquad (22)$$

Under the assumption that $(f-f_o)\tau$ and $(f-f_o)G$ are both small the approximate expression may be obtained from either Eq. (21) or Eq. (22)

$$\beta = 2\pi\,(f-f_o)\,\bar{G} \qquad (23)$$

where

$$\bar{G} = G\left[\frac{\tau}{G} - \frac{1}{(e^{G/\tau}-1)}\right]$$

$\bar{G}$ is thus the weighted value of the gate width. Comparing the values of β obtained from Eqs. (22) and (23) for $G = 2.5\ \mu$ sec (as used in this experiment) it is found that, for values $(f_p - f_p(\text{res})) = 30$ Kc/sec and 60 Kc/sec, the errors involved in using Eq. (23) are respectively 0.2° and 3°. These errors are much less than the corresponding statistical errors of this experiment so we may use Eq. (23) and take the phase plots, i.e. Eq. (21), as straight lines

$$\theta = \Phi + 2\pi\,(f-f_o)(T+\bar{G}) \quad . \tag{24}$$

It is seen that Eq. (24) is the relation that was anticipated in part A of this section.

An expression for the asymmetry as seen with the muon stroboscope may be obtained with the aid of Eq. (12) and Eq. (19)

$$A = \frac{2a}{\pi^2} \frac{\left| \sum_{n=0}^{N} e^{-n\tau_o/\tau + i\left[\Phi + 2\pi(f-f_o)(T+n\tau_o)\right]} \right|}{\sum_{n=0}^{N} e^{-n\tau_o/\tau}} \tag{25}$$

using $\frac{\tau_o}{\tau} \ll 1$ and $|f-f_o| \approx 0$ again we obtain

$$A = \frac{2a}{\pi^2} \frac{1}{\sqrt{1 + \left[2\pi(f-f_o)\tau\right]^2}} \frac{\sqrt{1 + e^{-2G/\tau} - 2e^{-G/\tau} \cos 2\pi(f-f_o)G}}{(1 - e^{-G/\tau})} \quad . \tag{26}$$

Because of its comparative insensitivity to $(f-f_o)$ no attempt was made to use A, or any of its terms, to find the resonance. [We note that the present Eqs. (24) and (26) are to be compared with Eq. (8) and a/RR_G respectively, in reference 24.] For future reference, the decrease in A at $(f_p - f_p(\text{res})) = 30$ Kc/sec, and 60 Kc/sec was calculated. With $G = 2.5\ \mu$ sec the respective drops were 8% and 32%.

An equation similar to Eq. (24) may be written for both the late gate (T_l to $T_l + G$) and the early gate (T_e to $T_e + G$). Then <u>under the assumption that is the same for both</u>, we have

$$(\theta_l - \theta_e) = 2\pi(f-f_o)(T_l - T_e) \quad . \tag{27}$$

Whereas Eq. (24) is approximately a straight line, Eq. (27) is exactly a straight line. As anticipated in Section II A, we see that $f = f_o$ when $\theta_l - \theta_e = 0$. Several independent checks were made to examine the constancy

of Φ and will be discussed as they arise. Also it will be shown in Appendix 2 that the introduction of an additional time delay Z in the signal line of the β counter changes the initial phase as follows

$$\Phi(Z) = \Phi - 2\pi f_o Z \quad . \tag{28}$$

During the positive muon run a measured delay $Z = 2.51 \pm 0.01$ nanosec was introduced to check that the initial phase did change as expected from Eq. (28) ($181^\circ \pm 1^\circ$). In addition, it was possible to check if there was any systematic dependence of resonance frequency on initial phase. From Eq. (27) there should be no such dependence.

C. Asymmetric Muon Stroboscope

Because it is impossible to set all the slots of equal width and maintain them equal, and because the various phase shifts cannot be done exactly, the actual muon stroboscope will be asymmetric. The asymmetric muon stroboscope is considered in Appendix 2 and it is shown that a large part of any systematic effect due to different slot widths may be removed by redefining tan 0 as follows

$$\tan\theta = \frac{R^x - L^x}{F^x - B^x} \tag{29}$$

with $R^x = (R^{ID})^x + (R^{IIA})^x + (R^{IIIB})^x + (R^{IVC})^x$

L^x = etc.

and

$$(R^{ID})^x = R^{ID} \frac{N_\mu N_\beta}{36 N_\mu^{\frac{1}{2}} N_\beta} D = R^{ID} \; k^{ID}$$

$$(R^{IIA})^x = \text{etc.}$$

In the same way we will redefine A

$$A = \frac{-2\sqrt{(F^x - B^x)^2 + (R^x - L^x)^2}}{\sum^x} \qquad (30)$$

with $\sum^x = R^x + L^x + F^x + B^x$. The definitions given in Eqs. (29) and (30) are the ones used throughout the remainder of this experiment, although a slight modification of Eq. (29) will later be necessary to allow for background events.

From Appendix 2, and also in view of the assumptions made in Section II B, it becomes quite clear we cannot prove in a simple manner that the early and late phase plots will cross at the resonance frequency even for an asymmetric muon stroboscope. The final test of the equipment must be as follows-- if the actual muon stroboscope were presented with polarized muons precessing at a known frequency under conditions as in the experiment, could it determine that frequency correctly? A run was made which simulated muon precession at a known frequency. The stroboscope did in fact determine the frequency correctly. The details will be given later.

D. Estimate of total matrix counts required for a statistical accuracy $\frac{\Delta g/m}{g/m} = 2 \times 10^{-5}$.

In all error work of this report, the symbol Δ denotes the standard deviation in the quantity it precedes. Here we consider only the errors associated with the counting statistics, the complete error treatment which includes all systematic effects is given in Section V(A). From Eq. (8)

$$\Delta^2 \left(\frac{g}{m}\right) = \left[\frac{g_e}{m_e}\left(\frac{f_p}{f_e}\right)\right]^2 \left[\frac{\Delta^2 f}{(f_p)^2} + \left(\frac{f}{f_p}\right)^2 \frac{\Delta^2 f_p}{(f_p)^2}\right] \qquad (31)$$

where it is assumed (and will be shown later) that the errors in g_e and $\left(\frac{f_e}{f_p}\right)$ are much smaller than those in this experiment. No error in

m_e is considered as we will later obtain m in terms of m_e. Now f is "measured" by statistics of Eq. (27) and f_p is measured directly by proton resonance so that $\triangle f_p$ is systematic in nature and is not considered here, i.e. we set $\triangle f_p = 0$. From Eq. (27)

$$\triangle^2 f = \frac{\triangle^2\theta_e + \triangle^2\theta_1}{\left[2\pi(T_1 - T_e)\right]^2} \tag{32}$$

where we have also taken $\triangle f_o = 0$. We now wish to obtain expressions for $\triangle\theta_e$ and $\triangle\theta_1$ from Eq. (29). In the usual manner

$$\triangle^2\theta = \left[\frac{1}{(1+\tan^2\theta)}\right]^2 \left[\frac{\triangle^2 R^x + \triangle^2 L^x + (\triangle^2 F^x + \triangle^2 B^x)\tan^2\theta}{(F^x - B^x)^2}\right] \tag{33}$$

with $\triangle^2 R^x = \triangle^2(R^{ID})^x + \triangle^2(R^{IIA})^x + \triangle^2(R^{IIIB})^x + \triangle^2(R^{IVC})^x$ etc. i.e. the separate errors in $\triangle^2 R^x$ etc. are considered independent. Inspection of Eq. (29) shows that in fact they are partially correlated. However, errors in N_μ and N_β need not be considered since both cancel from Eq. (29). By rigorously considering errors due to N_μ^I etc., N_β^D etc. in Eq. (29) it is easily shown that the correlation is such that our independence assumption above results in a slight overestimation of the error in θ. So we may proceed with Eq. (33), considering a typical term of $\triangle^2 R^x$, for example $\triangle^2(R^{ID})^x$,

$$\triangle(R^{ID})^x = \sqrt{\frac{7}{6}\, k^{ID}\, (R^{ID})^x} \tag{34}$$

where the close approximations $\frac{R^{ID}}{N^I} = 0$ and $\frac{R^{ID}}{N^D} = \frac{1}{6}$ have been used. Since systematic errors must be estimated later in the experiment there appeared to be no point in accurately calculating all 16 values as in Eq. (34). Instead a conservative value of $\sqrt{\frac{7}{6}\, k^{ID}}$ etc. was chosen and used for all 16. Only $\sim$ 20% of the experimental values of these terms exceeded 1.2 (all were < 1.3) so the use of the factor 1.2 in the 16

equations like Eq. (34) will result in a slightly conservative accuracy estimate. Thus from Eq. (33) we have

$$\Delta\theta = \frac{1.2\sqrt{(R^x+L^x) + (F^x+B^x)\tan^2\theta}}{(F^x - B^x)\sec^2\theta} \qquad (35)$$

For the present purposes we can note that even in the actual stroboscope the relation $R^x + L^x = F^x + B^x$ appeared always to be satisfied, as we would expect for the symmetrical stroboscope from Eq. (19), and thus we may simplify Eq. (35) to

$$\Delta\theta = \frac{1.2}{|A|}\sqrt{\frac{2}{\Sigma}x} \ , \qquad (36)$$

where use has been made of Eq. (30).

Returning to Eq. (31) and using Eq. (32) and Eq. (36) the final expression is obtained,

$$\frac{\Delta\left(\frac{g}{m}\right)}{(g/m)} = \frac{1.2}{2\pi f\left[T_1 - T_e\right]|A|}\sqrt{\frac{2}{\Sigma_1}x + \frac{2}{\Sigma_e}x} \ . \qquad (37)$$

Assuming $\Sigma_e^x \approx 2\Sigma_1^x$, and setting $(T_1 - T_e) = 2.9\ \mu$ sec., $|A| = 0.22$, f = 200 Mc/sec. (the values are shown to fit the conditions of this experiment) we obtain $\Sigma_e^x = 2.6 \times 10^4$. In the actual final result of this experiment $\Sigma_e^x \approx 3.4 \times 10^4$ for $\frac{\Delta g/m}{g/m} \approx 2 \times 10^{-5}$. The difference, of course, is due to the fact that the above work ignores systematic errors.

It is of interest to note what the above accuracy means in terms of stability of Φ, the initial phase. Using the above results we find $\Delta\theta_e = 2.4^o$ so changes in Φ must be small compared to 2.4^o. Also, from Eq. (28), $\Delta Z = 3.3 \times 10^{-2}$ nanosec., so any changes of relative delay or slot phase during the experiment must be small compared with 3.3×10^{-2} nanosec. We investigate this later.

E. Optimum Settings

Working from Eq. (37) it is possible to determine the optimum settings of various parameters so that the fractional error in g/m is a minimum for a given amount of running time. These settings obtained by assuming rather idealized running conditions, are discussed in Appendix 3.

III. DETAILS OF EXPERIMENT

A. Beam

The positive meson beam arrangement is shown in Fig. 4. The 215 Mev/c beam was produced at an internal target of the Berkeley 184" synchrocyclotron. The doublet quadrupole Q 1 produced a rather indistinct image just downstream from the exit of the collimator wheel. The beam was then bent through 25° by the H type bending magnet M1 and finally it was focussed at the muon target by means of Q 2. Both Q 1 and Q 2 were 8" quadrupoles. The muon target was located at the center of the air gap of the H magnet "Orion." This magnet was fitted with a circular pole tip assembly (see below) in order to produce a homogeneous field at the muon target. The target container was a brass box 2" x 2" x 1" with the 1" dimension lying in the beam direction. In the case of the positive meson run the walls of the box were 0.005" thick, and it was filled with bromoform. With the synchrocyclotron operating on the normal short duty cycle (~3%) approximately 5×10^5 mesons/minute were incident on 2" x 2" area at Orion at full beam. Copper absorber then stopped the pions and slowed the muons so that they stopped in the target. The pion to muon ratio was approximately 10. A "second dee" is available for increasing the duty cycle ("stretching the beam") but in this instance we were unable to obtain satisfactory operation of this device so that it became necessary to do the positive muon work of this experiment with 1/4 full beam (because of deadtime requirements, see later) and the short duty cycle. Scaling rates of interest will be given in Section IV(A).

The negative meson beam was obtained simply by reversing all magnets. In this case the brass walls of the muon target were 0.002" thick and the target was filled with distilled water. In this run we were able to operate the second dee satisfactorily and the duty cycle was improved by a factor ~ 20. About 50% of the beam was contained in an initial "spike" and this was gated out. Again, scaling rates of interest will be shown in Section IV(A).

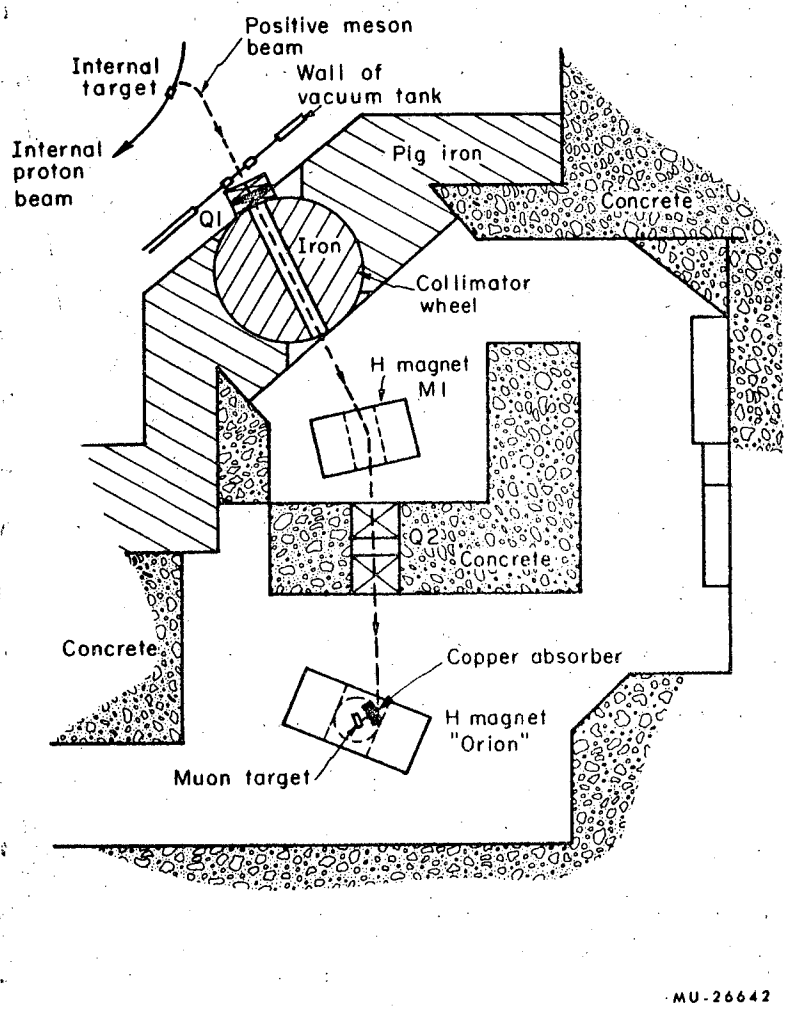

Fig. 4. Beam arrangement in meson cave at Berkeley 184-inch synchrocyclotron. Beam momentum was 215 Mev/c.

B. Counters

The layout of the counters is shown in Figure 5. The sizes of the plastic scintillators were as follows—

Counter	Scintillator Size
1	4" x 5" x 1/2"
2	3" x 4" x 1"
3	2" x 2" x 1/8"
4	4-1/2" x 4-3/4" x 1/8"
5	2" x 2" x 1/8"
6	3" x 4" x 1"
7	3" x 4" x 1/8"

In each case the first dimension stated is that in the plane of Fig. 5. A stopped muon is identified by the event 1 2 3 4 $\overline{5}$ 6 where the usual coincidence-anti-coincidence notation has been used. Similarly the emerging electron is given by the event 5 6 7 $\overline{4}$ 2. Counters 2 and 6 were used as the μ counter and the β counter respectively. A crossover signal was obtained from each, in a manner described in Appendix 4, and went to the appropriate fast mixer unit. Both counters used 1" thick scintillators in order to reduce multiplier phototube timing fluctuations. The use of counter 7 is primarily to ensure a definite lower limit to the output pulse from counter 6 as both fast mixer units had a pulse amplitude range within which they operated. This also is discussed in the above appendix.

R.C.A. Type 6810-A phototubes were used in counters 3, 4, 5 and 7 whereas counters 1, 2 and 6 employed R.C.A. Type 7746 phototubes. The latter phototubes have been shown[26] to have the faster rise time and smaller transit time spread, which are important factors in counters 2 and 6. Light pipes, up to 3 feet in length, were used to remove the phototubes to positions where they could be shielded against the stray field of Orion. At the positions of photo-

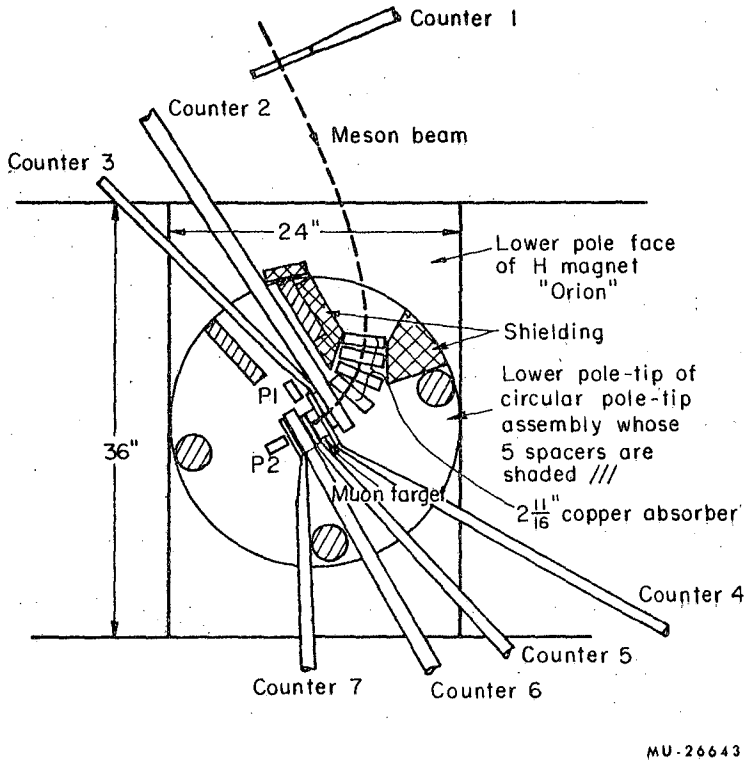

Fig. 5. Counter arrangement in air gap of Orion.

tubes 2 and 6 this stray field amounted to 1 kilogauss when the field at the center of the magnet was 14.7 kilogauss. A system of 3 steel pipes (outer one 5-1/2" O.D., 1/4" wall) and 1 inner mu metal pipe reduced this field to 0.2 gauss. This residual field did not seem to be lowered by adding another inner mu metal pipe, but it was added anyway as a "safety margin." The above residual field could perhaps have a very slight effect on the phototube gain and transit time. Delay curves done with the field on and with the field off showed that any transit time change was < 2 nanosec. In this experiment the magnetic field H is only swept in a range $< 10^{-3}$ H so we see that the above effects, if they exist at all, are constant and cannot enter into the result. The 6810-A phototubes were shielded by 2 steel pipes and 2 mu metal pipes only.

Also shown in Fig. 5 are the two proton resonance probes P1 and P2. The probe P2 provided the signal for the magnetic field regulator to be discussed below. Probe P1 was used for monitoring and exploring the field. It was mounted on a three way travel and when the target was removed it could move in a plane midway between the counters while they were still actually in place.

C. Magnetic Field Regulation and Measurement

The complete system used with Orion is shown in Fig. 6. The circular assembly A A' B' B carried an inner coil system consisting of 1 pair of pickup coils and 5 pairs of trim coils (nos. 1-5). This system of coils was recessed into the inner surfaces of the brass spacer as is indicated. In addition there was an outer coil assembly consisting of 2 pairs of coils wound around the outside of the assembly. One of these outer pairs was used as the correcting coil, the other as a trim coil (no. 6). As is seen from Fig. 6, the main coils of Orion were excited from a 250 K.W. generator equipped with a current regulator whose stability was $\sim$1 part in 10^4. The magnetic field regulator operated independently of this current regulator and had a correction field range of $\pm$ 7 gauss which was ample to cover the current excursions.

The electronic block diagram of the magnetic field regulator and monitor systems is shown in Fig. 7. As is shown, the regulator system has

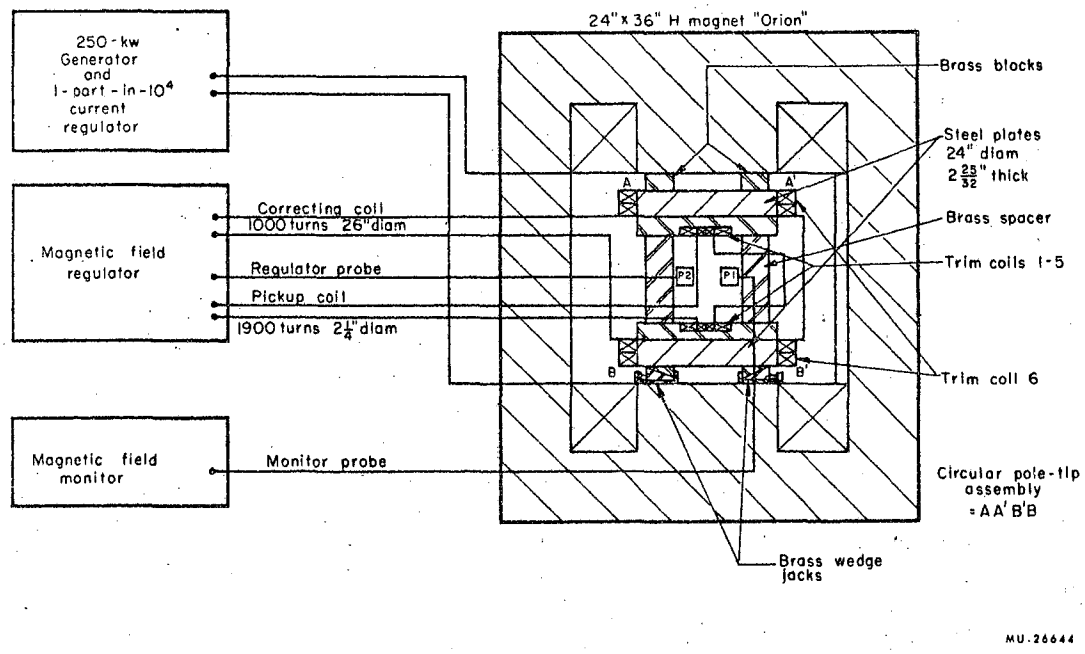

Fig. 6. Block diagram of complete system used with Orion.

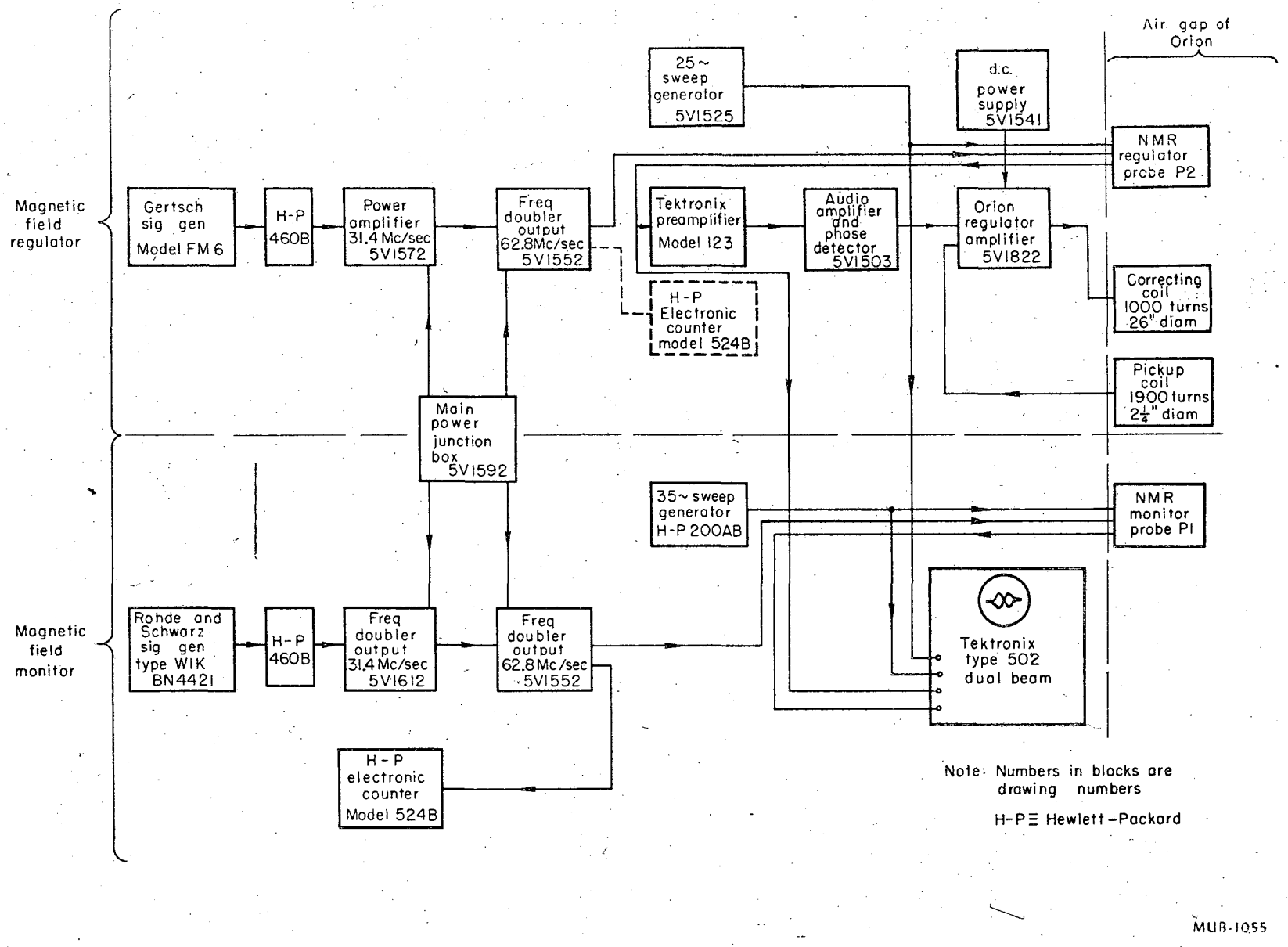

Fig. 7. Block diagram of Orion magnetic field regulator and monitor system.

two loops—a fast loop which receives its error signal from the pickup coil, and a slow loop which receives its error signal from P2 in conjunction with a phase detector. Both probes P1 and P2 were the simple amplitude bridge type described by Thomas et al[27, 28]. We will not discuss the design of the field regulator any further here, since a detailed description has been given elsewhere[29]. Instead we shall merely note that under actual operating conditions the monitor signal P1 seldom showed fluctuations larger than $\pm$ 2 parts in 10^6 about its average position. If the "orion regulator amplifier" unit was allowed ~20 minutes warm up, then the drift of average position seldom exceeded 1 part in 10^6 during a run of 1 hour.

D. Homogeneous Magnetic Field

The overall approach used here was to first produce a magnetic field which has circular symmetry about the central vertical axis. This field was then made homogeneous in the target region with the aid of pairs of circular coils. The pairs of rectangular coils involved in the first step, together with the coils of the second step, may be thought of as "current shims".[30]

The circular pole tip assembly produced much of the desired symmetry. Referring back to Fig. 6 we note that it consists of two outer steel plates (24" dia. and 2- $\frac{25}{32}$ " thick) bolted to an inner brass assembly consisting of two spaced plates (24" dia. 1" thick). The brass assembly was machined as a unit so that its outer surfaces were accurately parallel. The surfaces of each steel plate were also ground accurately parallel. The advantage of this type of pole tip assembly in reducing field non-uniformity associated with reluctance differences along the various flux paths through the magnet has been described by Goodman[31]. As is shown in Fig. 6, the assembly rested on four brass wedge jacks while four brass blocks separated its upper surface from the upper pole tip of Orion. The height of the jacks and the thickness of the blocks were approximately equal.

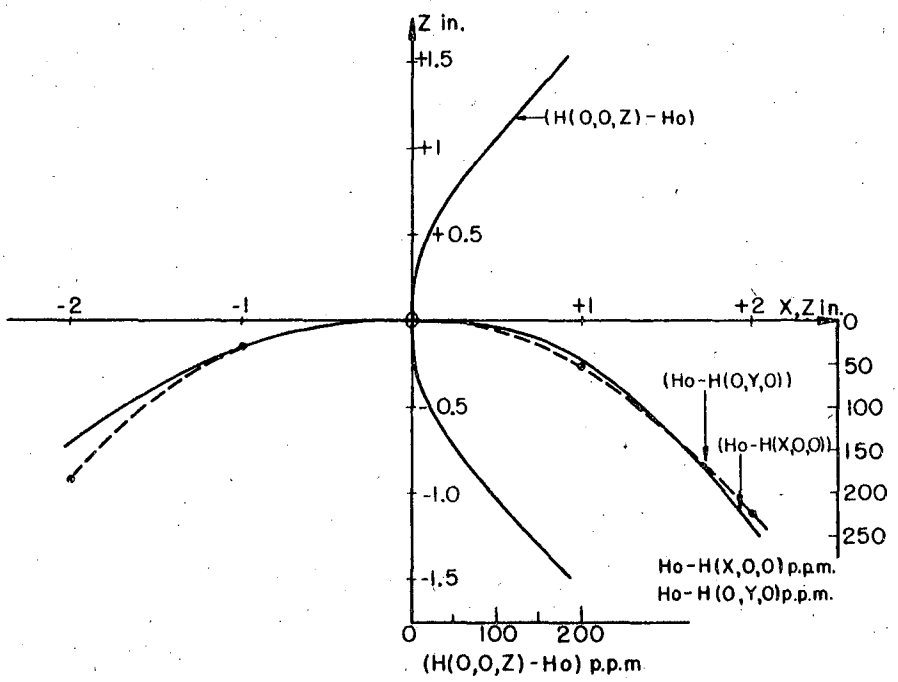

Fig. 8. Superimposed graphs showing magnetic field H along X, Y, Z axes (see Fig. 9) with only trim coil 6 in use. The magnetic field at the origin 0 is H_o = 14.7 kilogauss (1 p.p.m. = 10^{-6} H_o).

The symmetrizing procedure was to first balance (ie. $H(+X,0,0) = H(-X,0,0)$, etc.) the field on the 3 co-ordinate axes X, Y, Z shown on Fig. 9. (Note that the present Z is not to be confused with that of Eq. (28).) The vertical direction was done by a combination of shifting the assembly vertically in the air gap (the reason why the jacks and wedges were not exactly the same thickness) and by applying current in only the lower half of trim coil 6. Fig. 8 shows the resultant symmetrical distribution ($H(0,0,Z) - H_0$) that could be obtained in this way. (H_0 = field at origin 0, = 14.7 kilogauss.) Also shown are the distributions for ($H_0 - H(0,Y,0)$) and ($H_0 - H(X,0,0)$) before they were completely symmetrized. It should be noted that the outer points (relative to 0) are somewhat uncertain owing to the large line widths involved. The X and Y directions were each balanced by applying appropriate loading to the pole tip assembly by means of the wedge jacks. In fact it was necessary to first remove the load from the wedge jacks by means of small hydraulic jacks in order that the former could be adjusted. In this fashion it was possible to obtain, for example on the X axis, $H(X = +1) = H(X= -1)$ with an error of < 3 p.p.m. We use the notation 1 p.p.m. for "one part per million."

Even after the field has been balanced on the three co-ordinate axes as described above we still do not have circular symmetry about the Z axis because $H(X, Y, Z) \neq H(Y, X, Z)$. The rectangular pole tips of Orion cause this trouble. Although it is not shown on Fig. 6, we removed the normal 3" pole tips from Orion in order to get the main exciting coils closer together. This reduced the above effect by a factor of at least 2, the field still falling off faster in the Y direction than in the X direction. By applying current in trim coil 1 so as to obtain a reasonable line width, it was found that in the midplane on a 2" radius circle the field was closely given by $H(\theta) = H(2,0,0) + (50 \text{ p.p.m.}) \cos^2\theta$ where θ is indicated on Fig. 9 (θ not to be confused with Eq. (29)).

This field distribution is that of a pair of rectangular coils[30] (long side of

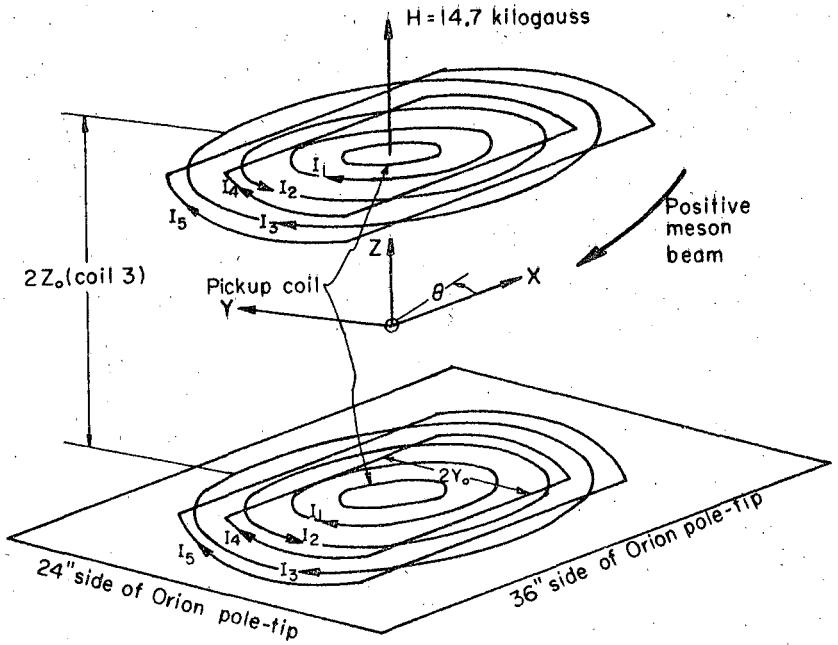

Coil	Total Turns	Dimension	$2Z_o$	I amps	Direction	12 Pin Plug
1	2 x 125	DIA. = 4.6" (average)	5.9"	0.20	-Z	1 - 7
2	2 x 100	" 6.5" "	5.9"	0.32	+Z	2 - 8
3	2 x 125	" 8.6" "	5.9"	1.43	-Z	3 - 9
4	2 x 10	$2Y_o$ = 3.0" "	5.6"	0.50	-Z	4 - 10
5	2 x 40	" 6.2" "	5.6"	1.23	-Z	5 - 11
6 (lower half)	500	DIA. ~~2.6~~ 26" "	—	0.45	-Z	—

Fig. 9. Trim coil arrangement with current directions used for positive meson beam.

rectangle parallel to X axis) as might have been anticipated on the basis of the origin of the trouble. With the aid of the 2 pairs of rectangular coils, the difference between the maximum and minimum field values on this same 2" circle was < 5 p.p.m.

The field now had a high degree of circular symmetry, and trim coils 1, 2 and 3 were adjusted in a rather empirical fashion to achieve the most homogeneous field in a cylinder 2" high ($Z = \pm 1$) and 2" in diameter ($X, Y = \pm 1$). Fine adjustments of the jacks, trim coil 6 and the rectangular coils could then be made with the circular coils near their correct values. In this way it was possible to attain a field in the cylinder such that no points fell outside the limits $H_o \pm 4$ p.p.m. The final trim coil arrangement is as shown in Fig. 9, the various current and field directions are those for the case of the positive muon work. During the actual run there were small long time variations in the above limits. There were also long time variations in the field difference between the monitor probe position and the target center. Both these effects are considered later. It is suspected they had their origin in the fact that the main exciting coils were not rigidly held down and could be heard to "creak" as the magnet came on. Wooden chocks were hammered into the cracks in an effort to reduce this creaking.

Finally we note that when the central field in Orion was set for 31 Mc/sec (half the present value) and a plot made as in Fig. 8, it was apparent that field fall off from the origin to a given point (expressed in p.p.m. of $H_o = 7.4$ kilogauss) was less by a factor of 5 or more. This shows the marked effect of saturation around the pole tip edges as the field is increased. Some work was also done with the pole tip assembly placed in the H magnet "Titan." The X and Y directions, in this case, were found to be almost symmetrical without any current in the rectangular coils. In fact the field along the Y direction fell off slightly less slowly than that in the X direction because Titan has its exciting coils close together. Thus the field of Titan would probably be a little easier to make homogeneous than that of Orion. Titan was

in use at the time of the present run.

E. Electronics

The electronics block diagram is shown in Fig. 10. Details of much of the equipment are given in the Radiation Laboratory Counting Handbook.[32] The basic muon stroboscope of Fig. 2 can be seen in the right of Fig. 10. It is noted that a "μ slow mixer" and a "β slow mixer" have now been placed between the 4 x 4 scaler matrix and the corresponding fast mixer unit in order that certain requirements may be demanded of both the muon and electron events before they may reach the matrix. As can also be seen, both negative and positive signals were taken from the μ counter and the β counter. In each case the negative and positive signals were combined in a crossover network C before being amplified by Hewlett-Packard 460 A and 460 B (linear) amplifiers. This output went to the appropriate fast mixer unit which was operated by the positive, limited part of the amplified crossover pulse. The purpose of the crossover pulse[33,24,34] is to reduce timing jitter associated with pulse amplitude variation. Both the crossover network and the fast mixer units are described in detail in Appendix 4.

The four discriminators following each fast mixer unit have been labelled according to the slow widths that they determine. These discriminator pulses must be delayed (~500 nanosec. of RG63/U) to allow sufficient time for the electronics to decide if the corresponding requirements have been met and, if so, to have the corresponding slow mixer gated "on." If both the muon and electron events do satisfy all the requirements, then the discriminator pulses pass through the slow mixers to the matrix, and for these events the system is identically that of Fig. 2 with one important exception— gates I, II, III, IV no longer determine the interval in which electrons are accepted. Instead this interval ($T_{\not e} - T_{\not e} + C$) is set on gate 1 which gates on the coincidence circuit W4.

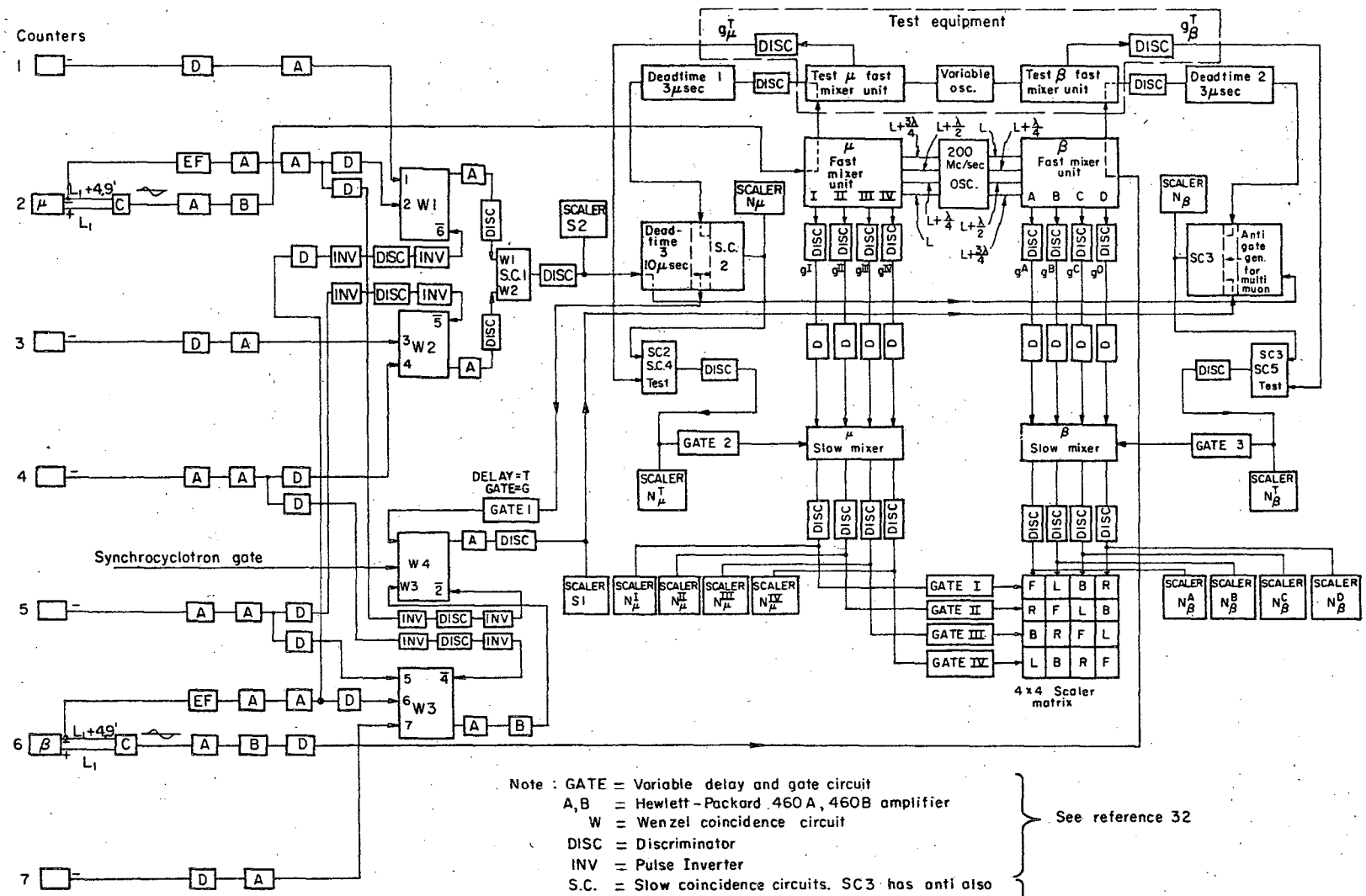

UCRL-10536

Fig. 10. Electronics block diagram.

In this way there is no possibility that a particular channel of the μ fast mixer may be favored and so perhaps introduce systematic error. The gates I, II, III, IV turned on at the 4 x 4 matrix about 0.2 μ sec before any electron could possibly arrive and did not turn off until about 0.2 μ sec after the latest possible electron.

The requirements placed on the muon events are summarized as follows:

a. $1\ 2\ 3\ 4\ \overline{5}\ 6$ — this is done in the usual way with coincidence-anticoincidence circuits W1 and W2. Events meeting this requirement are scaled by S2.

b. no S2 event in the previous 10 μ sec. —imposed by means of deadtime circuit 3 (see Appendix 4) and slow coincidence circuit SC2, in order that gate 1 has sufficient recovery time. All 7 gate units used in this experiment had been reworked so that they were capable of a 40% duty cycle within a 500 μ sec gate which repeated 60 times/second, a more exacting rate requirement than that imposed above.

c. no μ fast mixer input in previous 3 μ sec. — imposed by deadtime circuit 1 and S.C. 2. It was found that the fast mixers would operate continuously at a repetition rate $>$ 1 Mc/sec without deterioration of the output, so the above requirement is modest. If the above three requirements are all satisfied by the muon event, it is scaled by scaler N_{μ} and gate 2 is triggered to gate "on" μ slow mixer. In normal operation the "test" input to slow coincidence circuit 4, S.C. 4, is not required and the test equipment is not in use.

Similarly we may summarize the requirements to be met by the electron event:

(a) $5\ 6\ 7\ \overline{2}\ 4$ — performed with W3 and W4 in the usual manner.

(b) occurs during interval $T_{\not e}$ — $(T_{\not e} + G)$ after the muon arrival— this is done by feeding the gate 1 into one of the normal clipping line plugs of W4.

The gate is then direct coupled, with appropriate attenuation, to one of the actual coincidence diodes of the coincidence circuit. The synchrocyclotron gate was similarly introduced into W4, although it is probably not too important that this be done. Events satisfying (a) and (b) are scaled by S1.

(c) no β fast mixer input during previous 3 μ sec— imposed by deadtime circuit 2 and S.C. 3 for same reasons as in muon case.

(d) no other S2 event (stopped muon) occurs in the time interval between the triggering of gate 1 and the arrival of an electron during the gate — this requirement is made in order to reduce the probability that an electron gets assigned to the incorrect parent muon. Such occurrences probably could not introduce systematic error, but they would result in a lowering of the asymmetry A as seen by the stroboscope. From Eq. (37) we are obviously interested in having A as large as possible. Notice that although the following S2 event (or events), coming in the above time interval, could not trigger the gate 1 again (because of deadtime circuit 3), it is still necessary to "shut down" the electron detection initiated by the original S2 event. The electronics which performs this operation is called the "anti gate generator for multi muon events." On the arrival of the following S2 event, a 10 μ sec anti coincidence gate is sent to SC 3. The arrival of yet more S2 events within this 10 μ sec gate extends the gate 10 μ sec beyond the last arrival. The gate is capable of being extended indefinitely. The complete details of this system are given in Appendix 4.

Also shown in Fig. 10 is the equipment used to test the muon stroboscope. It is seen that after leaving the corresponding fast mixer units, both the μ counter and β counter signals went to test fast mixer units. Each test fast mixer unit contained just one mixing circuit, which was identical in design with the four mixing circuits contained in the normal fast mixer units. The two test units were driven from a variable frequency oscillator which operated in a range near 200 Mc/sec and was stable in frequency to 1 part in 10^6 for a one

hour run at a given setting in the range. The 200 Mc/sec oscillator and the variable oscillator were entirely independent of each other. During test runs, "test" inputs were required in both S.C.4 and S.C.5. Thus, for example, only the muons arriving in one of $g^{I} - g^{IV}$ and in g^{T}_{μ} were able to get to the 4 x 4 matrix. The slot width g^{T}_{μ} is determined by the ratio N^{T}_{μ} / N_{μ}. It is shown in Appendix 5 that the above test arrangement effectively presents to the muon stroboscope a muon precessing with the frequency set on the variable oscillator. It is thus possible to check if indeed the early and late phase plots cross when the frequencies of the two oscillators are equal.

F. Experimental Procedure

After the initial beam and electronics tune-up procedures had been completed, checks were run on various conditions which were relevant to the stroboscope operation. The decay curve for positive muons stopping in bromoform was traced out to delays $T_{\frac{1}{2}}$, as long as 6 μ sec (G = 2 μ sec) to investigate background conditions. Similarly a slow precession (1 Mc/sec) experiment was performed with positive muons stopping in bromoform so that the asymmetry coefficient obtained could be compared with that obtained at 200 Mc/sec with the stroboscope. Also the effect of background was examined by running the slow precession experiment at delays T as long as 6 μ sec (G = 0.2 μ sec). The output pulse heights from the μ counter and β counter were checked to verify that they fell in the operation range of the fast mixer. Checks were then run with the muon stroboscope in operation under "beam through" conditions, in which $\bar{2}$, $\bar{4}$, $\bar{5}$, $\bar{6}$ are all removed (also the range and the target) and 7 was required in W1 rather than W3. Delay curves were run by varying the delay Z in the signal line of the crossover signal coming from the β counter, and recording the matrix counts. These curves were repeated two days later to check for timing drifts. A typical curve is shown in the discussion of the fast mixer circuit in Appendix 4.

Checks were also made under "beam through" conditions to determine if the stroboscope showed any apparent phase angle change as the output voltage of the 200 Mc/sec oscillator, the voltage to counters 2 and 6, and the various slot widths were deliberately varied about their normal values. The meaning of the phase angle under beam through condition is discussed at the end of Appendix 5.

In the positive muon run the resonance was expected[21] near a monitor probe proton frequency f_p^m = 62.77 Mc/sec so the range within 30 Kc/sec of this frequency was swept in 10 Kc/sec steps. As noted earlier G = 2.5 μ sec was used, and phase plots were obtained for $T_{\not\equiv}$ = 0.2, 1.5 and 3.1 μ sec. in an effort to check that there was no systematic dependence of resonance frequency on the value of $T_{\not\equiv}$. These phase plots were obtained with the β counter delay normal, i.e. Z = 0, and with an extra 2.51 $\pm$ 0.01 nanosec introduced, i.e. Z = 2.51 $\pm$ 0.01. [The author is indebted to Mr. C. Kerns for the construction and calibration of this delay.] For most of the data taken, the following is a typical sequence—

(a) f_p^m = 62.75 Mc/sec, Z = 0 nanosec

(b) = 62.79 Mc/sec, Z = 0 nanosec

(c) = 62.75 Mc/sec, Z = 2.51 nanosec

(d) = 62.79 Mc/sec, Z = 2.51 nanosec

In this fashion it was hoped to minimize the effects of any drifts which could perhaps be present. About 20% of the final data was the combined results of runs spaced several days apart. Such runs allowed checks for drift to be made. During the data taking frequent checks were made on —

(a) The high voltage supplied to the μ and β counters.

(b) The power supply voltage of the fast mixer units.

(c) Currents in the 6 trim coils.

(d) Delay T and gate G.

(e) Internal check of frequency meter.

(f) Temperature in air cooled racks in which fast mixer units were mounted.

(g) Output voltage of 200 Mc/sec oscillator. Checks (a), (b) and (g) were made with the aid of a digital voltmeter (Non-Linear Systems, Inc. Model V64).

At less frequent intervals checks were also made on —

(a) Frequency of the 200 Mc/sec oscillator-checked several times.

(b) Field difference between the monitor probe position and the target center— checked 8 times during the run.

(c) The field distribution in target region was checked before the run and twice during the run. A 1" x 1" x 1" block of carbon was used to determine the relative weights for each quarter of the target.

At the conclusion of the positive muon run the target was emptied and background phase plots were run for just a few frequency settings at each value of T, and for Z = 0 only

For the negative muon run with water, the resonance was expected[21] near f_p^m = 62.83 Mc/sec. The range within 60 Kc/sec of this frequency was swept in 30 Kc steps (one point was also taken at 62.74 Mc/sec). The coarser steps were used because of the very small asymmetry in this run. Phase plots were made for G = 2.5 μ sec and T = 0.2 μ sec and 2.1 μ sec, the plots being obtained only for Z = 0. The checks made here were the same as in the positive muon run. Since no effort was made to finely readjust the 6 trim coils when the field of Orion and the trim coil currents were all reversed, the field is not as[50] homogeneous in this run. However, this does not matter as the statistical accuracy is much less for the negative muon run. At the conclusion of the run, the target was

emptied and just one background run made for each of T = 0.2 and 2.1 μ sec, the combined low asymmetry and low background rate making it impossible to obtain background phase plots.

During the negative muon run (because of the high rate) the test equipment was set up and phase curves were obtained for T = 0.2, and 3.1 μ sec for each delay $Z'^{\mu} = 0$ and $Z'^{\mu} = 2.27 \pm 0.01$ nanosec where Z'^{μ} is the additional delay inserted between the μ fast mixer unit and the test μ fast mixer unit. The meaning of the test run phase angle, θ^T, has been discussed in Appendix 5 where it is shown that θ^T is the weighted average phase difference between the muon stroboscope and the first harmonic of $F_{av}(t'')$ for the group of electrons observed. $F_{av}(t'')$ is the average probability that an electron signal may get through test β fast mixer at time t" after muon signal came through the test μ fast mixer. The average is taken over all possible arrival times, x', of the muon signal in the slot g_{μ}^{T} of the test μ fast mixer.

IV RESULTS OF EXPERIMENT

A. Typical Counting Rates

These have been summarized in Table I for both the positive and negative muon runs. In the positive meson run it is seen that the stopped muon rate dropped by a factor of 4 on emptying the target and apparently most of the residual rate is due to scattering out of muons, since removal of the target does not have much effect on this rate. From the lower line of Table I it is apparent that the rates during the negative meson run were more than 10 times those of the positive run. The maximum allowable rate (determined by deadtime requirements) for the duty cycle of the negative run was only a little higher than the rate of Table I. It is apparent that removal of the water from the target does not have a large effect on the stopped muon rate. Similarly removal of the target has little effect. The large stopped muon background probably is due to electrons in the negative beam as is discussed in IV(D). It should be noted that the "target-empty" and "target out" rates of Table I may have an error of 10% due to normalization. The matrix counting rate with empty target, and for each setting of T that was used, will be discussed below.

B. Initial Checks

Study of the positive muon decay curve showed that less than 10% background was encountered for delays T as long as 6 μ sec, but the background increased rapidly thereafter. The slow precession experiment for positive muons stopping in bromoform gave an uncorrected ratio

$$\frac{\text{Peak} - \text{Valley}}{\text{Peak} + \text{Valley}} = 0.22$$

with an error of $\sim$ 10%, and this ratio also did not change appreciably for delays T as long as 6 μ sec. Photographs of the outputs of the μ

and β counters (with Orion field off) showed that they were operating in the light level range 0.9 to 1.6. This range would be extended to somewhat higher values with the field on (curvature of the electron orbits) but it was clearly within the range for which the fast mixer units were designed.

The results of delay curve work done under "beam through" conditions showed that over a two day period any timing drift was $\leq 1/10$" of delay (1" = 0.169 nanosec.). Because the above period was only about half that of the positive run, the above drift was arbitrarily doubled to arrive at (from Eq. (28)) an estimated phase drift $\Phi_D \leq 2.2^\circ$. Variation of the output voltage of the 200 Mc/sec oscillator by +0.1V and -0.08V about its normal value (2.2 V rms) produced phase changes (end of Appendix 5) of $< 1.5^\circ$. During the experiment this voltage was always within 0.01 V of its normal value. The voltage to the μ counter and β counter was lowered 100 V from its normal value (2200 V) to produce a phase change $< 3^\circ$. This voltage was always within 4 V of its normal value during the actual experimental runs. The widths of the various slots were varied $\pm$ 20% about their normal values ($\sim \frac{\tau_e}{6}$) in order to check the effect of slot width on phase angle. By simply using Eq. (11) it was found that phase angle shifts $\leq 1^\circ$ were produced. Use of Eq. (29) reduced these shifts. Thus the system is to a large degree "self balancing" as regards slot width variations, even with the strongly peaked "beam through" distribution. This would explain how the actual experimental phase angles obtained using Eq. (29) were never significantly different from those obtained from Eq. (11).

C. Positive Muon Run

The results of full target runs are shown in Table II and have

been corrected for slot width by means of Eq. (29). In typical runs the asymmetry parameter obtained was $A = -0.22 \pm 0.02$ which indicates a value not significantly different from that obtained in the slow precession experiment. This shows that the overall timing jitter present is < 2.5 nanosec as was expected from the light pulser and "beam through" tests. The results in Table II represent about 5 days of running under the positive beam conditions.

It is also necessary to estimate the error in proton frequency f_p during the experiment. We have the relation

$$f_p(\vec{r}, t) = f_p^m(t) + f_p^{(1)}(t) + f_p^{(2)}(\vec{r}, t) \qquad (38)$$

where

$f_p^m(t)$ = monitor probe (P1) proton frequency at time t

$f_p^{(1)}(t)$ = "transfer field" at time t, i.e. the increase in proton frequency as the probe P1 is moved from the monitor position to the center of the target.

$f_p^{(2)}(\vec{r}, t)$ = increase in proton frequency as the probe P1 is moved from the center of the target to point $\vec{r}$, at time t. The quantities on the right hand side of Eq. (38) are the actual measured quantities. The time dependence will be taken into consideration by merely increasing the errors appropriately. Also we take $f_p^{(2)}(\vec{r}, t) = 0$ and assign an error to cover magnetic field variation in the target region for all t. With this scheme we have then

$$f_p = f_p^m + f_p^{(1)} \qquad (39)$$

with $f_p^{(1)}$ being the constant transfer field. The contributions to the errors in each of the quantities f_p^m, $f_p^{(1)}$ and $f_p^{(2)}$ are now listed

(again, we use the notation 1 p.p.m. = 10^{-6} f_p):

(A) f_p^m

(1) Time stability of the magnetic field. As noted in Section III C there were fluctuations which seldom exceeded ± 2 p.p.m. together with a drift which seldom exceeded ± 1 p.p.m. during a typical run of one hour. It was assumed these effects were independent and so an error of $\pm\sqrt{5}$ p.p.m. was assigned for time stability.

(2) Error in frequency measurement. The Hewlett Packard Electronic Counter Model 524 B used in this experiment was the one which is used with the frequency standard at this laboratory. During the run it was checked against another counter of the same type and the two agreed to closer than 2 p.p.m. (the second counter was then checked and found to be slightly out of adjustment). At the end of the run it was rechecked with the frequency standard. We will use the very conservative accuracy estimate of ± 2 p.p.m. here.

(3) Shift[36] of the proton resonance line of Pl due to the addition of $Fe(NO_3)_3$ to the water sample. The simple shape was cylindrical (height = 1.5 diameter) and was formed by drilling out a polystyrene rod. Samples of the same shape, but with different concentrations of $Fe(NO_3)_3$, were used to obtain a graph of resonance line frequency against concentration, at the fixed magnetic field of the experiment. This graph was extrapolated to zero concentration and it was concluded that, for the 0.1N solution used, the shift was $\leqslant$ + 1 p.p.m. This was taken into consideration by allowing a further error of ± 1 p.p.m.

Combining (1) (2) and (3) above we obtain

$$f_p^m = \sqrt{10} \text{ p.p.m.}$$

(B) $f_p^{(1)} \pm \Delta f_p^{(1)}$

As noted in Section III D there were long term variations associated with the transfer field and it was suspected that they may be associated with slight movements of the main exciting coils. It was found that setting $f_p^{(1)} = 0$ with $\Delta f_p^{(1)} = \pm 3$ p.p.m. covered the extreme deviations observed during the positive muon run.

(C) $\Delta f_p^{(2)}$

The extreme deviations from the central field were determined for each quarter of the target. These deviations were chosen to include long term variations. Since the statistical accuracy of this experiment was much less than the field deviations, the field was checked only three times, for the positive muon run, and a rather coarse grid was used. The extreme deviations of each quarter of the target were then weighted according to the 1" x 1" x 1" carbon block data. The results were:

measured extremes $\pm$ 5 p.p.m.

weighted extremes $\pm$ 4 p.p.m.

From (A) (B) and (C) we arrive at the final result

$$f_p = f_p^m$$

$$f_p = \sqrt{59} \text{ p.p.m.} \qquad (40)$$

where (B) and (C) errors have been combined in the most pessimistic fashion as there is a possibility of some correlation between them.

The frequency of the 200 Mc/sec oscillator was checked only a few times during the positive run since its accuracy was very much better than the statistical accuracy of the experiment. The result of these checks was

$$f_o = 199.82615 \pm 0.00010 \text{ Mc/sec} \qquad (41)$$

Finally for the positive run, we show in Table III the data obtained from the empty target runs. Only the β counter delay Z = 0 was run since the low counting rate excluded the possibility of accurate phase measurements and comparisons. The average asymmetry of this "background" was $A_b = -0.12 \pm .03$. It has meaning to average the values of A_b in Table III as we recall from Section II B that A decreases by only 8% for $(f_p - f_p(res)) = 30$ kc/sec. In the final column of Table III are shown the ratios of total matrix counting rates for full target and empty target (0.005" brass walls). This ratio was measured for each value of T . The matrix counting rate was reduced by a further factor of 2 when the empty target was removed. Part of the matrix counting rate, with the target out, would be due to muons stopping in the .002" aluminum wrapping of counters 4, 5 and 6.

D. Negative Muon Run

The β counter delay was left at Z = 0 throughout this run as the low decay asymmetry makes accurate phase comparisons impossible. Table IV shows the results obtained for the full target (H_2O) runs. These results represent ~ 1 day of running under the negative muon beam conditions. The shorter delay T = 2.1 μ sec was used in this case so that the error of each phase angle measurement could be reduced to a reasonable value in the running time remaining (Eq. (36)). For comparison with the positive run, the asymmetry coefficient A was calculated in the present case from the results for T = 0.2 μ sec and $f_p^m = 62.80$, 62.83, and 62.86 Mc/sec (these results contained more than half the total statistics). The average value obtained was $A = -(1.0 \pm 0.4) \times 10^{-2}$ as is shown (recall from Section II B, and above, that it is reasonable to take the present average).

This value contains no corrections (other than the slot width correction of the counts). It appears low when compared to the corrected value -0.043 ± 0.005 obtained by Ignatenko et al.[13] The difference may not immediately be assumed to have been caused by the stroboscope since it gave a good asymmetry in the positive muon run. Unfortunately we did not perform a slow precession experiment for negative mesons in water and so cannot make the direct comparison as we could for the positive run. Also shown in Table IV are the ratios of total matrix counting rates for full target and the empty target (0.002" brass walls). These ratios show that although, for the negative muon run, there was little effect on the stopped muon rate (S2) on emptying the target, there is a large effect on the total matrix rate. This effect is even slightly more pronounced than in the positive run, as might be expected since the target used here has thinner walls. This indicates that the large background present in S2 rate is due to stable particles (because we see no large number of extra decays). It is probably due to scattering out of electrons, since experiments[37,38] indicate a comparatively large electron contamination in negative meson beams. As in the positive meson run, the removal of the empty target decreased the matrix counting rate by a factor of ~ 2 in the present case.

Because the statistical accuracy of the present run is much worse than the positive run, no great effort was made to make the magnetic field very homogeneous again after all the currents had been reversed. Also we did not both to determine the weighting factors of each quarter of the target. Thus some of the errors are larger in the present case. The errors are as follows:

(A) $f_p^m = \sqrt{10}$ p.p.m.

$$(B)\ f_p^{(1)} \pm \Delta f_p^{(1)} = -(4 \pm 5)\ \text{p.p.m.}$$

$$(C)\ \Delta f_p^{(2)} = \pm 6\ \text{p.p.m.}$$

Thus we have

$$f_p = f_p^m - 4\ \text{p.p.m.}$$
$$\Delta f_p = \sqrt{131}\ \text{p.p.m.} \qquad (42)$$

where again we have combined (B) and (C) in the most pessimistic fashion.

The 200 Mc/sec oscillator was again monitored during the negative run. Unfortunately, it was damaged during this run and when repaired it stabilized at a slightly different frequency. Thus it was necessary to assign a frequency and error which "bridged" the gap. The result was

$$f_o = 199.8275 \pm 0.0014\ \text{Mc/sec} \quad . \qquad (43)$$

Even this error is $< 1 \times 10^{-5}\ f_o$ and so is very much less than the present statistical error.

E. Simulated Muon Test Run

Table V shows the results of this test. There was sufficient time to run only 3 points on each phase "plot." The range of ± 100 Kc/sec for the frequency of the variable oscillator corresponds roughly to the proton frequency range of ± 30 Kc/sec used in the positive run. The variable frequency oscillator was stable to ± 1 p.p.m. at a given frequency setting. The value of the frequency, f_o, of the 200 Mc/sec oscillator as shown in Table V is that at which it stabilized after being repaired. As can be seen, it was stable to ± 1/2 p.p.m. throughout this test. The magnetic field was held at a proton frequency of 62.83 Mc/sec throughout this run. As noted in Table IV, the value of A for negative muons stopping

in water was only -1×10^{-2} and so we note that its affect on the numbers shown in Table V is $<$ the statistical errors. Thus we may consider that the negative muons decay isotropically in this run. In the last two columns of the Table we show the calculated phase angle θ^T (Eq. (29)) and its error $\Delta\theta^T$ (Eq. (35)). The particular values of θ^T shown in Table V were obtained by arbitrarily assuming the "asymmetry coefficient" to be negative in the test run (just as it is for the actual muon decay asymmetry).

V. CALCULATIONS

A. Complete Expression for Equivalent Phase Error in Late-Early Phase Difference

Eq. (35) of Section II D gave only the statistical error that is to be assigned to a given phase measurement. Here we wish to determine the complete error which must be assigned to a determination of the phase difference. In order to correct for background we must rewrite Eq. (29) as follows

$$\tan \theta_o = \frac{R^x - L^x - (R_b^x - L_b^x)}{F^x - B^x - (F_b^x - B_b^x)} = \frac{R_o - L_o}{F_o - B_o} \tag{44}$$

where the counts R^x etc. refer to full target results and R_b^x etc. refer to empty target results. From Eq. (29), Eq. (30) and the fact that the actual stroboscope always satisfied the symmetric stroboscope relation $R^x + L^x = F^x + B^x$, we have

$$\tan \theta_o = \frac{R^x - L^x - (\Sigma^x/2) r A_b \sin \theta_b}{F^x - B^x - (\Sigma^x/2) r A_b \cos \theta_b} \tag{45}$$

with

$$\tan \theta_b = \frac{R_b^x - L_b^x}{F_b^x - B_b^x}, \quad r = \Sigma_b^x / \Sigma^x \quad \text{and} \quad A_b = \frac{2\sqrt{(R_b^x - L_b^x)^2 + (F_b^x - B_b^x)^2}}{\Sigma_b^x}.$$

For the purposes of error estimation it is necessary to rewrite Eq. (27) in the more general form

$$f = f_o + \frac{(\theta_o)_1 - (\theta_o)_e + \bar{\Phi}_e - \bar{\Phi}_1}{2\pi \left[T_1 - T_e + \bar{G}_1 - \bar{G}_e \right]} \tag{46}$$

In this way we obtain the following expression for the square of the error in the muon frequency

$$\Delta^2 f = \Delta^2 f_o + \frac{\Delta^2(\theta_o)_1 + \Delta^2(\theta_o)_e + \Phi_D^2}{\left[2\pi (T_1 - T_e)\right]^2} + \frac{\left[(\theta_o)_1 - (\theta_o)_e\right]^2}{\left[2\pi (T_1 - T_e)^2\right]^2}$$

$$\times \left[\Delta^2 T_e + \Delta^2 T_1 + 2\Delta^2 \bar{G}\right] \qquad (47)$$

where use has been made of the nominal relations $G_e = G_1 = G$ and $\Phi_e = \Phi_1 = \Phi$. The errors which have been considered in Eq. (47) are as follows:

$\Delta \theta_o$ — the statistical error in the phase angle expression after correction for background, i.e. Eq. (45). This error is analogous to that of Eq. (35) where no background was considered.

Φ_D — the possible drift in initial phase of the stroboscope during the run, i.e. we allow $|\Phi_e - \Phi_1| \leq \Phi_D$.

$\Delta T_e, \Delta T_1, \Delta G$ — these are variations of Gate 1 during the runs. These variations could be caused by setting errors and by jitter. We note that the effect of these errors on the experiment can always be made arbitrarily small by operating in a sufficiently narrow range about the resonance frequency. In the present experiment only the errors of the outermost phase determinations are increased by a few percent due to variations of Gate 1. The possible variations were estimated as $\left[\Delta^2 T + \Delta^2 \bar{G}\right]^{1/2} = \pm 3\% \left[T + \bar{G}\right]$ for both early and late gates. Thus we have from Eq. (47)

$$\Delta^2 f = \Delta^2 f_o + \frac{\Delta^2(\theta_o)_1 + \Delta^2(\theta_o)_e + \Phi_D^2 + 9 \times 10^{-4}\left[((\theta_o)_e - \Phi)^2 + ((\theta_o)_1 - \Phi)^2\right]}{\left[2\pi (T_1 - T_e)\right]^2} \qquad (48)$$

where Φ need be known only approximately in order to estimate the last term in the numerator.

It is now necessary to determine $\Delta\theta_o$ from Eq. (45). First we will consider the error contributions due to R^x, L^x, F^x and B^x. A typical derivative is as follows

$$\frac{\partial \theta_o}{\partial R^x} = \frac{(F_o - B_o) + \frac{1}{4}\sum_o^x A_o A_b \, r \sin(\theta_o - \theta_b)}{(F_o - B_o)^2 \sec^2 \theta_o} \tag{49}$$

with $\sum_o^x = \sum^x (1-r)$ and we have used Eqs. (29), (30) and the symmetric stroboscope relation $R_o + L_o = F_o + B_o$ in the second term of the numerator, which is usually a much smaller term (neglecting signs) than $(F_o - B_o)$. Expressions similar in form to Eq. (49) may be obtained for the other 3 contributions. Combining all 4 terms we obtain the following expression for the square of the error in θ_o due to the statistics of the <u>full</u> target data

$$\Delta^2 \theta_o^f = \left(\frac{\partial \theta_o}{\partial R^x}\right)^2 \Delta^2 R^x + \left(\frac{\partial \theta_o}{\partial L^x}\right)^2 \Delta^2 L^x + \left(\frac{\partial \theta_o}{\partial F^x}\right)^2 \Delta^2 F^x + \left(\frac{\partial \theta_o}{\partial B^x}\right)^2 \Delta^2 B^x$$

$$= \frac{(1.20)^2 \left[(F_o - B_o)^2 (R^x + L^x) + (R_o - L_o)^2 (F^x + B^x)\right]}{(F_o - B_o)^4 \sec^4 \theta_o} \,. \tag{50}$$

The numerical factor in the numerator is from Eq. (34) as usual. The term of next highest order in the numerator of Eq. (50), and which has been neglected, is

$$\frac{(1.20)^2}{2} \sum_o^x r \, A_o A_b \left[(F_o - B_o)(R^x - L^x) + (R_o - L_o)(B^x - F^x)\right] \sin(\theta_o - \theta_b) \,.$$

An upper limit for this term is obtained by setting $\sin(\theta_o - \theta_b) = 1$, and is given by $(1.20)^2 \left(\frac{\sum_o^x}{2}\right)^2 r \, A_o^3 A_b \sum^x$, where the symmetric stroboscope relation $R_o + L_o = F_o + B_o$ has been used. By also using this relation in the numerator of Eq. (50), it may be shown that the numerator of Eq. (50) is $\gg$ the above upper limit. Thus the omission of the above term from Eq. (50) is justified. We will write Eq. (50) in the more convenient form

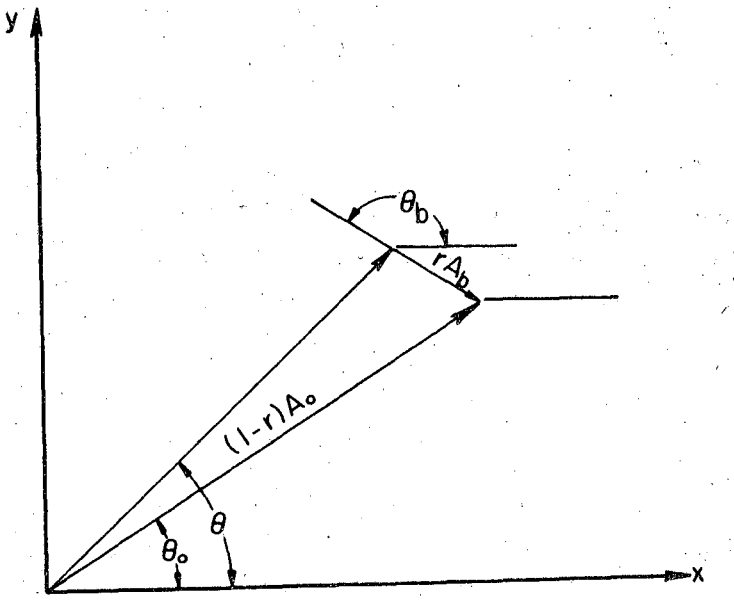

MU-26647

$\tan \theta = \frac{R^x - L^x}{F^x - B^x}$ where θ is the full target phase angle without background correction.

$\tan \theta_b = \frac{R_b^x - L_b^x}{F_b^x - B_b^x}$ where θ_b is the phase angle associated with the background (i.e. empty target). A_b is the corresponding asymmetry.

θ_o = background corrected phase angle.

A_b = background corrected asymmetry.

Fig. 11. Vector diagram of background corrections.

$$\Delta\theta_o^f = \frac{1.20\sqrt{(R^x + L^x) + (F^x + B^x)\tan^2\theta_o}}{(F_o - B_o)\sec^2\theta_o} \quad . \tag{51}$$

The contributions of the background errors (target empty) to $\Delta\theta_o$ will be considered next. From Eq. (45) we obtain, using $R_o + L_o = F_o + B_o$, Eq. (29) and Eq. (30)

$$\Delta^2\theta_o^b = \left[\frac{r\,A_b}{(1-r)A_o}\right]^2 \left[\left\{\left(\frac{\Delta r}{r}\right)^2 + \left(\frac{\Delta A_b}{A_b}\right)^2\right\}\sin^2(\theta_o-\theta_b) + \Delta^2\theta_b\cos^2(\theta_o-\theta_b)\right] \tag{52}$$

The significance of Eq. (52) is easily seen on the vector diagram of Fig. 11 in which the background is represented by a vector $r\,A_b\,e^{i\theta_b}$ and the background corrected data by $(1-r)A_o e^{i\theta_o}$. The sum of these two vectors gives the full target vector, as is stated by Eq. (45). Finally the complete expression for the error in θ_o is obtained from Eq. (51) and Eq. (52) as

$$\Delta^2\theta_o = \Delta^2\theta_o^f + \Delta^2\theta_o^b \tag{53}$$

From Eq. (48) and Eq. (53) we obtain the complete expression for the equivalent error to be assigned to a determination of the phase difference

$$\Delta^2\left[(\theta_o)_1 - (\theta_o)_e\right] = \Delta^2(\theta_o^f)_e + \Delta^2(\theta_o^f)_1 + \Delta^2(\theta_o^b)_e + \Delta^2(\theta_o^b)_1 + \Phi_D^2$$
$$+ 9\times10^{-4}\left[((\theta_o)_e - \Phi)^2 + ((\theta_o)_1 - \Phi)^2\right] . \tag{54}$$

Actually there will be some correlation between errors $\Delta(\theta_o^b)_e$ and $\Delta(\theta_o^b)_1$ since they have the common error ΔA_b. However it may be shown that Eq. (54) is actually a conservative statement of the accuracy because of the fact that it is the error in the difference between $(\theta_o)_1$ and $(\theta_o)_e$ which is involved.

B. Combination of Results in Positive Muon Run

The use of Eq. (48) in the error calculations is equivalent to assuming the gradients of our late-early phase difference plots, i.e.

$$\frac{d}{df_p^m}\left[(\theta_o)_l - (\theta_o)_e\right] = 2\pi (T_l - T_e)\ \frac{f}{f_p} \qquad (55)$$

where we have recalled that we actually plot $(\theta_o)_l - (\theta_o)_e$ versus f_p^m, and Eq. (39) has been used. In the positive muon work of the present experiment, a more general procedure will be used. By the method of least squares,[39] we will fit the straight lines

$$(\theta_o)_l - (\theta_o)_e = a_1 + a_2 X \qquad (56)$$

where $X = 100\ (f_p^m - 62.77)$ and f_p^m is Mc/sec units. The values of a_2 so obtained may be compared with the values calculated from Eq. (55), as a further check of our stroboscope theory.

The complete procedure involved in the combination of the positive muon results will now be outlined. It is designed to take into consideration, to a good approximation, the correlations which exist among some of the errors.

(1) The corrected phase angles θ_o, and the corresponding errors $\Delta\theta_o^f$ due to full target statistics, were calculated and are shown in Table VI. The relevant equations are Eq. (45) and Eq. (51).

(2) The 6 phase difference sets were calculated and the straight line of Eq. (56) was fitted to each set. In this work the square of the error assigned to each phase difference measurement was given by

$$\Delta^2 (\theta_o^f)_l + \Delta^2 (\theta_o^f)_e + 9 \times 10^{-4}\left[((\theta_o)_l - \Phi)^2 + ((\theta_o)_e - \Phi)^2\right.$$

after Eq. (54). This is a very good approximation because the last term is

small and so the fact that it does not represent a random error is of no importance. The results of straight line fitting are given in Table VII where a_2 is expressed in degrees per 10 Kc/sec (i.e. degrees per unit X). We note that the experimental gradient agrees quite reasonably with the calculated value. The last two columns of the table show $X_z(res)$ and $\Delta X_z(res)$ where the subscript z is added to denote the X value appropriate to β counter delay z. We have from Eq. (27) and Eq. (56)

$$X_z(res) = -\frac{a_1}{a_2} \tag{57}$$

$$\Delta X_z(res) = |X_z(res)| \sqrt{\left(\frac{a_1}{a_1}\right)^2 + \left(\frac{a_2}{a_2}\right)^2} \quad . \tag{58}$$

In Fig. 12 and Fig. 13 we show graphs of the experimental phase difference points and their errors (as assigned above and therefore essentially $\sqrt{\Delta^2(\theta_o^f)_1 + \Delta^2(\theta_o^f)_e}$). The errors $\Delta X_z(res)$ are also shown horizontally near the X axis. By inspection of the graphs for a given Z value it is seen that to the present experimental accuracy there is no dependence of resonance frequency on the values of T which are involved. This is as expected. The three results for each Z value were then combined considering only the errors $\Delta X_z(res)$. The two combined results had a χ^2 probability of 0.03. This is low, but it will appear below (Table IX columns 3 and 6) that the final errors are ~ 50% greater than those obtained from $\Delta X_z(res)$ alone. Thus the two combined results are reasonably consistent.

(3) The background phase angle data was fitted with straight lines whose slope was obtained from Eq. (21) and Eq. (23). This is justified by the notes below Eq. (23), and the good agreement in slope shown in Table VII, since the statistical error is large in the background run. The resultant values of $(\theta_o - \theta_b)$ and $\Delta\theta_b$ are shown in Table VIII. Also shown are values of A_o obtained by averaging several runs for both Z = 0 and Z = 2.51 ± 0.01 nanosec at each delay T. In the last column of Table VIII are shown the phase angle errors due to background, as given by Eq.

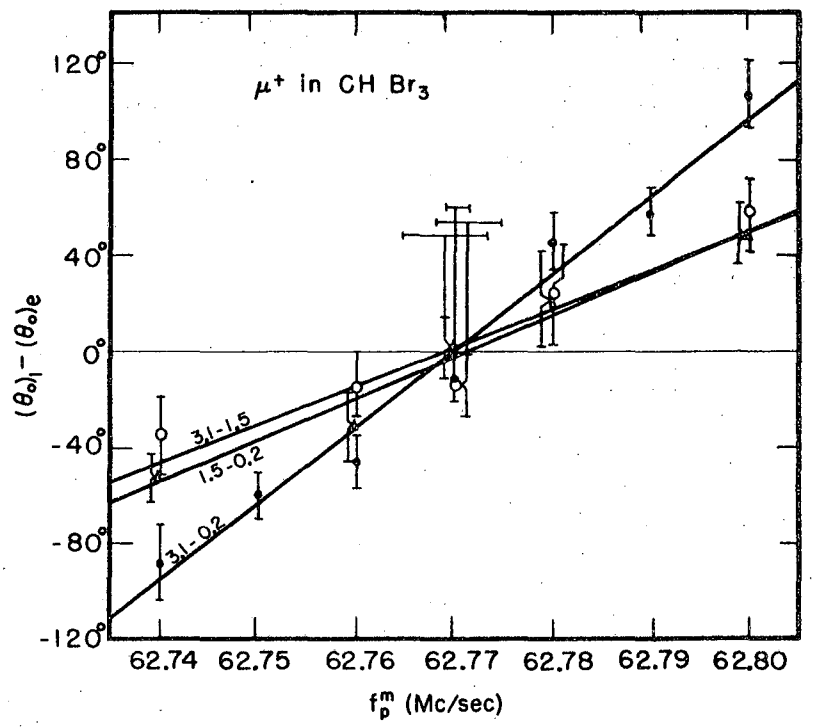

MU-26648

Z = 0

● $(T_1 - T_e) = 3.1 - 0.2\ \mu$ sec

○ $(T_1 - T_e) = 3.1 - 1.5\ \mu$ sec

Δ $(T_1 - T_e) = 1.5 - 0.2\ \mu$ sec

Vertical error flags are

$$\sqrt{\Delta^2(\theta_o^f)_1 + \Delta^2(\theta_o^f)_e + 9 \times 10^{-4} \left[((\theta_o)_1 - \Phi)^2 + ((\theta_o)_e - \Phi)^2\right]}$$

Fig. 12. Graph of late-early phase difference versus proton monitor frequency for positive run with Z = 0. Horizontal flags show errors ΔX_o(res), (see text).

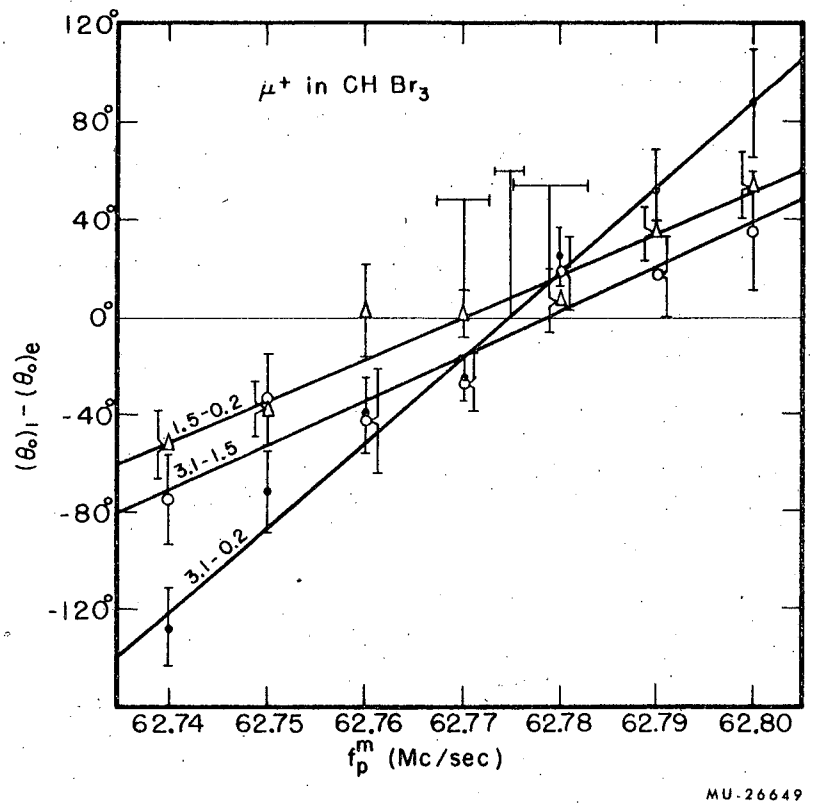

Z = 2.51 ± 0.01 nanosec.

● $(T_1 - T_e)$ = 3.1 - 0.2 μ sec.

○ $(T_1 - T_e)$ = 3.1 - 1.5 μ sec.

△ $(T_1 - T_e)$ = 1.5 - 0.2 μ sec.

Vertical error flags are

$$\sqrt{\Delta^2(\theta_o^f)_1 + \Delta^2(\theta_o^f)_e + 9 \times 10^{-4} \left[((\theta_o)_1 - \Phi)^2 + ((\theta_o)_e - \Phi)^2 \right]}$$

Fig. 13. Graph of late-early phase difference versus proton monitor frequency for positive run with Z = 2.51 ± 0.01 nanosec. Horizontal flags show errors ΔX_z (res), (see text).

(52). Where $\Delta\theta_b$ is large, the last term of Eq. (52) is written as $\left[\Delta \sin(\theta_o - \theta_b)\right]^2$ and the extreme deviation for $\pm\Delta\theta_b$ is used. Since only Z = 0 was run, the same $\Delta\theta_o^b$ is used for both the Z = 0 and Z = 2.51 ± 0.01 nanosec results of Table VII.

(4) We next take into account the errors $\sqrt{\Delta^2(\theta_o^b)_1 + \Delta^2(\theta_o^b)_e}$ and Φ_D in measurements of the phase difference. The first of these errors is common to all points on both Z lines for a given value of $(T_1 - T_e)$, but is independent for different values of $(T_1 - T_e)$. The second one, Φ_D, is common to all points on all lines. It will appear below that results from the lines $(T_1 - T_e) = 3.1 - 0.2\ \mu$ sec carry ~70% of the weight in the final result, and also that Φ_D makes only a small contribution to the errors in the points of the other $(T_1 - T_e)$ lines. Thus, it is a good approximation to assign a <u>common</u> error $\sqrt{\Phi_D^2 + \Delta^2(\theta_o^b)_1 + \Delta^2(\theta_o^b)_e}$ to all points on both lines corresponding to the <u>same</u> $(T_1 - T_e)$ value, but to assume these errors are <u>independent</u> for points on lines corresponding to <u>different</u> $(T_1 - T_e)$ values. From Eq. (56) we see that for a given value of $(T_1 - T_e)$, the common error to be included with both errors ΔX_z is given by $\frac{1}{a_2}\sqrt{\Phi_D^2 + \Delta^2(\theta_o^b)_1 + \Delta^2(\theta_o^b)_e}$. The procedure for combining this common error and the two errors ΔX_z (all three errors are independent) is discussed in Appendix 6 and is given as follows,

$$X(\text{res}) = \frac{\sum_z \frac{X_z(\text{res})}{\Delta^2 X_z(\text{res})}}{\sum_z \frac{1}{\Delta^2 X_z(\text{res})}} \qquad (59)$$

$$\Delta X(\text{res, final}) = \sqrt{\frac{\Phi_D^2 + \Delta^2(\theta_o^b)_1 + \Delta^2(\theta_o^b)_e}{a_2^2} + \Delta^2 X(\text{res})} \qquad (60)$$

$$\text{with} \quad X(\text{res}) = \sqrt{\frac{1}{\sum_z \frac{1}{\Delta^2 X_z(\text{res})}}} \tag{61}$$

and $\Delta X(\text{res, final})$ is the final error in X(res). All of the above work is tabulated in Table IX. The errors $\Delta X(\text{res, final})$ are then considered as independent (note on Φ_D above) and the usual weighted mean (similar to Eq. (59)) is taken, together with its error (similar to Eq. (61)). These are shown on the bottom of the table. All the errors of Eq. (54) have now been taken into account. Changing from f_p^m to f_p brings in Δf_p (Eq. (31), Eq. (40)) and using the resonance condition Eq. (6) includes the error Δf_o of Eq. (48) which is the last error contribution to Δf. The final result for positive muons stopping in bromoform is

$$\overline{\left(\frac{\bar{\imath}}{f_p}\right)'} = 3.18336 \pm 0.00007 \quad . \tag{62}$$

Strictly, Eq. (62) applies for f_p measured in water and f measured in bromoform. However we assume[21] that the muons and protons experience very similar shielding in bromoform. Then to the present experimental accuracy Eq. (62) may be considered to give the ratio of precession frequencies for free muons and free protons in the same magnetic field, since the chemical shift of protons in bromoform relative to protons in water is only -1.8 p.p.m. (i.e. less shielding in bromoform).

C. Calculation of Initial Phase Φ

This was calculated from the positive muon results for both Z = 0 and Z = 2.51 ± 0.01 nanosec. In this way we could check to see if the initial phase changed as expected (Eq. (28)). Also Φ for Z = 0 will be used in the negative muon work below. Straight lines of the form

$$\theta_o = a_1 + a_2 X \tag{63}$$

were fitted to the three phase plots for each Z value. This is justified because the predominantly statistical error $\sqrt{\Delta^2(\theta_o^f) + 9 \times 10^{-4} [\theta_o - \Phi]^2}$ assigned to each point is much greater than the deviation of the true phase curve from linearity (see notes below Eq. (23)). Since in the positive run we have $f_p = f_p^m$, Φ and $\Delta\Phi$ are given by using in Eq. (63) the conditions

$$X = + 0.20$$
$$X = 0.14 \quad . \tag{64}$$

The results of this work are then

$$\Phi\ (Z = 0) \quad = + (1^\circ \pm 3^\circ)$$
$$\Phi\ (Z = 2.51 \pm 0.01) = -(177^\circ \pm 2^\circ) \tag{65}$$
$$\therefore \text{ Change of } \Phi \ = -(178^\circ \pm 4^\circ) \ .$$

Using Eq. (28) to obtain the expected phase change we obtain $-(2\pi f_o Z)$ $= -(181^\circ \pm 1^\circ)$ and so we see that the agreement is quite reasonable.

D. Combination of Results in Negative Muon Run

The procedure used here is slightly different from that of the positive run. In the present case it is not possible to measure θ_b (Eq. (45)) owing to the combined low badkground (target empty) rate and low asymmetry. Thus instead of θ_o we will use the phase angle θ of Eq. (29), and estimate the maximum effect of background from Eq. (52). No known substance gives a muon decay asymmetry coefficient[13,14] which is appreciably higher than that obtained in water so we will assume $\frac{A_b}{A_o} = 1$. This almost certainly is an overestimate of A_b since we know by experiment that approximately half the background is due to negative muons stopping in the brass walls of the target. Such muons suffer additional depolarization due to the fact that the copper nucleus has spin ($\frac{3}{2}$). It has been

shown[42,43] that for a nucleus of spin I there is an additional reduction in muon polarization by the factor $\frac{1}{3}\left[1+\frac{2}{(2I+1)^2}\right]$. For brass this factor is ~ 0.5. Furthermore the negative muons which stop in the brass suffer a large Knight shift[44] ($\sim 0.1\% = 63$ Kc/sec) and hence there is a further reduction in A_b by a factor of ~ 0.5, from Eq. (26). Similar remarks to those above also apply to the negative muons which stop in the aluminum wrapping of the counters. By writing the last term of Eq. (52) in the form $\Delta\left[\sin(\theta_o - \theta_b)\right]$ and taking the maximum variation possible we obtain the estimated maximum phase angle error due to background as

$$\Delta\theta^b(\max) = \frac{r}{1-r} \quad . \tag{66}$$

The significance of Eq. (66) on the vector diagram of Fig. 11 is obvious.

A further difference between the present procedure and that of the positive run is that here we will use the initial phase Φ as determined on the positive run. This will enable us to extract the most information from our somewhat meagre negative muon statistics. If the change from positive run conditions to negative run conditions consisted of merely reversing all magnets, then we would expect[12] from CP invariance that Φ would be unchanged. However, an additional change was made in that the muon target was changed from bromoform to water. We will now consider three corrections to be made to the positive run Φ in order to take the target change into account.

(1) The average energy of the muons which stop in the target will now be less than in the positive case. Returning to Eq. (13) we see that this will mean a slight change in the precession frequency between the time when the muon crosses the μ counter and when it stops. The initial phase will involve the quantity

$$\Phi^{(1)} = -2\pi\int\left[f(1) - f(y)\right]dt \tag{67}$$

where the integral extends from the time the muon crosses the μ counter ($t = 0$) to the time the muon comes to rest. The negative sign is chosen because the moving muon will be precessing more slowly than the rotating frame at resonance and so it will appear to loose a small amount of initial phase. Eq. (67) may be rewritten as

$$\Phi^{(1)} = \frac{-eH}{mc} \int \sqrt{\frac{\gamma(\gamma-1)}{\gamma^2-1}} \, ds \tag{68}$$

where s is measured along the muon orbit from the μ counter. We wish to estimate $\Phi^{(1)}(CHBr_3) - \Phi^{(1)}(H_2O)$. This was done roughly by taking the average muon orbit (of length s_o) as passing through the 1" scintillator of the μ counter, the two 1/8" scintillators of counters 3 and 4, and half of the target. In this way the γ values at the instant of striking the μ counter were estimated as 1.25 for water and 1.30 for bromoform. Then the integrand in each case was assumed constant, at the above maximum values for the entire s_o. In this way it was estimated that $\Phi^{(1)}(H_2O) - \Phi^{(1)}(CHBr_3) < 0.7^\circ$.

(2) Due to their lower average momentum, the muons which stop in the water target will have orbits which cross the μ counter at a slightly larger angle ϕ (see Fig. 2) than the orbits in the positive run. This will appear as a slight change of initial phase. Since $(\frac{g-2}{2}) = 0.001$, the change in initial phase of the "polarization vector" will be closely equal to the change in the orbit direction ϕ. The change in ϕ was estimated using the following relation

$$\phi_2 - \phi_1 = \frac{e}{c} \int \frac{P_1 - P_2}{P_2} \quad \frac{H}{P_1} \, ds_1 \tag{69}$$

where we have used the suffix 1 for the bromoform case and the suffix 2 for the water case. It has been assumed that to first order the orbits have the same length since it will appear below that $(\phi_2 - \phi_1)$ is small.

The orbit was assumed to end at the centre of the target in each case. The section of the orbit up to counter 3 was divided into 7 regions and for each region the value of $\frac{P_1-P_2}{P}$ was determined at the midpoint of the region and at the end of the region. The increase in angle of the orbit, i.e. $\frac{e}{c}\int\frac{H}{P_1}\,ds_1$, was determined for each region from an approximate orbit. From this rough numerical integration of Eq. (69) an "average" value of $(\phi_2 - \phi_1)$ was obtained (used the midpoint values of ratio above) and an upper limit to $(\phi_2 - \phi_1)$ was also obtained (used the maximum values of the ratios). We list them as follows:

$$\begin{aligned} &\text{"Average"} \quad (\phi_2 - \phi_1) \approx 3^\circ \\ &\text{Limit} \qquad\quad (\phi_2 - \phi_1) < 5^\circ \,. \end{aligned} \tag{70}$$

Taking the "average" value we have for the change of initial phase due to this effect

$$\Phi^{(2)}(H_2O) - \Phi^{(2)}(CHBr_3) = 3^\circ \,. \tag{71}$$

(3) There may be a range dependence[20] of the initial phase of the "polarization vector." An error of $\pm 8^\circ$ was assigned to cover this possibility. Combining (1), (2) and (3) we obtain the total correction

$$\Phi(H_2O) - \Phi(CHBr_3) = + (4^\circ \pm 8^\circ) \,. \tag{72}$$

It was found that the correction contained by Eq. (72) represents a resonance frequency shift $\sim$20% of the final error and so this correction is not very important. From the first of Eq. (65) (since Z = 0 was used here) and from Eq. (72) we arrive at the initial phase to be used in the negative muon run

$$\Phi(H_2O) \pm \Delta\Phi(H_2O) = + (5^\circ \pm 8^\circ) \,. \tag{73}$$

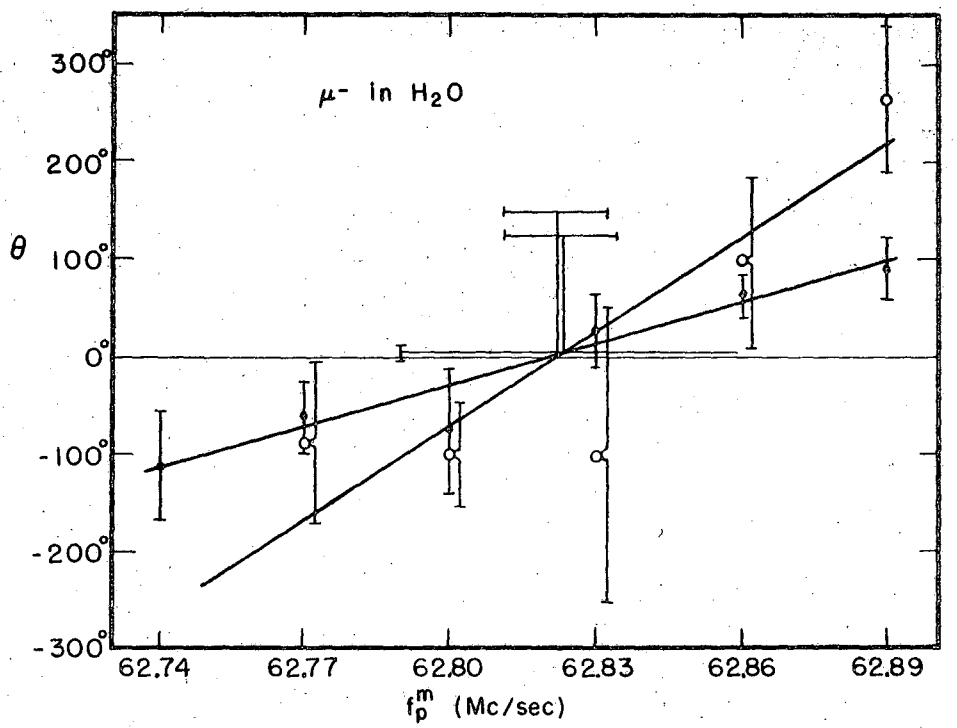

$Z' = 0$

• $T = 0.2\ \mu$ sec

○ $T = 2.1\ \mu$ sec

Vertical error flags are

$$\sqrt{\Delta^2\theta + 9 \times 10^{-4}(\theta - \bar{\theta})^2}$$

Fig. 14. Graph of phase angle versus proton monitor frequency for negative run with Z = 0. Horizontal flags show errors $\Delta X'$(res, final), (see text).

The procedure used for the negative muon run may now be outlined:

(1) The phase angles θ were calculated from Eq. (29) and each was assigned an error $\sqrt{\Delta^2\theta + 9 \times 10^{-4} (\theta - \bar{\Phi})^2}$ with $\Delta\theta$ given by Eq. (35).

(2) Straight lines of the form

$$\theta = a_1 + a_2 X' \tag{74}$$

with $X' = 100 (f_p^m - 62.83)$, were fitted by the method of least squares. Fig. 14 shows a graph of the experimental points and the straight lines of best fit.

(3) The maximum phase angle error due to background, $\Delta\theta^b(\max)$, is calculated from Eq. (66). The effect of drift in initial phase is already included from the positive run (it has a negligible effect here). Since $\Delta\theta^b(\max)$ is common to all points on a given phase line, it may be combined with the error of $\bar{\Phi}(H_2O)$. Then we obtain X'(res) and its final error $\Delta X'$(res, final) from the following relations

$$X'(\text{res}) = \frac{\bar{\Phi}(H_2O) - a_1}{a_2} \tag{75}$$

$$X'(\text{res, final}) = \left|X'(\text{res})\right| \sqrt{\frac{\Delta^2\bar{\Phi}(H_2O) + \Delta^2\theta^b(\max) + \Delta^2 a_1}{(\bar{\Phi}(H_2O) - a_1)^2} + \frac{\Delta^2 a_2}{a_2^2}} \tag{76}$$

Since the statistical errors Δa_1 and Δa_2 are the dominant ones, we may combine the results from our two phase lines by the usual method and obtain $\bar{X}'$(res) and its error $\Delta\bar{X}'$(res). Then using Eq. (42) we proceed as in the positive case and obtain the final result for negative muons stopping in water

$$\left(\frac{f}{f}\right)^-_{p\,H_2O} = 3.1808 \pm 0.0004 \tag{77}$$

All the above work has been tabulated in Table X. Here we may not assume that this is also the ratio for free negative muons as will be discussed in the next section.

E. Calculation of g/m for Both Runs

Before we use Eq. (8) it is necessary to correct the experimental value of f_e/f_p so that both electron and proton are in the same field, since the stated value of the ratio is for f_p taken as the frequency of protons in distilled water. Hutchinson et al.[21] obtained the corrected ratio f_e/f_p (both free) = 658.2107 after applying a correction[45] of 25.6 p.p.m. to allow for diamagnetic shielding of protons in water. No details are given of the water sample used in the experimental determination of f_e/f_p and so it is not known if there is also a bulk susceptibility correction[36] which must be applied. Apparently this is the main uncertainty in the corrected ratio and since it is at most ~ few p.p.m., for this experiment we may assume no error in the ratio f_e/f_p(both free). The g/m ratio for positive muons (we have assumed that this is the g/m ratio for free positive muons) is then given directly from Eq. (8).

$$\left(\frac{g}{m}\right)^{+} = (9.6840 \pm 0.0002) \times 10^{-3}\ m_e^{-1} \quad . \qquad (78)$$

For the negative muons we must first correct f_p to obtain the frequency of free protons. The diamagnetic correction of 25.6 p.p.m. will be used to obtain f_p(free). The bulk susceptibility correction due to F_e^{+++} ions was shown to be ≤ 1 p.p.m. in Section IV C(3) and that due to bulk diamagnetic susceptibility of water is smaller[36] so we ignore both. In this way we obtain from Eq. (8) an equivalent g/m ratio for negative muons in water

$$\left(\frac{g}{m}\right)^{-}_{H_2O} = (9.6760 \pm 0.0013) \times 10^{-3}\ m_e^{-1} \quad . \qquad (79)$$

Assuming that the masses of positive and negative muons are equal, we obtain for the fractional difference between the g value of free positive muons, g^+, and the equivalent g value of negative muons in water, $g^-(H_2O)$

$$\frac{g^-(H_2O)-g^+}{g^+} = -(8.3 \pm 1.4) \times 10^{-4} \quad . \tag{80}$$

As noted earlier, $g^-(H_2O)$ is really the g value for negative muons in the oxygen in water.

F. Simulated Muon Test Run

Straight lines of the form

$$(\theta^T)_1 - (\theta^T)_e = a_1 + a_2 \; f_o^{var} \tag{81}$$

were fitted to the data of Table V. The error assigned to each θ^T was given by $\sqrt{\Delta^2 \dot{\theta}^T + 9 \times 10^{-4} (\theta^T - \bar{\theta}^T)^2}$ where for error calculations $\bar{\theta}^T$ may be obtained merely by inspection from Table V. The usual resonance condition $(\theta^T)_1 - (\theta^T)_e = 0$ was used and the two resonance frequencies found were as follows:

$$Z = 0, \; f_o^{var} \text{ (res)} = 199.8290 \pm 0.0028 \text{ Mc/sec}$$

$$Z = 2.27 \pm 0.01, \; f_o^{var} \text{ (res)} = 199.8243 \pm 0.0036 \text{ Mc/sec} \; .$$

A common error $\frac{\bar{\theta}_D^T}{a_2}$ was then allowed with $\bar{\theta}_D^T = \frac{1}{2}\theta_D = 1.1^\circ$ since test run only lasted $\sim 1/2$ day and so the arbitrary factor of 2 is not included here. Using Appendix 6 we obtain for the combined result

$$\bar{f}_o^{var} \text{ (res)} = 199.8272 \pm 0.0024 \tag{82}$$

and we had $$f_o = 199.82860 \pm 0.00010$$

Thus we see that the two frequencies are in very good agreement, the error present in $\bar{f}_o^{var}$ (res) is $\sim$1 part in 10^5 and is only half the final error of the positive muon work in this experiment. Furthermore the error of $\bar{f}_o^{var}$(res) as given above is predominantly due to lack of statistics. The above test shows under actual operating conditions that any unknown systematic effects are small compared with the error of the positive muon work, and completely negligible in the negative muon work. By proceeding in a manner similar to that described in part C of this section, the phase angle change corresponding to a Z'' change of 2.27 $\pm$ 0.01 nanosec could be determined. The result was

$$\text{Measured change} = -(170^\circ \pm 3^\circ)$$

$$\text{Expected change Eq. (A18)} = -(163 \pm 1^\circ).$$

This agreement was considered reasonable because of the fact that there will be small phasing errors (ψ^{IA} etc. of Appendix 2) in the stroboscope. A sharp distribution will be more sensitive to these errors. Also there is a possibility of a systematic error associated with the delay change. During the test run this change was made by simply inserting a short cable and coupling in the signal line. The delay measured was the increase in delay when the same cable and coupling were inserted in <u>another</u> system, and so we did not measure the actual delay change experienced by the test system. This is in contrast to the 2.51 $\pm$ 0.01 nanosecond delay which was the actual delay change made during the experiment.

VI. DISCUSSION

A. Positive Muon Work

Eq. (78) may be combined with the recent (g-2) experiment[20] which gave $g = 2(1.001162 \pm 0.000005)$. In this way we obtain the positive muon mass value

$$m^+ = (206.766 \pm 0.005)\, m_e \quad . \tag{83}$$

Recently Hutchinson[21] obtained the results $f/f_p = 3.18338 \pm 0.00004$ and $m^+ = (206.765 \pm 0.003) m_e$ (13 p.p.m.) after further analysis of the preliminary report of Hutchinson et al. The CH_2I_2 and $CHBr_3$ work used in the preliminary report was discarded in the recent results, which therefore involve only the H_2O and HCl work. Hutchinson noted that there may be appreciable rates for the formation of compounds in the cases of CH_2I_2 and $CHBr_3$ and that consequently the chemical shift corrections ~~are~~ are uncertain for these two materials. However, neither Hutchinson's $CHBr_3$ result nor that of the present experiment (see Eq. (62) and Eq. (83)) shows significant deviation from the combined H_2O-HCl results. Thus it seems reasonable to combine the present experimental result with that of Hutchinson. This results in a mass value

$$m^+ = (206.765 \pm 0.002)\, m_e \quad 12 \text{ p.p.m.} \tag{84}$$

The muon mass value obtained with mesic X-rays (Section I) is in good agreement with Eq. (83) and Eq. (84) but it is not as accurate as the present results.

B. Negative Muon Work

Ford et al.[46] have discussed the corrections to be applied to the g value of a free muon in order to obtain the g value of a negative muon bound in a μ mesic atom. In their notation the g value of a free muon

is given by $(g_o + g_1)$ where $g_o = 2$ (i.e. Dirac particle) and g_1 is the radiative correction. Thus $(g_o + g_1)$ is our Eq. (1). We list the other corrections and give the numerical values for $_g0$.

(1) Binding correction to radiative corrections, g_2

$$\frac{g_2}{g_o}\,(_g0) = -0.000013.$$

(2) Direct binding correction, g_3. This is the largest correction and results from the relativistic treatment of the magnetic moment of a Dirac particle in a central field

$$\frac{g_3}{g_o}\,(_g0) = -0.001104 \quad .$$

(3) Nuclear polarization correction, g_4 .

$$\frac{g_4}{g_o}\,(_g0) = +0.000012 \quad .$$

(4) Electronic polarization correction, g_5. This term is negligible unless the ground electronic state has fine structural levels.

(5) Diamagnetic shielding by the atomic electrons, g_6. This will be very similar to the shielding experienced by the nucleus and it is the second largest correction considered,

$$\frac{g_6}{g_o}\,(_g0) = -0.00032.$$

(6) Center of mass correction, g_7. It may be neglected. From the above corrections we obtain the result

$$\frac{g^-(_g0) - g^+}{g^+} = -14.3 \times 10^{-4}$$

where we have taken the positive muon as the free muon. This is to be compared with the experimental result of $-(8.3 \pm 1.4) \times 10^{-4}$ as given in Eq. (80) . Ford et al. feel that the agreement is reasonable in view of

the facts that it was necessary to make assumptions about the electronic state of the μ-mesic atom and also there may be chemical shifts present. The above results indicate that the g values of free positive and negative muons are the same to within 6 parts in 10^4. Hutchinson et al.[21] obtained the result

$$\frac{g^-(H_2O) - g^+}{g^+} = -(9.3 \pm 1.0) \times 10^{-4} ,$$

and again it is seen that the two experiments are in quite reasonable agreement. The combined result of both experiments is

$$\frac{g^-(H_2O) - g^+}{g^+} = -(8.9 \pm 0.8) \times 10^{-4} .$$

VII. ACKNOWLEDGEMENTS

The experiment was suggested to the author by Professor Kenneth M. Crowe who also outlined the scheme used.

Dr. Hans Kruger undertook a large part of the actual running at the 184" synchrocyclotron. The author is also indebted to Messrs. R. Beck, B. Czirr, N. Dairiki, Tin Maung, J. Ryan, G. Sheldon and R. Spencer for assistance with this phase of the work. Dr. O. Shapiro took a keen interest in the experiment and made a number of helpful suggestions.

A number of the support groups of this laboratory assisted with the design, construction and maintenance of the equipment used. The author desires to acknowledge especially the assistance of Mr. Q. Kerns and his counting research group in the problems associated with the design of the fast mixers. Mr. R. Brown designed and constructed an appreciable fraction of the circuitry used, as well as performing much of the testing and setting up for the experiment. Mr. K. Lamers did most of the 200 Mc/sec oscillator work, part of which was done by Mr. H. Lancaster. The author is indebted to Mr. S. Smiriga and Mr. C. Dols for their work on the field regulator system.

The crew of the 184" synchrocyclotron, directed by Mr. J. Vale and Mr. L. Houser, were of every assistance throughout the work, as were also the accelerator technicians led by Mr. R. Walton and Mr. L. Sylvia.

It is a pleasure to acknowledge the typing assistance of Mrs. M. White and Mrs. B. Bole.

This work was performed under the auspices of the U. S. Atomic Energy Commission.

VIII. APPENDICES

Appendix 1. Estimate of Effect of Finite Solid Angle of β Counter

This is done by considering the very simple case shown in Fig. (A1). The β counter is assumed to be a spherical disc of radius ρ, with half angle $\mathcal{E}_o$. We assume that the polarized muons stop at O, the center of sphere. Referring to Eq. (14) of text, the following is now the expression for the number of IA counts d^4F_o due to all I muons in dx at x and to electrons in dt at t of the first A slot in O

$$d^4F_o = N_\mu f_o\, dx\, \frac{\sin\mathcal{E}\, d\mathcal{E}\, d\phi'}{4\pi} \left\{1 + a\cos\theta\right\} e^{-t/\tau}\, \frac{dt}{\tau} \quad . \quad (A1)$$

Eq. (A1) considers only the element $\Delta\Omega = \sin\mathcal{E}\, d\mathcal{E}\, d\phi'$ as shown in Fig. A1. Also θ is given by

$$\cos\theta = \sin\mathcal{E}\, \sin\phi'\, \sin(\Phi + 2\pi ft) + \cos\mathcal{E}\, \cos(\Phi + 2\pi ft) \quad . \quad (A2)$$

Then

$$d^2F_o = \int_o^{\mathcal{E}_o}\int_o^{2\pi} d^4F_o\, d\phi'\, d\mathcal{E} \quad . \quad (A3)$$

It is seen that term of d^4F_o which involves $\sin^2\mathcal{E}\, \sin\phi'$ gives no contribution integrated on ϕ' in Eq. (A3), and we have

$$d^2F_o = N_\mu f_o\, dx\, \frac{(1-\cos\mathcal{E}_o)}{2} \left\{1 + \frac{a(1-\cos 2\mathcal{E}_o)}{4(1-\cos\mathcal{E}_o)} \cos(\Phi + 2\pi ft)\right.$$

$$\left. e^{-t/\tau}\, \frac{dt}{\tau}\right\} \quad . \quad (A4)$$

Comparing Eq. (A4) and Eq. (14) of text we see that the only difference has been the reduction of the muon asymmetry coefficient by the factor $\frac{1}{4}\,\frac{(1-\cos 2\mathcal{E}_o)}{(1-\cos\mathcal{E}_o)}$. In this experiment it was roughly estimated that $\mathcal{E}_o \approx 20^\circ$ and so this reduction only amounts to a few percent. The expression for

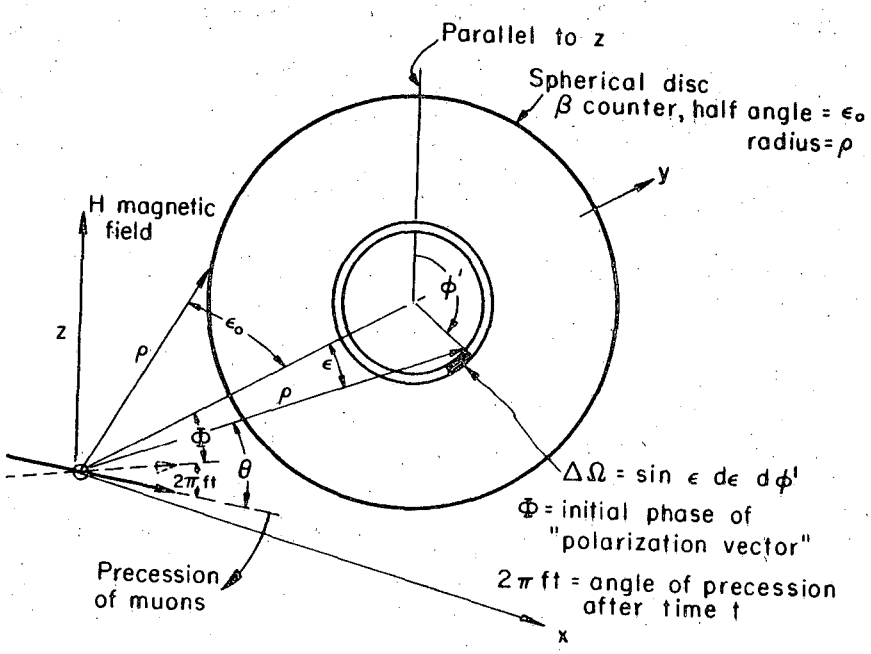

Fig. A1 Spherical disc β counter for detecting decay electrons from polarized muons stopped at 0, the center of the sphere.

tan θ, Eq. (20) remains unaltered. From Eq. (A2) this will also be true in the more general case where the counter is symmetrical with respect to the change $\phi' \rightarrow \phi' + 180^{\circ}$.

Appendix 2. Asymmetric Muon Stroboscope

In this appendix we investigate the effect due to the slots of the muon and electron fast mixers being unequal in width. It is also assumed that the slots are not exactly centered at the quarter cycle positions and that the signal delay time between the β counter and its fast mixer is a time Z longer than that between the μ counter and its fast mixer. The symbols g^I etc. denote the slot widths of I etc. and the symbols ψ^{IA} etc. denote the shifts of the slot centers of β fast mixer unit relative to quarter cycle times defined by slot I. The timing diagram is that shown in Fig. A2, where again it is not possible to draw T and G to scale.

Referring back to Eq. (14) of text we have now

$$t = T + y + t' - Z$$

and

$$N' = f_o\left(T + y + x - \psi^{IA} + \frac{g^A}{2} - \frac{g^I}{2}\right) .$$

The cosine form in Eq. (15) now becomes

$$\cos\left[\Phi + 2\pi(f-f_o)(T + y) + 2\pi f(t' - Z) - 2\pi f_o\left(x - \psi^{IA} + \frac{g^A}{2} - \frac{g^I}{2}\right)\right] .$$

Again $y \ll T$ and $y + t' - Z \ll \tau$ may be used. Since Z is small in this experiment, $|f-f_o| \leq 10^{-3} f_o$ may still be used as an approximation here. The calculations proceed just as in the text and we obtain

$$F^{IA} = \frac{N \mu f_o \Delta\Omega g^I g^A}{4\pi\tau} \sum_{n=0}^{N} e^{\frac{-(T+n\tau_o)}{\tau}} \left\{1 + \eta^{IA} \cos\left[\Phi^{IA} + 2\pi(f-f_o)(T+n\tau_o)\right]\right\} \qquad (A5)$$

where F^{IA} refers to the counts in element IA only, as the counts in IIB, etc. will differ slightly now,

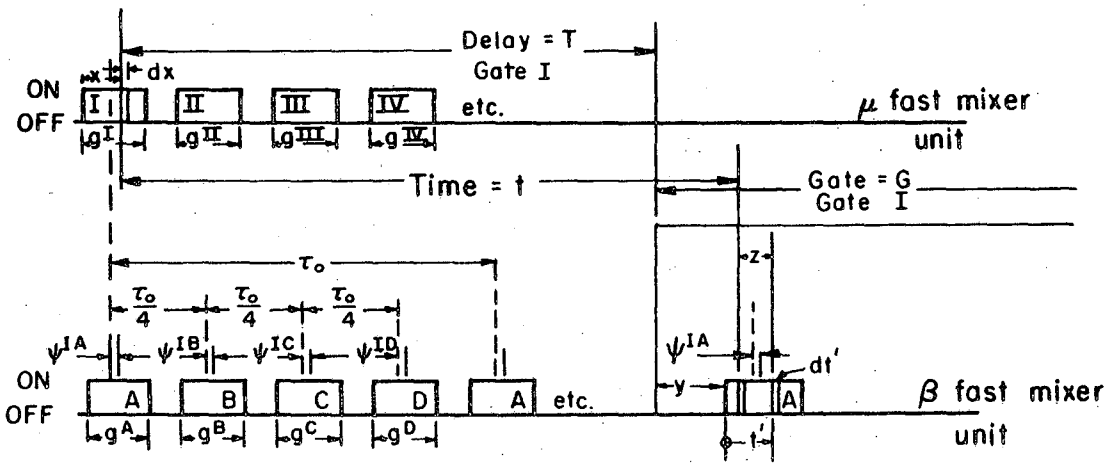

Slot centers are marked by short vertical full lines.

Z = time delay of β signal line relative to that of μ signal line.

Fig. A2. Timing diagram of asymmetric muon stroboscope. Notice that T and G are not to scale.

$$\Phi^{IA} = \Phi - 2\pi f_o(Z - \psi^{IA}) \quad , \tag{A6}$$

$$\eta^{IA} = \frac{a \sin(\pi f_o g^I)\sin(\pi f_o g^A)}{\pi^2 f_o^2 g^I g^A} \quad . \tag{A7}$$

With the substitutions $g^I = g^A = \tau_o/6$ and $Z = \psi^{IA} = 0$, Eq. (A7) reduces to Eq. (18) as would be expected. From Eq. (A6) we note the effect of adding delay Z to β counter signal line is that stated in text with Eq. (28). Eq. (A7) indicates how the asymmetry (as seen by the stroboscope) falls as the slot widths are increased. The factor $\frac{9}{\pi^2}$ is the appropriate one for the symmetric stroboscope, as can be seen by inspecting the text. Thus with slot widths of $\tau_o/6$ the asymmetry is reduced only ~10%. It is useful to rewrite Eq. (A5) in terms of quantities actually scaled during the experiment.

$$F^{IA} = \frac{N_\mu^I N_\beta^A}{N_\mu} \left\{ 1 + \frac{\eta^{IA}}{f_o \tau (1 - e^{-G/\tau})} \sum_{n=0}^{N} e^{-n\tau_o/\tau} \cos\left[\Phi^{IA} + 2\pi(f - f_o)(T_1 + n\tau_o)\right] \right\} \tag{A8}$$

where N_μ^I is the number of muons which arrived in slot I and N_β^A is the number of electrons which emerged in slot A. Expressions similar in form to Eq. (A8) may be obtained for the other 15 elements of the matrix.

By studying Eq. (A5) or Eq. (A8) the difficulty of the asymmetric muon stroboscope (i.e. the actual muon stroboscope) is immediately apparent. All slot widths, all Φ values, and all η values will in general be slightly different and so the simple expression for tan θ (Eq. (20) of text) will no longer be true. Apparently part of this difficulty is overcome if we redefine tan θ by the following expression

$$\tan\theta = \frac{R^X - L^X}{F^X - B^X} \tag{A9}$$

where $$R^x = (R^{ID})^x + (R^{IIA})^x + (R^{IIB})^x + (R^{IVC})^x$$

$$L^x = \text{etc.}$$

and

$$(R^{ID})^x = R^{ID} \frac{N_\mu N_\beta}{36\, N_\mu^I N_\beta^D} = R^{ID}\, k^{ID}$$

$$(R^{IIA})^x = \text{etc.}$$

with N_β being the total number of electrons detected in the run in which N_μ muons were stopped. In this new scheme Eq. (A8) becomes

$$(F^{IA})^x = \frac{N_\beta}{36}\left\{1 + \frac{\eta^{IA}}{f_o \tau\,(1-e^{-G/\tau})} \sum_{n=0}^{N} e^{-n\tau_o/\tau} \cos\left[\Phi^{IA} + 2\pi(f-f_o)(T_x + n\tau_o)\right]\right\} \qquad (A10)$$

with similar expressions for the other 15 elements of the matrix. We see now that the first term (the larger one since η^{IA} involves a) will be the same for all elements. In addition η^{IA} is only varying slowly with respect to changes of I or A slot width at slot widths near $\tau_o/6$. Thus the use of Eq. (A9) should largely compensate out any systematic effects due to different slot widths, or to small slot width changes during the experiment. Actually θ was calculated from both Eq. (11) and Eq. (A9) to see if there was any effect. It was found that the difference between the two values of θ was always $\ll 1$ standard deviation. From this it is included that the matrix is largely "self balancing" as regards slot width. A given slot width occurs once in each group R^s, L^s, F^s, B^s and so there is a large degree of cancellation of slot width differences in Eq. (11).

Appendix 3. Some Optimum Settings

In this appendix we will examine the optimum values of the parameters involved in $\frac{\Delta(g/m)}{(g/m)}$. Since the allowable rate for stopping muons is not dependent on T_1, T_e for this experiment it is relevant to find optimum values from the condition that $\frac{\Delta g/m}{g/m} = E$ be a minimum for a given total number of stopped muons.

Equation (37) of text gave the relation

$$E = \frac{1.2}{2\pi f(T_1-T_e)\,|A|}\sqrt{\frac{2}{\sum_1^x}+\frac{2}{\sum_e^x}} \quad . \tag{A11}$$

From Eq. (A4) and Eq. (26), for the symmetric muon stroboscope near resonance we have

$$A = \frac{9a(1-\cos 2\mathcal{E}_o)}{4\pi^2(1-\cos\mathcal{E}_o)} \quad . \tag{A12}$$

The values of $\sum_1^x$ and $\sum_e^x$ will be simply replaced by those of $\sum_1$ and $\sum_e$ as given from Eq. (19) (i.e. symmetric muon stroboscope)

$$\sum^x \approx \frac{2N_\mu e^{-T/\tau}(1-\cos\mathcal{E}_o)(1-e^{-G/\tau})}{9} \quad . \tag{A13}$$

It is noted from Eq. (A12) and (A13) that a β counter of finite solid angle is being considered. From Eqs. (A11), A12) and (A13)

$$E = \frac{0.8\,\pi\sqrt{(1-\cos\mathcal{E}_o)}}{a\,f\,(T_1-T_e)(1-\cos 2\mathcal{E}_o)\sqrt{(1-e^{-G/\tau})}}\sqrt{\frac{e^{T_1/\tau}}{(N_\mu)_1}+\frac{e^{T_e/\tau}}{(N_\mu)_e}} \tag{A14}$$

with the condition $(N_\mu)_1 + (N_\mu)_e$ = constant = K.

Optimum solid angle of β counter.

From Eq. (A14) we find that E is at a minimum when $\cos \varepsilon_o = 1/3$ i.e. $\varepsilon_o = 71^o$. ∴ optimum solid angle, $\Delta\Omega$ (opt) = $\frac{4\pi}{3}$ sterad.

Optimum gate width G. (we assume the same width in each run)

By inspection of Eq. (A14) G should be as large as possible. However in that case the repetition rate would be lowered due to increased dead-time of the gate. The value G = 2.5 μ sec was chosen so that the allowable repetition rate was the same for any value of T up to ~3 μ sec. In any case the value of E does not show much further decrease for larger values of G, as would be expected since most of the muons have already decayed.

Optimum setting of T_e.

From Eq. (A14)

$$E = \frac{0.8\,\pi\sqrt{1-\cos\varepsilon_o}\; e^{T_e/2\tau}}{a\, f(1-\cos 2\varepsilon_o)\sqrt{(1-e^{-G/\tau})_{T'}}}\sqrt{\frac{1}{K-(N_\mu)_1}+\frac{e^{T'/\tau}}{(N_\mu)_1}} \qquad (A15)$$

where T_e, $T' = T_1 - T_e$, and $(N_\mu)_1$ will be taken as the independent parameters. By inspection we want $T_e = 0$ in order that E should be as small as possible. In practice the smallest value of T_e that could be used was $T_e = 0.2$ μ sec.

Optimum values of $(N_\mu)_1$ and T'

These are obtained by the conditions $\frac{\partial E}{\partial (N_\mu)_1} = \frac{\partial E}{\partial T'} = 0$ with the results-

optimum $T' = 2.6\tau = 5.7$ μ sec.

optimum ratio $\frac{(N_\mu)_1}{(N_\mu)_e} = \frac{(\sum^x)_e}{(\sum^x)_1} = e^{T'/2\tau} = 3.7$.

The above work does not allow for fact that background is

becoming appreciable at delays $\sim 6\ \mu$ sec and also that the running of such a long delay would in fact mean that the stopping muon rate would have to be reduced for the T_1 run. In the actual experiment the longest delay used was $T_1 = 3.1\ \mu$ sec. Also the solid angle is determined by the electron orbits (allowing for energy loss) in the magnetic field and in this experiment $\varepsilon_o \approx 20^\circ$. There was no way to increase ε_o appreciably and still retain a reasonably simple counter design.

Appendix 4. Details of Electronics

A. Crossover Pulse Network

The actual pulse conditions under which we wished to operate were first determined by placing the actual μ and β counters in an electron beam at the 184" synchrocyclotron. The light level corresponding to electrons transversing the 1" thick scintillators was given a relative value of 1 unit. Then in the actual experiment the muons would be expected to give a light level slightly greater than 1 unit due to their higher ionization, while the electrons detected would be expected to give light levels in the rough range 1-3 units owing to their curved orbits (estimate obtained by drawing orbits). Thus it was decided to seek operation in the range of levels 0.5 - 4 for safety. The R.C.A. Type 7746 multiplier phototubes were set up viewing a light pulser[32] calibrated for this range, and typical average outputs are shown in Fig. A3(a). These traces were obtained with a recorder used in conjunction with a sampling oscilloscope [this was constructed by the counting research group directed by Mr. Q. Kerns, since most of the above investigation was done before commercial models were generally available] whose bandwidth was 700 Mc/sec. Clearly timing shifts ~2 nanosec. would be obtained with such a pulse height range if we attempted to standardize the pulses merely by limiting them.

Instead of using the usual overclipping arrangement to form a crossover pulse, a more general arrangement was used in which both positive and negative signals were taken from the tube. The behaviour of the crossover pulse may then be influenced by varying R_1 and R_2 (see Fig. A3(b)), the relative cable delay inserted in the signal paths, or the resistors of the summing function. The values of these parameters were determined so that the crossover point (positive → negative) remained steady as the

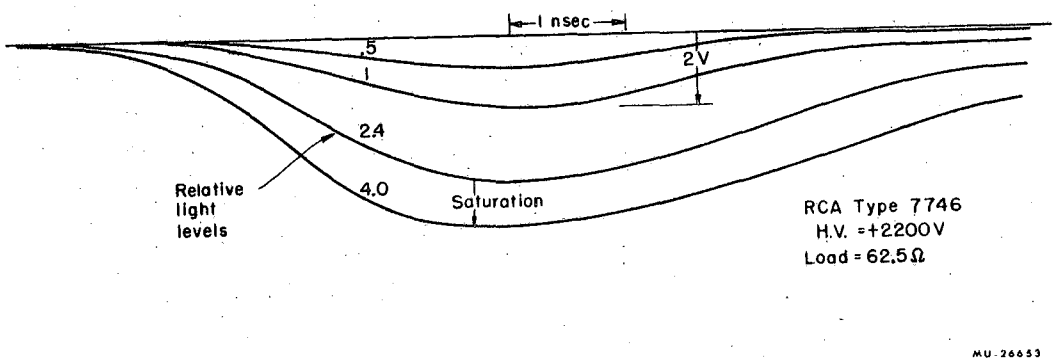

Fig. A 3(a). Average output pulses from R.C.A. Type 7746 phototube for four different light levels. Relative light level = 1 corresponds to approximately 130 photoelectrons arriving at the first dynode of the tube. The operating conditions are as indicated and the divider used was similar to that shown in Fig. A 3(b), except that R_1 = 160 K, R_2 = 220 K, R_3 = 150 K in the present case.

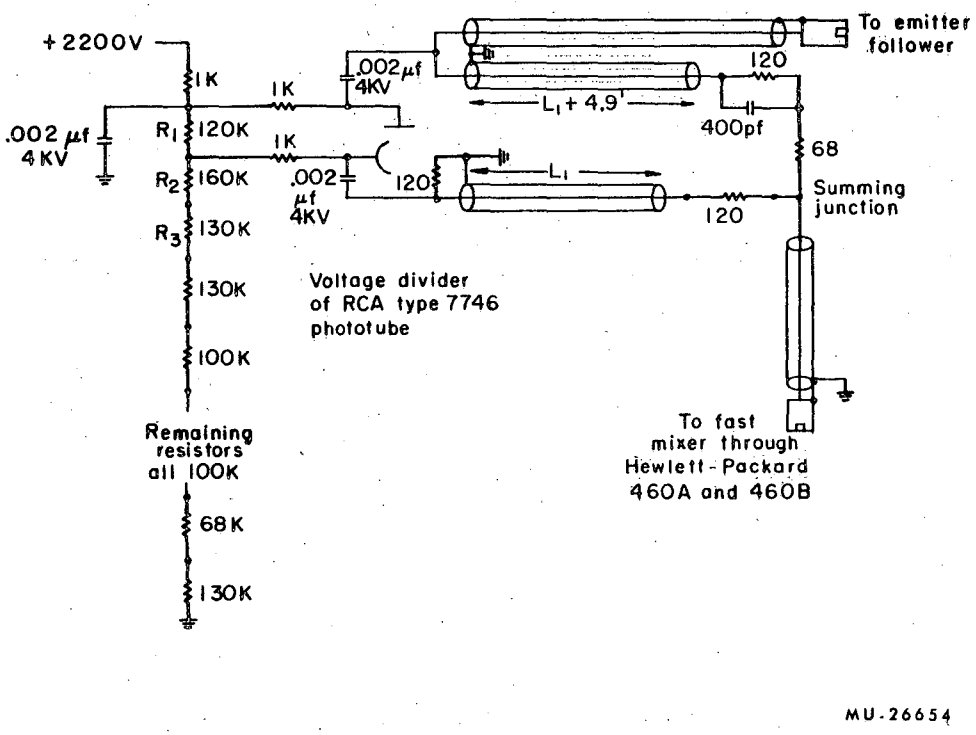

Fig. A 3(b). Final arrangement used to form crossover pulse. Note that the capacitors of the voltage divider have not been shown.

light level was varied (using crossed polarizers). Actually we are more interested in the behaviour of the spiked pulse (see below) which is mixed with the 200 Mc/sec wave, so the parameters were chosen to minimise its movement. However, it was found that the behaviour of the crossover point was very similar to that of the spiked pulse. The final system arrived at, is shown in Fig. A3(b) and the timing shift of the spiked pulse was < 0.2 nanosec as the light level was changed from 0.5 to 4. The purpose of the 400 p.f. condenser at the summing function was to prevent operation of the fast mixer units by the somewhat ragged tail of the amplified crossover pulse (see Fig. A4). As is seen from Fig. A3(b) a separate negative pulse was taken for use in the standard coincidence circuits. This pulse had a small trailing positive pulse originating from the summing function, and it was necessary to remove this by a suitably biased emitter follower. Recalling that the stroboscope is required to have a average timing stability ~ 0.01 nanosec (Section IID) both the μ and β phototubes were supplied from the same high voltage line. In this way it was estimated that a high voltage change of ~ 100 V was required to produce a relative $\mu - \beta$ delay change of 0.1 nanosec. During the actual experimental run the high voltage variation was $< \pm 4$ V.

B. Fast Mixer Units

The circuit diagram of one mixing circuit is shown in Fig. A4. Each fast mixer unit has four of these circuits. The input amplified crossover pulse is sketched in the upper part of the figure. The swing from negative to positive takes 3 nanosec., with the positive portion rising in 1 nanosec and being limited by the Hewlett-Packard 460B(linear) amplifier. A fast rising pulse is then obtained[35] by feeding the amplified crossover pulse into a grounded base stage (2N1143, near cutoff). Only the positive part of the pulse operates the input stage. After clipping,

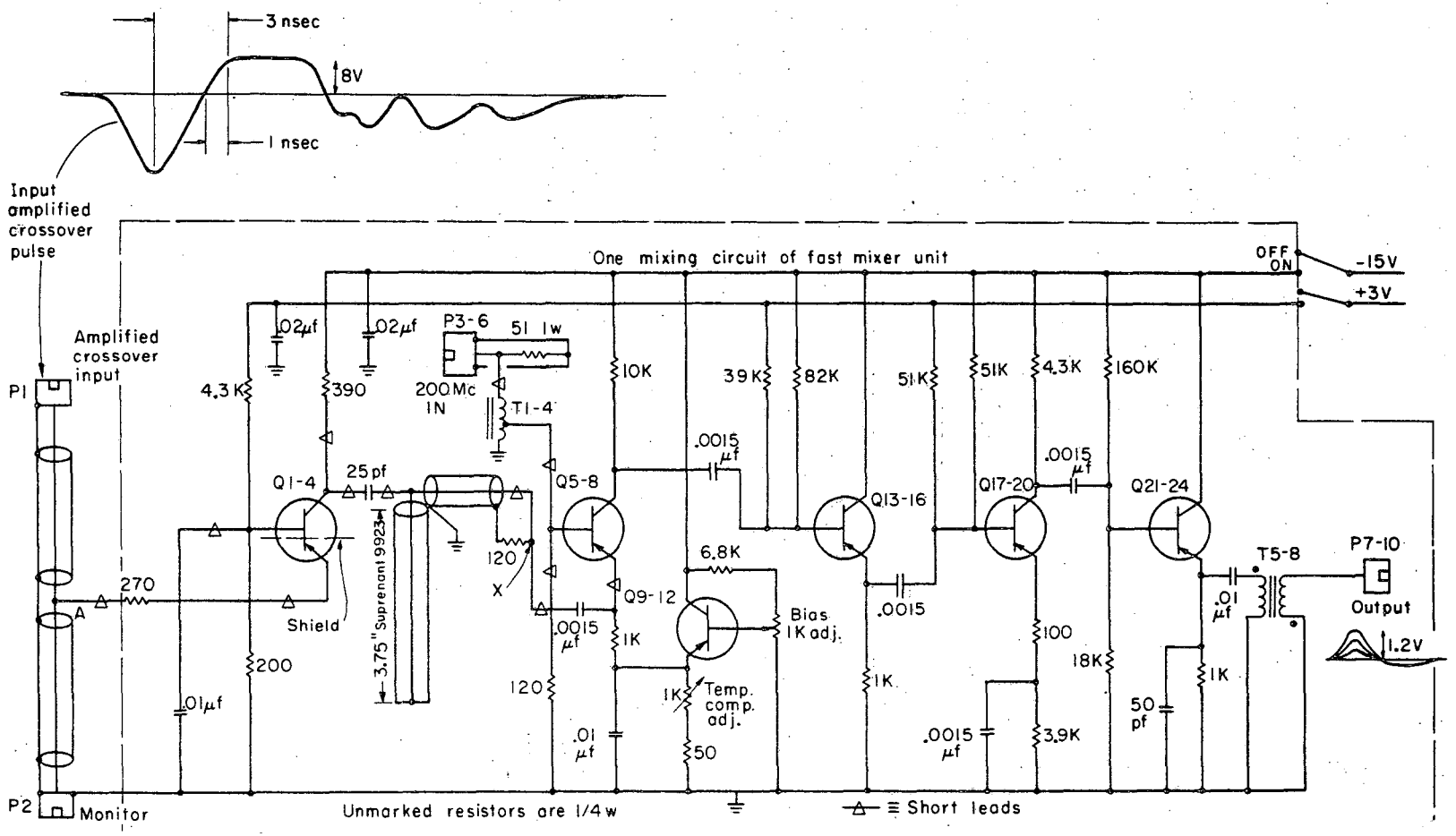

NOTES: (1) μ and β fast mixer units each contain 4 mixing circuits as above, connected in parallel at point A.
(2) T1-4 8:2 turn auto transformer wound on Type 102 core.
(3) T5-8 inverting transformer (Pulse Eng. PE 2679-7).
(4) Transistors Q1 - 12 2N 1143
Q13-24 2N 501

Fig. A 4. Circuit diagram of one mixing circuit of fast mixer units.

a spiked pulse is obtained whose amplitude is ~1/2 V and whose full width at half maximum is 1 nanosec. This pulse was monitored at point x by removing the 120Ω resistor. The spiked pulse was mixed with the 200 Mc/sec wave in the second state (2N1143) and the overlap was integrated on the collector capacitance and then amplified. The bias adjust was normally set so the output envelope was + 1.2V into 125Ω load. Under light pulser test conditions it was found that when the following discriminator was set for a slot width of $\tau_o/6$ (i.e. triggered by 1/6 of input pulses), then its level was ~0.6 V. In the experimental run this corresponding setting was ~0.8 V so that the scintillation pulses may not be quite as fast as those of the light pulser.

The input from the 200 Mc/sec oscillator was normally set at 2.2 V r.m.s. and this was then stepped down to minimize loading of the terminated line. In order that mixing circuit output variations could be associated only with relative timing it is necessary that the amplitude of the 200 Mc/sec wave be held constant, and that the crossover pulse be well limited. The amplitude of 200 Mc/sec wave was regulated by means of a feedback circuit which controlled the supply voltage of the output stage. It was found that there were still some long time drifts present and these were corrected manually with a helipot. The fractional amplitude variation during the experimental run was $< \pm 4 \times 10^{-3}$. It should be noted that because all mixing circuits of μ and β fast mixer units are driven from the same 200 Mc/sec, the effects of amplitude variation will tend to cancel. The limiting action of the crossover pulse was examined by setting the slot width for $\tau_o/6$ at light level = 1 and then finding how the slot width varied as a function of light level. This is shown in Fig. A5(a) where we see that the limiting in the range of interest (1 - 3) is very good and in fact

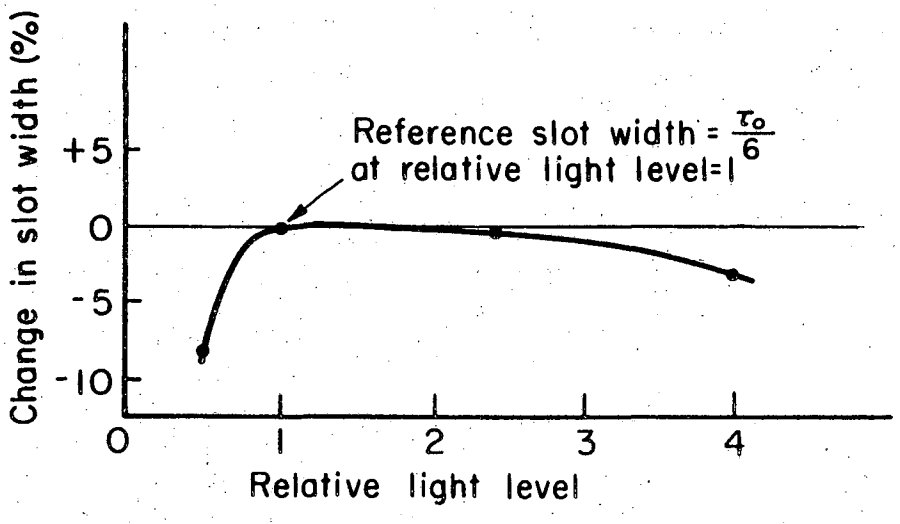

MU-26655

Fig. A 5(a) Graph showing percent change in slot width as relative light level is varied.

is reasonable over the entire range (0,5- 4). It should be noted that this curve was influenced by choice of series resistor in emitter of input stage.

Each mixing circuit was temperature compensated as indicated in Fig. A4. The adjustment was made so as to minimize the change produced by a heat lamp. In the actual run the temperature variation was only $3^{\circ}C$. The fast mixer units were symmetrized as much as possible by choosing sets of 4 transistors with equal delay times for use as Q1-4 and Q5-8. The delay times were obtained by plugging successive transistors into say Q1 socket and tracing the spiked pulses. It was found that the timing distribution for 2N1143 transistors had a width of ~ 0.5 nanosec while that for 2N501 transistors was ~ 1 nanosec and this is the reason behind the choice of transistors as shown on Fig. A4. Further symmetrization was done by studying, for example, the pulse heights in outputs A and C of β unit when an output was received in B (used to trigger oscilloscope).

Before the experimental run the muon stroboscope was tested in a setup in which both μ and β phototubes viewed the same light pulser (set for light level = 1). The relative delay Z of the β signal relative to the μ signal was varied and a delay curve could be obtained for a given matrix element. In Fig. A5(b) the solid line graph is the idealized curve we would expect, the element IA being taken as an example. We assume the center of the I and A slots are exactly aligned and we do not consider timing jitter. Then the ordinate at relative delay Z is simply the product of the number of light pulses N_p considered and the fraction of a cycle during which pulses of relative delay Z find that both slots I and A are turned on. The above follows from the fact that the 200 Mc/sec oscillator and the light pulser are operating independently of each other. (It is probably easier to see how the idealized curve is obtained if we imagine that we leave the μ and β pulses exactly aligned and instead vary the time displacement of the

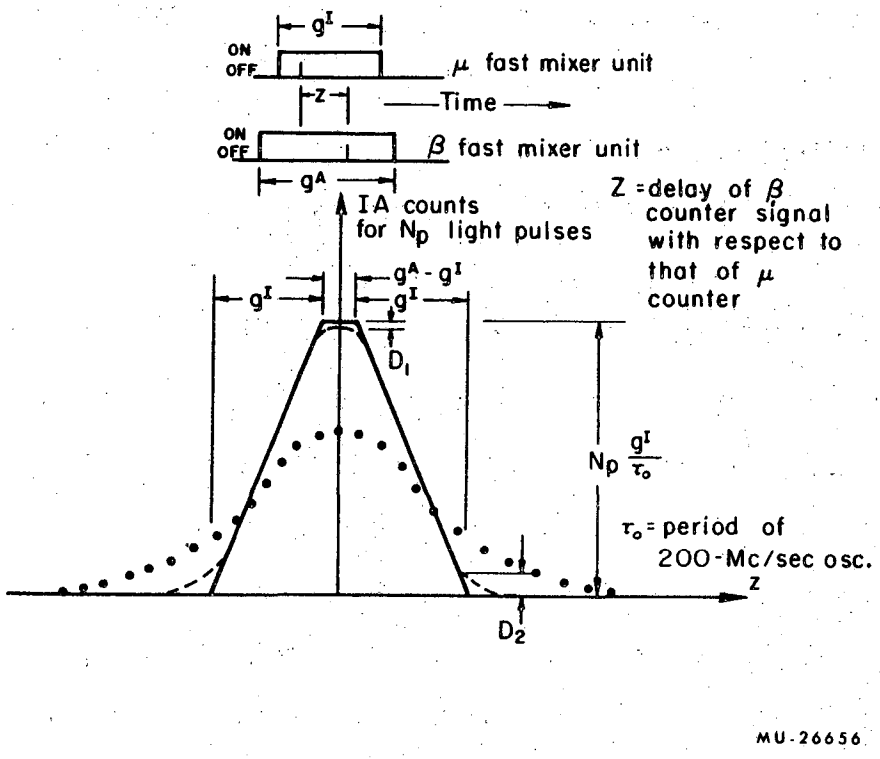

Fig. A 5(b). — Solid line graph is the idealized IA delay curve for N_p light pulses per run.

-- Dashed lines show deviations from the idealized curve and were obtained in light pulser tests.

.. Dotted curve is delay curve obtained with meson beam traversing both μ and β counters ("beam through").

slot centers.) The dashed sections on Fig. A 5(b) represent the deviations from the idealized curve as measured in the light pulser tests. Such deviations can be explained by timing jitter in the phototubes. Typically D_1 and D_2 were $\sim 5\%\ N_p \frac{g^I}{\tau_o}$. Also D_2 dropped by a factor of 2 in a Z change of 0.1 nanosec which indicates the order of the phototube jitter. This checks reasonably with that expected[26] in the above case. Tests were made on the timing stability of the system by setting Z to obtain $N_p \frac{g^I}{2\tau_o}$ counts (i.e. on the steep sides) and looking for counting changes over a period of time. In a typical run of several hours any timing shift was < 0.01 nanosec. For comparison we have also shown on Fig. A 5(b), with the dotted curve, a typical delay curve run during the experiment. In this run the meson beam traverses both μ and β counters, i.e. the "beam through" run described in text (Section III F). As would be expected, the timing jitter appears much worse here (D_1 and $D_2 \sim 40\%\ N_p \frac{g^I}{\tau_o}$, D_2 drops by factor 2 for Z change ~ 0.3 nanosec.). In the actual precession experiment we may expect that the timing jitter will be even worse because of the various electron orbits. Timing jitter alone cannot introduce systematic error in the experiment but it can lower our accuracy by lowering A, the magnitude of the asymmetry as seen by the muon stroboscope.

C. Deadtime Circuitry (This circuitry was designed and constructed by Mr. R. Brown.)

(1) Deadtime generators 1 and 2

These circuits could be set for deadtimes in the range 1-10 μ sec. They were set for 3 μ sec in the present work. The same circuit was used for both units and is shown in Fig. A6. On receiving an input discriminator pulse it put out a positive 12 V signal provided there had been no previous input in the preceding 3 μ sec. The arrival of further inputs during a deadtime merely extended the deadtime to 3 μ sec after the last arrival. As is shown by the various waveforms, the arrival of an input

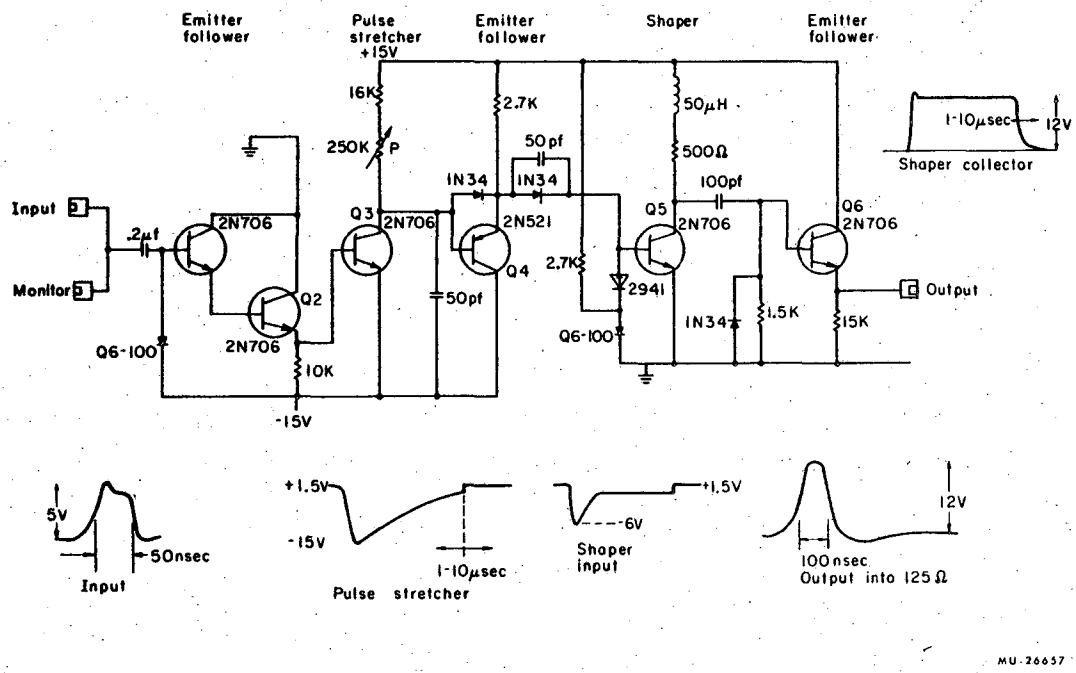

Fig. A 6. Circuit diagram for both deadtime generators nos. 1 and 2. The deadtime may be set in the range 1-10 μ sec by setting P.

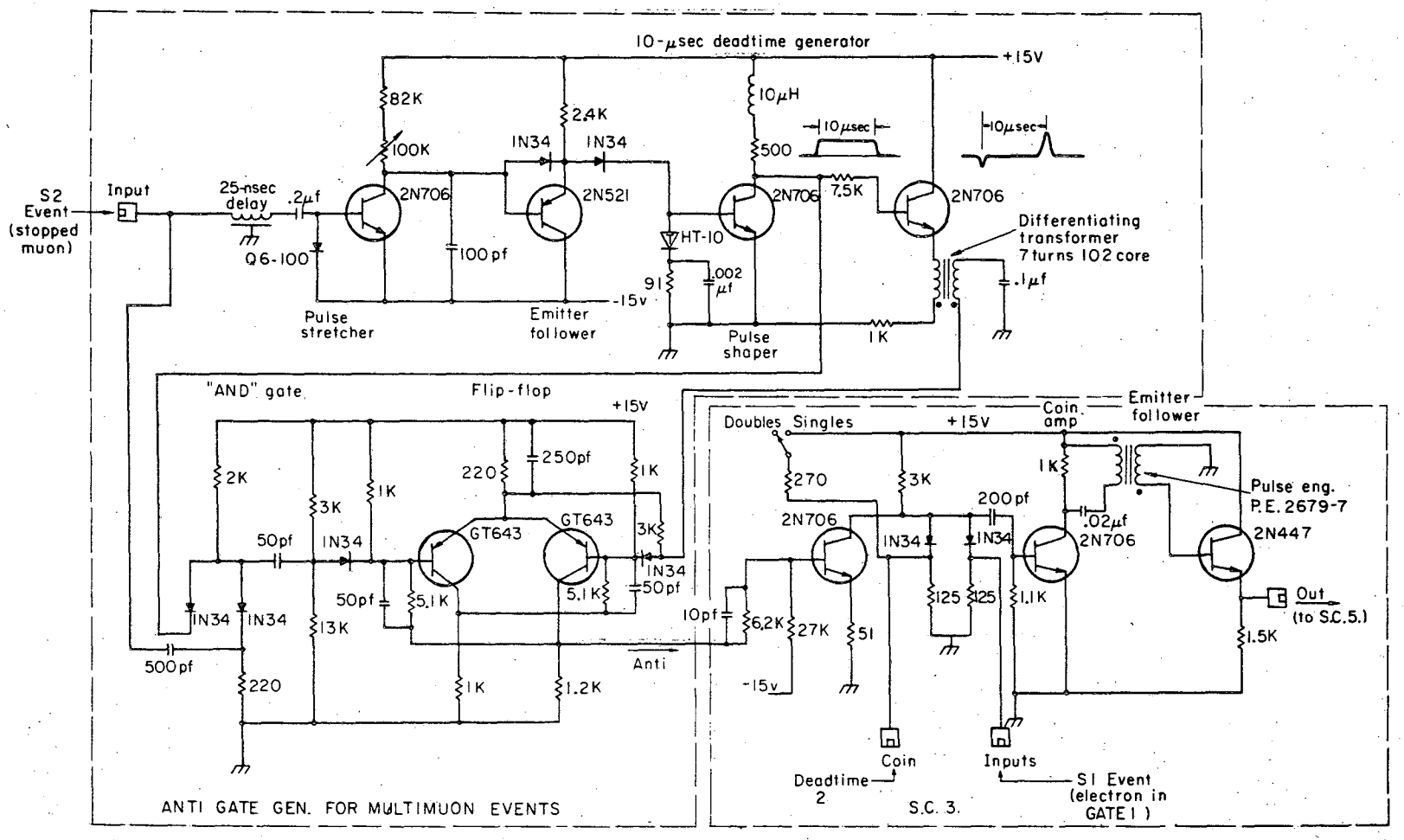

Fig. A 7. Anti gate generator for multimuon events. Also shown is S.C. 3, which is a slow 2-channel coincidence circuit with 1 anti-input for the anti gate.

pulse (we are assuming no preceding pulse) discharges the 50 pf capacitor which then charges towards + 15 V through P. The input pulse also drives Q5 (shaper) from saturation to cutoff. As the 50 pf capacitor charges to near +1 V, Q5 is held in cutoff by the tunnel diode. Near +1 V the tunnel diode switches to its high impedance state, driving Q5 into saturation. The output is then obtained by differentiation so that we observe only the leading edge of the shaper collector waveform. The various properties of the circuit are now clear.

(2) Deadtime generator 3 and SC 2.

This deadtime generator is similar to the ones above except that its range of operation was 3-35 μ sec. In this run the deadtime was set at 10 μ sec. The output went to a slow coincidence circuit S.C. 2 similar to S.C. 3 (see below).

(3) Anti gate generator for multi muon events, and S.C. 3. The circuit diagram is shown in Fig. A7. Its purpose is to prevent electrons being assigned to the wrong muon parent as noted in the text. The incoming stopped muon pulse is split, one path goes through a 25 nanosec delay and a 10 μ sec deadtime generator, while the other goes to a two fold coincidence circuit, or "and" gate, which receives its other input from the deadtime generator as shown. For just one muon input there is no output from the "and" gate because of the 25 nanosec delay. But if a second muon arrives, within 10 μ sec, it finds the "and" gate open and so triggers the flip-flop which sends an anticoincidence gate to S.C. 3. Then if no more muons arrive, the flip flop is reset, 10 μ sec after the second muon, by the trailing edge of the deadtime circuit output. The operation of S.C. 3 is clear. All other slow coincidence circuits S.C. 1, S.C. 2, S.C. 4, S.C. 5 are similar to S.C. 3 except that they have no anti-input.

Appendix 5. Simulated Muon Precession

In this appendix we shall show how the test run described in the ~~test~~ text (Section III E) does indeed simulate muon precession at the frequency set on the variable oscillator.

Figure A8 shows the complete timing diagram for test operation. The upper two lines refer to the μ and β test fast mixer units (driven by $f_o^{var.}$) and the lower two lines refer to the μ and β fast mixer units of the symmetric stroboscope (Fig. 3). The relative phase of f_o and f_o^{var} is completely random and the muons will thus enter in a random manner with respect to both oscillators. We assume a phase difference ϕ^T between the μ and β slots in the test fast mixer units (recall there is only one slot in each), and also a relative time delay Z^{μ} between the stroboscope and test μ fast mixer units (compared with the time delay between the corresponding β units).

The periodic curve $F_{\varepsilon v}(t'')$ represents the probability that an electron signal could get through the test β unit at time t" after a muon signal got through test μ unit, averaged over all arrival times x' in g^T_{μ}. (By putting $Z = (t'' + \frac{\phi^T}{2\pi f_o^{var}})$ we see that $F_{av}(Z)$ will be very similar to the delay curves of Fig. A 5(b). The only difference between the two cases is that the timing jitter will not be the same.) We will assume that the "pips" of $F_{av}(t'')$ are symmetrical and so from Fourier analysis we write

$$F_{av}(t'') = \sum_{m=0}^{\infty} a_m \cos m(\phi^T + 2\pi f_o^{var} t'') \qquad (A16)$$

Thus for the test fast mixer units we have—

Probability that μ counter signal arrives in $g^T_{\mu} = f_o^{var}\ g^T_{\mu}$.

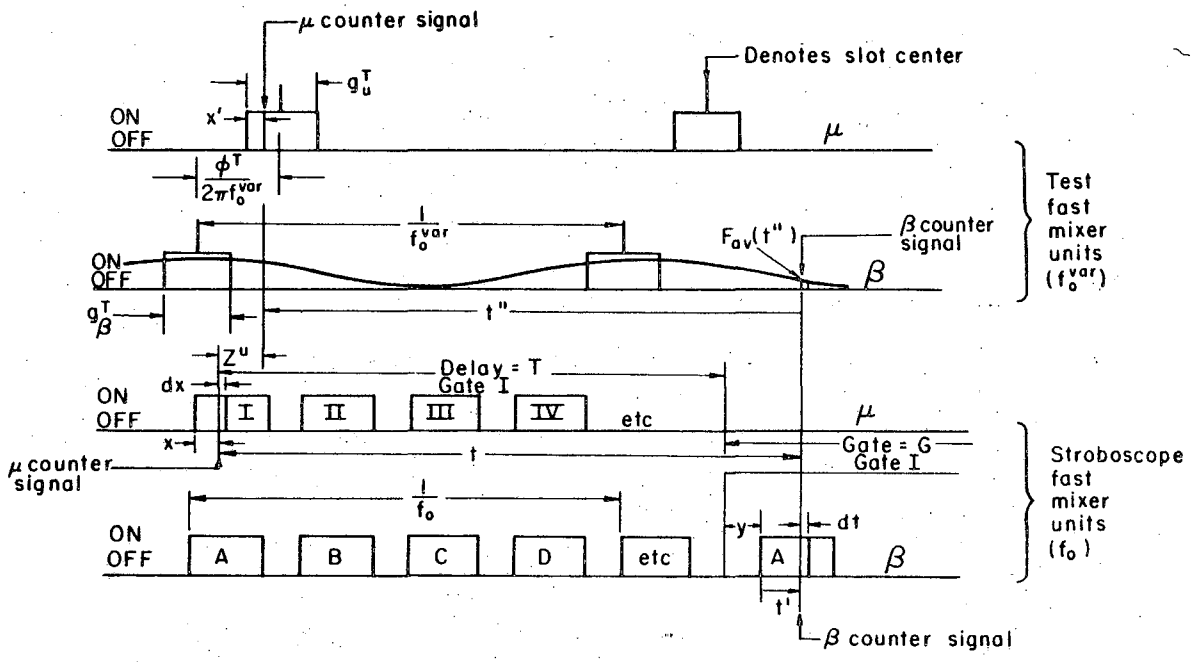

f_o^{var} = frequency of variable frequency oscillator.

f_o = frequency of 200 Mc/sec oscillator.
= 199.82860 ± 0.00010 Mc/sec.

ϕ^T = phase difference between muon and electron test fast mixer.

$F_{av}(t'')$ = average probability (averaged over x') that β gets through β test unit at time t'' after μ got through μ test unit.

Fig. A 8. Complete timing diagram for test operation. A typical event is shown. Muons enter randomly with respect to both f_o, f_o^{var} because oscillators are independent.

Probability of a β counter signal in dt at time t after muon signal arrives

$$= \frac{\Delta\Omega}{4\pi}\, e^{-t/\tau}\, \frac{dt}{\tau}\left\{ \sum_{m=0}^{\infty} a_m \cos m \left[\phi^T + 2\pi f_o^{var}(t-Z^{\mu}) \right] \right\} \quad (A17)$$

where we have used $t'' = (t-Z^{\mu})$. The asymmetry of the muon (negative) decay is too small to affect the present work. Thus we have assumed an isotropic decay distribution.

For the stroboscope fast mixer units we have—

Probability that μ counter signal falls in $dx = f_o\, dx$. (note that the averages with respect to x' and x can be made separately because of the fact that the relative phases of f_o and f_o^{var} are random).

Probability that β counter signal arriving in dt gets through β fast mixer unit = 1.

Thus the total number of IA counts in interval dt within first A slot of gate G is given by

$$d^2F_o = N_{\mu} f_o^{var} g_{\mu}^T f_o\, dx\, \frac{\Delta\Omega}{4\pi}\, e^{-t/\tau}\, \frac{dt}{\tau}\left\{ \sum_{m=0}^{\infty} a_m \cos m \left(\Phi^T + 2\pi f_o^{var} t \right) \right\} \quad (A18)$$

where N_{μ} is the number of muons stopped in the run and $\Phi^T = \phi^T - 2\pi f_o^{var} Z^{\mu}$. We note that Eq. (A18) is very similar to Eq. (14) the only differences being the additional factor $f_o^{var}\, g_{\mu}^T$ and the additional harmonics in the above case. Proceeding in the usual way we obtain (as in Eq. 18)

$$F = \sum_{n=0}^{N} \sum_{m=0}^{\infty} h\, e^{-(T+n\tau_o)/\tau} \left\{ a_m \frac{\sin^2 \frac{m\pi}{6}}{\pi^2 m^2} \cos m \left[\Phi^T + 2\pi (f_o^{var} - f_o)(T + n\tau_o) \right] \right\} \quad (A19)$$

with

$$h = N_{\mu} \frac{g_{\mu}^T}{\tau} \frac{\Delta\Omega}{4\pi} .$$

The expressions for L, B, and R may be obtained from Eq. (A19) with the following substitutions–

$$\text{L} \quad \Phi^T \rightarrow \Phi^T + \frac{\pi}{2}$$

$$\text{B} \quad \Phi^T \rightarrow \Phi^T + \pi$$

$$\text{R} \quad \Phi^T \rightarrow \Phi^T + \frac{3\pi}{2} \quad .$$

We also define the test phase angle in the usual manner (Eq. 11)

$$\tan \theta^T = \frac{R^S - L^S}{F^S - B^S} \quad . \tag{A20}$$

Thus we obtain

$$\tan \theta^T = \frac{\sum_{n=0}^{N} \sum_{m=1,3,5..} (-1)^{(m-1)/2} a_m \frac{\sin^2 m\pi/6}{\pi^2 m^2} e^{-n\tau_o/\tau} \sin m \left[\Phi^T + K_n\right]}{\sum_{n=0}^{N} \sum_{m=1,3,5..}^{\infty} a_m \frac{\sin^2 m\pi/6}{\pi^2 m^2} e^{-n\tau_o/\tau} \cos m \left[\Phi^T + K_n\right]} \tag{A21}$$

where $K_n = 2\pi (f_o^{var} - f_o)(T + n\tau_o)$ and we see that only the odd harmonics enter. Comparing Eq. (A21) with Eq. (20) we see that, although the early and late phase plots must still be equal at $f_o^{var} = f_o$, they may not be closely approximated by straight lines in the present case. The first coefficient to complicate matters is a_3, but it is probably quite small compared with a_1 since the frequency response of the system is already falling off at 200 Mc/sec. If we assume $F_{av}(t")$ "pips" are triangular, with base $\frac{1}{m' f^{var}}$, then $a_3 \frac{\sin^2 \pi/2}{9\pi^2} \leq 5\%\ a_1 \frac{\sin^2 \pi/6}{\pi^2}$ for m' in range 1-2. This range covers the shape of the "beam through" delay curve of Fig. A 5(b). This curve will be similar to $F_{av}(t")$ as noted earlier. (Experiment shows that $F_{av}(t")$ is slightly less peaked than the "beam through" delay curve.) In the test runs the statistical accuracy of $(F^S - B^S)$ and $(R^S - L^S)$ was only $\sim 5\%$ so we assume that the higher harmonics may be neglected. Then we have

$$\tan \theta^T = \frac{\sum_{n=0}^{N} e^{-n\tau_\phi/\tau} \sin \left[\Phi^T + 2\pi (f_o^{var} - f_o)(T + n\tau_o) \right]}{\sum_{n=0}^{N} e^{-n\tau_\phi/\tau} \sin \left(\Phi^T + 2\pi (f_o^{var} - f_o)(T + n\tau_o) \right]} \qquad (A22)$$

Comparing with Eq. (20) and Eq. (28) we get the analogies

$$\begin{aligned} \Phi^T &\equiv \Phi \\ z^{\mu} &\equiv z \\ f_o^{var} &\equiv f \end{aligned} \qquad (A23)$$

Thus it is seen that the behaviour of the combined muon stroboscope and test system, viewing isotropic muon decay, is the same as that of the muon stroboscope alone viewing the precessing asymmetric muon decay at frequency f_o^{var}. Recalling Eq. (21) and Eq. (23) we see that θ^T is the weighted average phase difference between the muon stroboscope and the first harmonic of $F_{av}(t'')$ for the electron gate in use. For the actual experimental results the counts were corrected for slot width so that θ^T was defined after Eq. (29) rather than Eq. (11).

If we set $g_\beta^T = \frac{1}{6 f_o^{var}}$ we may write Eq. (A 16) in the form

$$F_{av}(t'') = \frac{1}{6} \left[1 + a^T \cos (\phi^T + 2\pi f_o^{var} t'') \right] + \sum_{m=2}^{\infty} a_m \cos m (\phi^T + 2\pi f_o^{var} t'') \qquad (A24)$$

where $a^T = 6\, a_1$ is the test run "asymmetry coefficient" analogous to that of Eq. (4). We see that it is related to the coefficient of the first harmonic of $F_{av}(t'')$. If we also set $g_\mu^T = \frac{1}{6 f_o^{var}}$ then the counting rate for test operation will be only 1/36 that for normal operation since the muon and electron signals each have a probability of 1/6 to get through their respective test circuits.

Note on "Beam Through" Operation

The matrix counts $N[\theta\ (e-\mu)\ ]$ are considered a function of average electron-muon phase difference, $\theta(e-\mu)$, in which we neglect multiples of 2 π. Thus we consider that we have four points— F^s corresponding to $\theta(e-\mu) = 0$, L^s corresponding to $\theta(e-\mu) = \pi/2$, etc., and fit the curve (by least squares or Fourier analysis)

$$N[\theta(e-\mu)\ ] = a_o\ [1 + b_o \cos\ (\theta(e-\mu) + \phi_o)\ ] \quad . \qquad (A25)$$

It can be shown that $\tan \phi_o = \frac{R^s - L^s}{F^s - B^s}$ and so we have the significance of the "phase angle" under "beam through" conditions.

Appendix 6. Partially Correlated Errors

We consider two measurements, x_1 and x_2, of a quantity x. The errors in these two measurements are considered to be made up of a random error with standard deviations δ_1 and δ_2 respectively, together with an error of standard deviation Δ_o which is common to both x_1 and x_2. It is considered that δ_1 and δ_2 and Δ_o are all independent (Δ_o may be random or systematic) and that we desire to determine the weighted mean of x_1 and x_2 together with its standard deviation. It may be shown[40] that these quantities are given respectively by

$$\bar{x} = \frac{\sum_{i=1,2} \frac{x_i}{\delta_i^2}}{\sum_{i=1,2} \frac{1}{\delta_i^2}} \qquad (A26)$$

and

$$\Delta \bar{x} = \sqrt{\Delta_o^2 + \frac{1}{\sum_{i=1,2} \frac{1}{\delta_i^2}}} \qquad (A27)$$

IX. DEFINITIONS OF SYMBOLS

a	experimental asymmetry coefficient
a'	theoretical asymmetry coefficient
$a_1 a_2$	coefficients of straight line fitted by least squares
A,B,C,D	slots of β (electron) fast mixer unit
I,II,III,IV	slots of μ (muon) fast mixer unit
A	muon decay asymmetry as seen by stroboscope
A_b	background asymmetry as seen by stroboscope
A_o	muon decay asymmetry after background subtraction
c	velocity of light
e	electron charge
E	fractional error in g/m
f	muon precession frequency
f_e	electron precession frequency
f_p	proton precession frequency in water
$\frac{df(\theta")}{d\Omega}$	energy averaged angular distribution of electrons from muon decay (relative to muon spin)
$\frac{df(\theta')}{d\Omega}$	energy averaged angular distribution of electrpns from muon decay (relative to "polarization vector")
f_o	frequency of 200 Mc/sec oscillator
f_o^{var}	frequency set on variable frequency oscillator
$f_p(\vec{r},t)$	proton frequency (water) at $\vec{r}$ at time t
$f_p^m(t)$	monitor probe proton frequency (water) at time t
$f_p^{(1)}(t)$	transfer proton frequency (water) at time t
$f_p^{(3)}(\vec{r},t)$	proton frequency (water) increase between target centre and point $\vec{r}$ at time t

$F_{av}(t'')$	probability that electron gets through test β unit at time t'' after muon got through test μ unit, averaged over arrival times of muon in slot of test μ unit
$F_n$etc	forward counts etc due to electrons in the $(n+1)^{th}$ contributing slot within gate
F,L,B,R	forward, left, back, right counts
F^s,L^s,B^s,R^s	sum of four forward scalers, etc. of matrix
F^x,L^x,B^x,R^x	sum of four forward scalers, etc of matrix after each has been corrected for slot width
F_b^x,L_b^x,B_b^x,R_b^x	sum of four forward scalers, etc, of matrix during background run. Each scaler has been corrected for slot width.
F_o,L_o,B_o,R_o	$(F^x - F_b^x)$ etc.
g	muon g value
g_p	proton g value
g_e	electron g value
g^A,g^B,g^C,g^D	slot widths of β fast mixer unit
$g^I,g^{II},g^{III},g^{IV}$	slot widths of μ fast mixer unit
G	width of gate set on Gate 1
H	magnetic field
k	$\frac{N_\mu \Delta\Omega}{144 \pi f_o \tau}$
m	muon mass
m_p	proton mass
m_e	electron mass
N	number of cycles of 200 Mc/sec oscillator within gate
N'	an integer
N_μ	number of stopped muons

N_β	number of detected electrons
N_μ^I etc.	number of muons arriving in slot I etc.
N_β^A etc.	number of electrons arriving in slot A etc.
$N\left[\theta(e-\mu)\right]$	matrix counts considered as function of average electron muon phase difference (in which multiples of 2π are not considered)
r	ratio of matrix counting rates for empty target and full target runs
R_p	muon polarization at decay
t	time after muon stops
t'	time after start of A slot
T_e	early gate set on Gate 1
T_l	late gate set on Gate 1
T	any gate set on Gate 1
x	time after start of I slot
X	frequency scale used for fitting results of positive run
X'	frequency scale used for fitting results of negative run
y	time between start of gate and first A slot
Z	relative delay of β counter signal line
Z^μ	relative delay between stroboscope and test μ fast mixer units
α	fine structure constant
β	electron
γ	muon total energy $= m\gamma c^2$

δ_1, δ_2	statistical errors in x_1, x_2
Δ_o	common error in both x_1 and x_2
$\Delta\Omega$	element of solid angle
Δ	in error discussions it denotes the standard deviation of the quantity it precedes.
ϵ	angular coordinate of finite solid angle β counter
θ	phase of muon in rotating frame
θ_o	phase of muon in rotating frame after correction for slot width and background
θ_b	phase of background in rotating frame
θ^T	equivalent phase for test run
$\theta(e-\mu)$	average electron-muon phase difference neglecting multiples of 2π
θ''	angle between muon spin and direction of electron emission
θ'	angle between muon "polarization vector" and direction of electron emission
μ	muon
$\sum$	sum of F, L, B, R
$\sum^S$	sum of F^S, L^S, B^S, R^S ie. total matrix counts
$\sum^X$	sum of F^X, L^X, B^X, R^X ie. total matrix counts after correction for slot width
$\sum_b^X$	sum of F_b^X, L_b^X, B_b^X, R_b^X ie. total background matrix counts after correction for slot width
$\sum_o^X$	sum of F_o, L_o, B_o, R_o ie. total matrix counts after correction for slot width and subtraction of background

τ	muon mean life (2.2 μ sec)
τ_o	period of 200 Mc/sec oscillator
ϕ	angle between muon orbit and axis of β counter at instant muon crosses μ counter
ϕ'	angular coordinate of finite solid angle β counter
ϕ^T	phase difference between μ and β test fast mixer units
ϕ_o	equivalent initial phase under beam through conditions
Φ	initial phase of muon "polarization vector"
$\Phi(CHBr_3)$	initial phase in positive run with Z = 0
$\Phi(H_2O)$	initial phase in negative run with Z = 0
Φ_D	drift of initial phase
ψ^{IA} etc	delay of centre of A slot relative to centre of I slot, etc.

X. TABLES

Table I. Typical counting rates.

Beam	Target	Stopped Muons/min. (S2)			Σ/min. T = 0.2 μ sec
		Target Full	Target Empty	Target Out	Target Full
Positive					
1/4 Full Beam Short Duty Cycle	$CHBr_3$	9.0×10^3	2.0×10^3	1.8×10^3	60
Negative					
Full Beam "Stretched"	H_2O	1.5×10^5	1.0×10^5	7.8×10^4	720

T = Delay of Gate 1 (width of gate G = 2.5 μ sec).

Σ = Total 4 x 4 matrix counts.

Table II. Data obtained from full target runs with positive muons. Counts shown are obtained from actual counts with Eq. (29).

T	f_p^m	Z = 0				Z = 2.51 ± 0.01 nanosec.			
μ sec	Mc/sec	L^X	B^X	R^X	F^X	L^X	B^X	R^X	F^X
0.2	62.74	762	1114	1088	774	1151	885	911	1214
	75	1077	1378	1370	971	2483	1770	2086	2673
	76	1142	1426	1256	926	1189	827	1016	1267
	77	3238	3943	3313	2523	2589	2088	2742	3342
	78	1071	1310	1037	804	1165	977	1296	1552
	79	1336	1422	1026	959	1240	1085	1429	1605
	80	1044	1122	840	795	834	774	1123	1174
1.5	62.74	741	946	1171	986	708	591	479	601
	75					617	481	415	598
	76	237	334	332	228	324	263	287	367
	77	348	413	346	215	871	695	936	1097
	78	340	346	294	255	420	365	495	555
	79					485	522	763	715
	80	727	636	472	600	464	590	674	591
3.1	62.74	196	200	275	280	349	405	311	258
	75	766	969	1311	1053	437	367	322	346
	76	536	732	792	595	678	568	509	641
	77	335	460	394	258	749	533	643	814
	78	769	760	579	574	572	547	725	767
	79	926	695	535	697	320	313	435	359
	80	697	513	524	684	308	338	386	295

Typical asymmetry $$A = \frac{-2\sqrt{(R^X - L^X)^2 + (F^X - B^X)^2}}{\Sigma^X}$$

$$= -0.22 \pm 0.02$$

Z = Delay of β counter

T = Delay of Gate 1 (gate width G = 2.5 μ sec)

f_p^m = Proton resonance frequency of monitor probe Pl in Mc/sec

Table III. Data obtained from empty target runs with positive muons. The β counter delay Z = 0 was used.

T μ sec	f_p^m Mc/sec	L_b^x	B_b^x	R_b^x	F_b^x	A_b x 10	ΔA_b x 10	r
0.2	62.74	108	119	135	97	-1.5	0.8	
	77	125	140	136	96	-1.8	0.7	0.112
	80	138	137	145	119	-0.7	0.7	±0.007
1.5	74	67	70	86	72	-1.3	1.0	0.135
	80	91	87	75	91	-0.9	0.9	±0.010
3.1	74	37	43	44	43	-0.9	1.3	0.139
	80	35	44	31	35	-1.5	1.9	±0.013
					Av.	-1.2	0.3	

T = Delay of Gate 1 (gate width G = 2.5 μ sec.)

f_p^m = Proton resonance frequency of monitor probe P1.

$$A_b = \frac{-2\sqrt{(R_b^x - L_b^x)^2 + (F_b^x - B_b^x)^2}}{\Sigma_b^x}$$

$$\Delta A_b \approx \frac{1.20}{\sqrt{\Sigma_b^x/2}}$$

$$r = \frac{\text{Target empty } \Sigma_b^x/\text{beam monitor}}{\text{Target full } \Sigma^x/\text{beam monitor}}$$

Σ^x, Σ_b^x = Total matrix counts corrected for slot width Eq. 29.

Table IV. Data obtained from full target (H_2O) runs with negative muons. Notation is same as that of Tables II and III.

T μ sec	f_p^m Mc/sec	L^x	B^x	R^x	F^x	r
0.2	62.74	2510	2339	2432	2309	
	77	10179	10179	10424	10117	
	80	22210	22125	22427	22072	0.080
	83	10357	10411	10239	10177	±0.008
	86	28884	28850	28247	28524	
	89	13041	12862	12694	12873	
2.1	77	9701	9770	9817	9768	
	80	2436	2474	2524	2492	
	83	2638	2592	2670	2599	0.12
	86	2449	2518	2393	2526	±0.01
	89	7458	7540	7572	7550	

β counter delay Z = 0

Average asymmetry $$A = \frac{-2\sqrt{(R^x - L^x)^2 + (F^x - B^x)^2}}{\Sigma^x}$$

$$= -(1.0 \pm 0.4) \times 10^{-2} \text{ (see text)}$$

T = Delay of Gate 1 (gate width G = 2.5 μ sec)

Table V. Results of simulated muon test run.

Z^{μ} nanosec	T μ sec	f_o^{var} Mc/sec	L^x	B^x	R^x	F^x	θ^T	$\Delta\theta^T$
0	0.2	199.73	511	199	2	85	+ 77.4°	2.3°
		83	506	16	3	266	+116.4	2.2
		93	199	1	42	424	+159.6	2.5
	3.1	199.73	20	359	206	1	- 27.5	2.7
		83	209	8	0	128	+119.9	3.5
		93	2	68	317	112	+262.1	2.9
2.27 ± .01	0.2	199.73	2	91	357	87	- 89.4	2.6
		83	5	299	379	3	- 51.7	2.6
		93	85	481	229	2	- 16.7	2.5
	3.1	199.73	36	1	24	132	-185.2	4.1
		83	1	65	80	1	- 51.0	5.3
		93	104	23	0	38	+ 98.2	5.1

Z^{μ} = additional delay placed between normal and test muon fast mixers.

T = delay of Gate 1 (gate width G = 2.5 μ sec.)

f_o^{var} = frequency set on variable frequency oscillator.

L^x etc. obtained from actual counts by Eq. 29.

f_o = 199.82860 ± 0.00010 Mc/sec.

θ^T = is obtained from Eq. 35.

Table VI. Positive muon phase angles after correction for background.

Z nanosec	f_p^m Mc/sec	T = 0.2 μsec		T = 1.5 μsec		T = 3.1 μsec	
		θ_o	$\Delta\theta_o^f$	θ_o	$\Delta\theta_o^f$	θ_o	$\Delta\theta_o^f$
0	62.74	-43.0°	6.7°	-96.0°	7.5°	-131°	13.6°
	75	-35.2	7.2			- 95.4	6.0
	76	-11.6	7.0	-42.9	12.2	- 57.8	9.0
	77	- 2.1	4.2	+ 0.6	9.7	- 13.3	9.1
	78	+ 4.2	6.6	+26.6	18.7	+ 50.7	9.7
	79	+35.2	6.4			+ 93.6	6.7
	80	+32.4	8.3	+81.5	10.1	+139	10.2
2.51 ± .01	74	-214.5	8.2	-267.5	11.3	-342.3	12.2
	75	-202.4	5.0	-240.1	10.4	-274.3	15.9
	76	-200.9	7.3	-198.3	17.3	-241.1	13.9
	77	-171.6	4.2	-170.1	7.8	-196.9	9.0
	78	-166.2	6.2	-159.1	11.0	-140.9	9.7
	79	-159.5	6.9	-125.3	7.6	-107.7	15.6
	80	-143.5	6.5	- 90.0	12.2	- 55.4	21.3

θ_o is obtained from Eq. 45

$\Delta\theta_o^f$ is obtained from Eq. 51

Table VII. Results of fitting straight lines, Eq. 56, to positive muon phase difference data. a_2 is expressed in degrees per 10 Kc/sec.

Z nanosec	$T_1 - T_e$ μsec	a_2 Eq. 55	Experimental a_2	Δa_2	a_1	Δa_1	X_2(res)	ΔX_2(res)
0	3.1 - 0.2	33.2	32.5	2.4	- 1	4	+0.02	0.13
	3.1 - 1.5	18.4	15.9	3.5	+ 2	7	-0.11	0.44
	1.5 - 0.2	14.9	17.7	2.7	- 3	6	+0.15	0.33
2.51 ± .01	3.1 - 0.2	33.2	34.7	3.3	-16	5	+0.47	0.16
	3.1 - 1.5	18.4	18.3	3.7	-16	6	+0.87	0.39
	1.5 - 0.2	14.9	17.1	2.5	0	5	+0.01	0.27

Table VIII. Tabulation of phase angle error $\Delta\theta_o^b$ due to background in positive muon run.

T μ sec	A_o	$\theta_o - \theta_b$	$\Delta\theta_b$	$\Delta\theta_o^b$
0.2	-0.24 ± 0.01	10^o	18^o	1.1^o
1.5	-0.24 ± 0.02	0^o	34^o	2.6^o
3.1	-0.26 ± 0.02	60^o	47^o	2.9^o

Z = 0 in background run.

$\Delta\theta_o^b$ is given by Eq. 52.

Table IX. Final results for positive muon run. The frequency ratio for free positive muons and free protons may also be assumed to be given by $(f/f_p)^+$.

$T_1 - T_e$ μ sec	X(res)	ΔX(res)	$\frac{\sqrt{\Delta^2(\theta_o^b)_1 + \Delta^2(\theta_o^b)_e}}{a_2}$	$\frac{\phi_D}{a_2}$	ΔX (res, final)
3.1 - 0.2	+0.20	0.10	0.094	0.067	0.15
3.1 - 1.5	+0.45	0.29	0.23	0.13	0.39
1.5 - 0.2	+0.07	0.21	0.17	0.13	0.30
$\bar{X}$(res) = +0.20				$\Delta\bar{X}$(res) = 0.13	

$$\bar{f}_p^{\,m}(\text{res}) \pm \Delta\bar{f}_p^{\,m}(\text{res}) = 62.7720 \pm 0.0013 \text{ Mc/sec}$$

$$\left.\begin{aligned} \Delta f_p(\text{res}) &= \sqrt{\Delta^2 f_p^m(\text{res}) + \Delta^2 f_p} \\ \Delta f_p &= 4.8 \times 10^{-4} \text{ Mc/sec} \\ f_p &= f_p^m \end{aligned}\right\} \quad \text{Eq. 40}$$

$$\therefore f_p(\text{res}) \pm \Delta f_p(\text{res}) = 62.7720 \pm 0.0014 \text{ Mc/sec}$$

$$f = f_o \pm \Delta f_o = 199.82615 \pm 0.00010 \text{ Mc/sec.}$$

$$\therefore (f/f_p)^+ = 3.18336 \pm 0.00007$$

f = positive muon frequency in bromoform

f_p = proton frequency in water

Table X. Final results for negative muon run.

T μ sec	a_2 Eq. 24	Experimental a_2	Δa_2	a_1	Δa_1	$\Delta\theta^b$(max)	X'(res)	ΔX' (res, final)
0.2	13.9	14.0	3.1	+16°	14°	4.8°	-0.79	1.24
2.1	35.7	32.5	8.0	+26°	35°	7.9°	-0.65	1.13
						$\bar{X}'(res) = -0.72$		
								$\Delta\bar{X}'(res) = 0.84$

$$\bar{f}_p^m(res) \pm \Delta\bar{f}_p^m(res) = 62.8228 \pm 0.0084 \text{ Mc/sec}$$

$$\Delta f_p(res) = \sqrt{\Delta^2 f_p^m(res) + \Delta^2 f_p}$$

$$\left.\begin{aligned} \Delta f_p &= 7.2 \times 10^{-4} \text{ Mc/sec} \\ f_p &= f_p^m - 2.5 \times 10^{-4} \end{aligned}\right\} \text{ Eq. 42}$$

$$\therefore f_p(res) \pm \Delta f_p(res) = 62.823 \pm 0.008$$

$$f = f_o \pm \Delta f_o = 199.8275 \pm 0.0014$$

$$\left(\frac{f}{f_p}\right)^{-}_{H_2O} = 3.1808 \pm 0.0004$$

f = negative muon frequency in water.

f_p = proton frequency in water.

XI. REFERENCES

1. M. Gell-Mann, Revs. Modern Phys. 31, 834 (1959).
2. H. Suura and E. H. Wichmann, Phys. Rev. 105, 1930 (1957).
3. A. Petermann, Phys. Rev. 105, 1931 (1957).
4. E. M. Sommerfield, Phys. Rev. 107, 328 (1957).
5. A. Petermann, Helv. Phys. Acta 30, 407 (1957).
6. V. B. Berestetskii, O. N. Krokhin, and A. K. Khlebnikov, J. Exptl. Theoret. Phys. (U.S.S.R.) 30, 778 (1956) [translation: Soviet Phys. J.E.T.P. 3, 761 (1956)]
7. S. D. Drell, Annals of Physics 4, 75 (1958).
8. R. L. Garwin, L. M. Lederman, and M. Weinrich, Phys. Rev. 105, 1415 (1957).
9. J. D. Jackson, The Physics of Elementary Particles (Princeton University Press, 1958) p. 119.
10. R. A. Swanson, Phys. Rev. 112, 580 (1958).
11. Hans Kruger, University of California thesis 1961 (to be published).
12. J. D. Jackson, loc. cit., p. 95.
13. A. E. Ignatenko, L. B. Egorov, B. Khalupa, and D. Chulten, J. Exptl. Theoret. Phys. (U.S.S.R.) 35, 1131 (1958) [translation: Soviet Phys. J.E.T.P. 8, 792 (1959)].
14. A. Astbury, P. M. Hattersley, M. Hussain, M.A.R. Kemp, H. Muirhead, and T. Woodhead, Proc. Phys. Soc. 78, Pt. 6(i) No. 505, 1144 (1961).
15. Michel Schiff, Nuovo cimento 22, 66 (1961).
16. E. R. Cohen, K. M. Crowe, and J. W. DuMond, Fundamental Constants of Physics (Interscience Publishers, New York, 1957) p. 268, 269.
17. Y. Lathrop, R. A. Lundy, V. L. Telegdi, R. Winston, and D. D. Yovanovitch, Nuovo cimento 17, 109 (1960).

18. J. Lathrop, R. A. Lundy, S. Penman, V. L. Telegdi, R. Winston, D. D. Yovanovitch, and A. J. Bearden, Nuovo Cimento 17, 114 (1960).

19. S. Devons, G. Gidal, L. M. Lederman, and G. Shapiro, Phys. Rev. Letters 5, 330 (1960).

20. G. Charpak, F. J. M. Farley, R. L. Garwin, T. Muller, J. C. Sens, and A. Zichichi, A New Measurement of the Anomalous Magnetic Moment of the Muon, CERN Report 2878/N.P./ih Feb. 12, 1962. See also G. Schrank, An Experiment to Determine (g-2) for the Free Muon, Princeton-Pennsylvania Accelerator Report, P.P.A.D. 304 D.

21. D. P. Hutchinson, J. Menes, G. Shapiro, A. M. Patlach, and S. Penman, Phys. Rev. Letters 7, 129 (1961). Earlier references may be obtained from this reference; D.P. Hutchinson, A Precise Determination of the Magnetic Moment of the Positive Muon, Nevis-103, March 1962.

22. A. A. Schupp, R. W. Pidd, and H. R. Crane, Phys. Rev. 121, 1 (1961).

23. J. W. M. DuMond, Annals of Physics 7, 365 (1959).

24. R. L. Garwin, D. P. Hutchinson, S. Penman, and G. Shapiro, Phys. Rev. 118, 271 (1960).

25. For example see V. Bargmann, Louis Michel, and V. L. Telegdi, Phys. Rev. Letters 2, 435 (1959).

26. Yahia El Hakim, A Preliminary Investigation of the System Time Spread for Some Types of Multiplier Phototubes, UCRL-9200, May 1960.

27. H. A. Thomas, R. L. Driscoll, J. A. Hipple, Journal of Research of the National Bureau of Standards, 44, 569 (1950).

28. H. A. Thomas, Electronics 25, 114 (1952).

29. S. Smiriga, C. Dols, and G. Bingham, A Magnetic Field Regulator with a Stability of Three Parts in a Million, U.C.L.R.L. Electronics Engineering Note 827.

30. Weston A. Anderson, Rev. Sci. Instr. 32, 241 (1961).

31. L. S. Goodman, Rev. Sci. Instr. 31, 1351 (1960).

32. Radiation Laboratory Counting Handbook, UCRL 3307 (revised).

33. H. W. Lefevre and J. T. Russell, Rev. Sci. Instr. 30, 159 (1959).

34. A. E. Bjerke, Q. A. Kerns, and Thomas A. Nunamaker, Pulse Shaping and Standardizing of Photomultiplier Signals for Optimum Timing Information Using Tunnel Diodes, UCRL 9838, August 1961.

35. Robert M. Sugarman, Non Saturating Transistor Circuitry for Nanosecond Pulses, B. N. L. 4436.

36. W. C. Dickinson, Phys. Rev. 81, 717 (1951).

37. C. Scott Johnson, E. P. Hincks, and H. L. Anderson, Mu Mesic X-Rays in the Iron Region, University of Chicago, E. F. I. N. S.-61-59 (submitted to Phys. Rev. October 1961).

38. A. Astbury, K. M. Crowe, J. Deutsch, Tin Maung, and R. Taylor (private communication).

39. Jay Orear, Notes on Statistics for Physicists, UCRL 8417, August 13, 1958.

40. Yardley Beers, Introduction to the Theory of Error (Addison-Wesley Publishing Company, Inc., 1957) p. 37.

41. J. A. Pople, W. G. Schneider, and H. J. Bernstein, High-resolution Nuclear Magnetic Resonance (McGraw-Hill Book Co., Inc., 1959) p. 89, 279.

42. H. Überall, Phys. Rev. 114, 1640 (1959).

43. Elihu Lubkin, Phys. Rev. 119, 815 (1960).

44. W. D. Knight, Solid State Physics (Academic Press, New York, 1956) II, p. 93.

45. Pople, et al., loc. cit. p. 90, 169, 403.

46. Kenneth W. Ford, Vernon W. Hughes, and John G. Wills, Phys. Rev. Letters 7, 135 (1961).